TU Delft

Delft University of Technology

Defect Identification through Partial Discharge Analysis on HVDC

Partial Discharge Fingerprinting

Abdul Madhar, S.

DOI
10.4233/uuid:052aa674-20a1-4af5-a543-52acf5c4f90b

Publication date
2021

Document Version
Final published version

Citation (APA)
Abdul Madhar, S. (2021). *Defect Identification through Partial Discharge Analysis on HVDC: Partial Discharge Fingerprinting*. [Dissertation (TU Delft), Delft University of Technology]. https://doi.org/10.4233/uuid:052aa674-20a1-4af5-a543-52acf5c4f90b

Important note
To cite this publication, please use the final published version (if applicable).
Please check the document version above.

Copyright
Other than for strictly personal use, it is not permitted to download, forward or distribute the text or part of it, without the consent of the author(s) and/or copyright holder(s), unless the work is under an open content license such as Creative Commons.

Takedown policy
Please contact us and provide details if you believe this document breaches copyrights.
We will remove access to the work immediately and investigate your claim.

This work is downloaded from Delft University of Technology.
For technical reasons the number of authors shown on this cover page is limited to a maximum of 10.

Defect Identification through Partial Discharge Analysis on HVDC

Partial Discharge Fingerprinting

Defect Identification through Partial Discharge Analysis on HVDC

Partial Discharge Fingerprinting

Proefschrift

ter verkrijging van de graad van doctor
aan de Technische Universiteit Delft,
op gezag van de Rector Magnificus Prof.dr.ir. T.H.J.J. van der Hagen,
voorzitter van het College voor Promoties,
in het openbaar te verdedigen op donderdag 16 september 2021 om 10:00 uur

door

Saliha ABDUL MADHAR

Elektrotechnisch ingenieur,
Technische Universiteit Delft, Nederland,
geboren te Chennai, India.

Dit proefschrift is goedgekeurd door de

Promotor: Prof.dr. R. Ross
Copromotor: Dr. A. Rodrigo Mor

Samenstelling promotiecommissie:

Rector Magnificus,	voorzitter
Prof.dr. R. Ross,	Technische Universiteit Delft, *promotor*
Dr. A. Rodrigo Mor,	Technische Universiteit Delft, *copromotor*
Onafhankelijke leden:	
Prof.dr.ir. A.J. van der Veen,	Technische Universiteit Delft
Prof.dr. R. Plath,	Technische Universität Berlin
Prof.dr.-Ing. S. Tenbohlen,	University of Stuttgart
Prof.dr.ir. E.F. Steennis,	Technische Universiteit Eindhoven
Overige leden:	
Prof.dr. P. Palensky,	Technische Universiteit Delft, *reservelid*
Ing. P. Mráz, Ph.D.,	HAEFELY AG

Ing. P. Mráz, Ph.D. heeft de totstandkoming van het proefschrift bijgedragen.



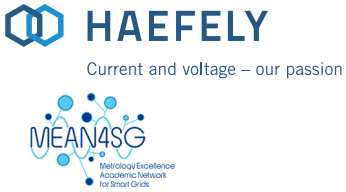

Keywords: partial discharge, dielectric testing, HVDC, pattern recognition, corona, defect identification

Printed by: Ipskamp printing

Front & Back: Initial design and concept by: Lukas Walder, HAEFELY AG, Basel
Realization in final form by: Syed Arshad, NODEStudio, Chennai

Copyright © 2021 by S. Abdul Madhar

ISBN 978-94-6366-449-3

An electronic version of this dissertation is available at
http://repository.tudelft.nl/.

Contents

Summary ix

Samenvatting xi

1 Introduction 1
- 1.1 Background . . . 2
- 1.2 Scope of the thesis . . . 3
- 1.3 State of the art . . . 4
  - 1.3.1 Defect identification under AC voltage stress . . . 4
  - 1.3.2 Defect identification under DC voltage stress . . . 6
- 1.4 Research goals . . . 9
- 1.5 Research approach and thesis outline . . . 11

2 Partial Discharge Basics 17
- 2.1 Introduction . . . 18
- 2.2 Origin and types of partial discharges . . . 18
- 2.3 Equivalent circuit for partial discharge . . . 20
- 2.4 PD phenomenon under AC vs. DC voltage . . . 21
- 2.5 Standardization in PD measurement: IEC 60270 . . . 24

3 Description of experimental setup 29
- 3.1 Introduction . . . 30
- 3.2 Artificial PD defect models . . . 30
  - 3.2.1 Corona defect . . . 30
  - 3.2.2 Floating electrode defect . . . 31
  - 3.2.3 Surface discharge defect . . . 31
- 3.3 PD measurement . . . 33
- 3.4 PD acquisition . . . 35
- 3.5 PD Evaluation . . . 35
  - 3.5.1 Data processing . . . 36
  - 3.5.2 Derived quantities . . . 36
  - 3.5.3 Visual tools . . . 37
  - 3.5.4 Statistical tools . . . 38
  - 3.5.5 Discriminatory tools . . . 38

4 Study of Corona Configurations under DC 43
- 4.1 Introduction . . . 44
- 4.2 Corona configurations . . . 46
  - 4.2.1 Configuration I: Negative DC with needle at HV . . . 46

4.2.2 Configuration II: Positive DC with needle at HV 49
4.2.3 Configuration III: Negative DC with needle at ground 53
4.2.4 Configuration IV: Positive DC with needle at ground 54
4.3 Discrimination of corona configuration under DC 57
4.4 Conclusion 60

5 Study of the Floating Electrode Defect under DC 65
5.1 Introduction 66
5.2 Understanding floating discharge under AC stress 67
5.2.1 Discharge behaviour 68
5.2.2 Corona from floating objects 72
5.3 Floating electrode under negative DC 73
5.4 Floating electrode under positive DC 77
5.5 Conclusion 77

6 Study of Surface Discharges under DC 83
6.1 Introduction 84
6.2 Measurement of electrical properties of the dielectric surface 85
6.3 Simulation of the surface defect model 86
6.3.1 Model setup 87
6.3.2 Results and Observations 89
6.4 Partial discharge testing of surface defect model 92
6.4.1 AC test 93
6.4.2 DC tests 96
6.5 Surface defect: Similarities between AC and DC patterns 100
6.6 Conclusion 102

7 Defect Identification under DC: Corona, Floating and Surface defect 107
7.1 Introduction 109
7.2 Analysis based on visual patterns 110
7.2.1 PSA patterns 110
7.2.2 Weighted PSA or WePSA patterns 112
7.2.3 Other derived patterns 119
7.3 Analysis based on statistical classification of discharge parameters . . 119
7.3.1 Classification of time between discharge occurrence 119
7.3.2 Classification of difference in discharge magnitude 120
7.4 Discharge trends with respect to voltage 122
7.5 Discriminatory process 124
7.6 Conclusion 126

8 Conclusions and Recommendations 131
8.1 Conclusions 132
8.2 Recommendations for future work 134

Appendix A 135

List of Abbreviations **137**

Acknowledgements **139**

Curriculum Vitæ **141**

List of Publications **143**

Summary

The electricity grid spanning hundreds of thousands of kms is one of the most complex man-made network built in human history. Today, after a century of growth, progress and innovation, the electricity grid is in the process of undergoing another landmark shift in its operation. The introduction of renewable energy sources, especially, offshore wind connected to the load centres through >80 kms of underground subsea cable has caused a shift from AC transmission towards DC transmission. This is because AC cables suffer from high charging currents that reduce the useful current carrying capacity for long cables. On the contrary, High Voltage DC (HVDC) is acclaimed with higher current capacity for the same conductor dimension as AC and as a result the more sustainable alternative. Therefore, the infrastructure developed around the AC grid is now under pressure to adapt itself to the DC technology. This implies a dramatic change in a cascade of procedures and processes, beginning from designing new DC components, its testing and qualification, its validation and up to its commissioning, control and operation. Every step in the process is expected to be crucial and challenging given the newness of the technology and lack of experience.

In the current scenario, this research rests itself in the testing and qualification phase of these DC components. The field of HV testing has not been exclusive to this pressure to adapt and improvise its processes to accommodate the newest DC technological trends. New requirements are being defined to determine the quality of HVDC components and new methodologies developed to fulfil this. One of the most widespread test methodologies that has come to become a part of several tests such as factory acceptance tests (FATs), site acceptance test (SATs), routine tests and type tests is the measurement of Partial Discharge (PD). Partial discharge is a dielectric phenomenon that when measured is used as a proven marker for insulation quality. The inherent differences in the performance of the insulation under AC and DC operation have not allowed a direct adaption of the PD analysis techniques from AC to DC.This research will investigate the possibilities of defect identification through PD measurements under DC.

With increasing HVDC installations such as GIS/GIL, cable links, convertors etc., the method for its design validation and fitness through partial discharge measurement is gaining increasing popularity. This is only expected to rise with the introduction of renewable energy, electric vehicles (EVs) and its related infrastructure, lowered dependency on fossil fuels and an international policy shift towards the reduction of greenhouse gases. Moreover, given the remarkable success of partial discharge measurements in defect identification under AC, mounting expectations for a similar prospect under DC conditions is a thriving notion. Therefore, as a first steps towards characterizing PD defects under DC conditions this thesis studies the

physics of discharge progression of 3 common defect types namely, corona, floating electrode and surface discharge in detail, in order to recognize minor if not major differences that will enable defect recognition. With this investigation, a comprehensive procedure is devised, enabling the identification of the three defects that were studied under DC conditions. The research also proposes the novel WePSA (Weighted Pulse Sequence Analysis) patterns discussed in chapter 7, section 7.2.2 as a prospective defect fingerprint that will allow identification of defects under DC. The simplicity and robust nature of these patterns make them self-explanatory and easy to interpret. Several other unique defect behavioural features discovered during the study add value to this research and bring it closer to accomplishing the final goal of PD defect identification under DC stress conditions.

This research could serve as a starting point for the scientific community to investigate further the other defect models and extend the defect discrimination strategy proposed in this thesis, chapter 7, section 7.5.

Samenvatting

Het elektriciteitsnet, dat honderdduizenden kilometers bestrijkt, is een van de meest complexe door de mens aangelegde netwerken in de geschiedenis van de mensheid. Tegenwoordig, na een eeuw van groei, vooruitgang en innovatie, bereikt het elektriciteitsnet een nieuwe mijlpaal in zijn werking. De invoering van hernieuwbare energiebronnen, met name offshore windenergie die met de het elektriciteitsnet/de gebruikers zijn verbonden via >80 km kilometers onderzeese kabel, heeft geleid tot een verschuiving van AC-transmissie naar DC-transmissie. Dit komt door-dat AC-kabels te lijden hebben van hoge laadstromen die de bruikbare stroom-capaciteit voor lange kabels verminderen. Hoogspanningsgelijkstroom (HVDC) daarentegen geniet de voorkeur vanwege een hogere stroomcapaciteit met dezelfde geleider-afmetingen als wisselstroom en is bijgevolg het duurzamere alternatief. Daarom staat de infrastructuur die rond het wisselstroomnet is ontwikkeld, nu onder druk om gelijkstroomtechnologie op te nemen. Dit impliceert een drastische verandering in een reeks procedures en processen, te beginnen met het ontwerpen van nieuwe gelijkstroomcomponenten, het testen en kwalificeren, het valideren en tot aan de inbedrijfstelling, controle en werking. Elke stap in het proces zal naar verwachting cruciaal en uitdagend zijn, gezien de nieuwheid van de technologie en het gebrek aan ervaring.

In het huidige scenario berust dit onderzoek op de test- en kwalificatiefase van deze DC-componenten. De druk om de processen aan te passen en te improviseren om tegemoet te komen aan de nieuwste technologische trends op het gebied van gelijkstroom is niet exclusief voor het gebied van het testen van HV. Er worden nieuwe eisen vastgesteld om de kwaliteit van HVDC-componenten te bepalen en nieuwe methodologieën ontwikkeld om hieraan te voldoen. Een van de meest wijdverbreide methodologieën die deel is gaan uitmaken van diverse tests, zoals fabrieksacceptatietests (FAT's), locatieacceptatietests (SAT's), routinetests en typetests, is de meting van partiële ontladingen (PD). Deelontladingen zijn een diëlektrisch fenomeen dat kenmerkend kan zijn voor de isolatiekwaliteit. Meetresultaten worden gebruikt als beproefde toetsing. De inherente verschillen in de prestaties van de isolatie bij wisselstroom- en gelijkstroomwerking verhinderen een directe aanpassing van de PD-analysetechnieken van wisselstroom aan gelijkstroom. Dit onderzoek richt zich op de defectidentificatie via PD-metingen bij gelijkstroom.

Het aantal HVDC-installaties zoals GIS/GIL, kabelverbindingen, convertors enz. toeneemt, groeit het meten van deelontladingen aan populariteit voor de validatie van het ontwerp en de geschiktheid ervan. Dit zal naar verwachting alleen maar toenemen met de introductie van hernieuwbare energie, elektrische voertuigen (EV's) en de bijbehorende infrastructuur, verminderde afhankelijkheid van fossiele brandstoffen en een internationale beleidsverschuiving naar de vermindering

van broeikasgassen. Bovendien, gezien het opmerkelijke succes van gedeeltelijke ontladingsmetingen bij het onderscheiden van defecten onder wisselstroom, is de verwachting voor een soortgelijk vooruitzicht onder gelijkstroomcondities een stimulerende gedachte. Als een eerste stap naar het karakteriseren van PD defecten onder DC condities bestudeert dit proefschrift daarom de fysica van het gedetailleerde ontladingsverloop van 3 veel voorkomende defecttypes, namelijk corona, zwevende elektrode en oppervlakteontlading, om zo kleine of zelfs grote verschillen te herkennen die defectherkenning mogelijk zullen maken. Met dit onderzoek wordt een uitgebreide procedure ontworpen, die de identificatie mogelijk maakt van de drie defecten die werden bestudeerd onder DC condities. In het onderzoek worden ook de nieuwe WePSA-patronen (Weighted Pulse Sequence Analysis) voorgesteld, die besproken worden in hoofdstuk 7, sectie 7.2.2, als een toekomstige vingerafdruk waarmee defecten onder gelijkstroom kunnen worden geïdentificeerd. De eenvoud en robuustheid van deze patronen maken ze zelfverklarend en gemakkelijk te interpreteren. Verscheidene andere unieke gedragskenmerken van defecten die tijdens de studie werden ontdekt, voegen waarde toe aan dit onderzoek en brengen het dichter bij het bereiken van het uiteindelijke doel van PD defectidentificatie onder DC spanningsomstandigheden.

Dit onderzoek kan als uitgangspunt dienen voor de wetenschappelijke gemeenschap om overige defectmodellen verder te onderzoeken en de in dit proefschrift voorgestelde defect-discriminatiestrategie uit te breiden, hoofdstuk 7, sectie 7.5.

1

Introduction

The introduction chapter provides background to the subject of 'partial discharge defect identification' that is dealt with in this research. It outlines the significance and relevance of the topic during the current times and defines the scope of this particular thesis. The state of the art in the field has been described in order to brief the reader with regard to the existing techniques and methodologies. Further, based on the above, the gaps in research are identified and clear-cut research goals are defined. In the final section, the chapter describes the research approach that is adopted in this thesis and outlines the thesis structure.

1

1.1. Background

A growing global demand for energy has led to an increasing number of interconnectors and wind parks being constructed up to 100's of km's offshore, connected through submarine cables. This has left the energy markets across Europe and generally across the World becoming increasingly cohesive in terms of energy trade. The need for long distance energy transmission has become crucial as a result. However, the existing energy infrastructure which works on the principle of High Voltage Alternating Current or HVAC has a large reactive power consumption when it comes to long distance transmission, the charging current of the cable becomes so high that the useful current carrying capacity is highly reduced. Therefore, an alternative means of transmission using High Voltage Direct Current or HVDC which is not limited by its charging current for long distance transmission has been increasingly adopted. This mounting interest in the field of HVDC and since being casted as the poster tool of "green" and "sustainable" energy has resulted in government policies and funding that authorize the design and installation of large HVDC projects across Europe and across the World. Figure 1.1 shows the map of Europe with the already existing HVDC links, the projects under construction and the planned projects as was in the year 2008. In the year 2018, the HVDC infrastructure was estimated at a whooping USD 8.3 billion. And it is expected to rise at an annual rate of 7 % over the next 4 years to an estimated USD 12.3 billion [1]. Although the HVDC transmission technology is lauded with high transmission efficiencies, there is a lack of deep understanding towards the DC behaviour of network components such as circuit breakers, isolators and insulation systems. This haste in decision making and lack of thorough preparation and study has resulted in the failure of several newly installed HVDC links. As reported in the annual Entsoe (European Network of Transmission System operators for Electricity) report [2]; there were a total of 48 registered disturbance outages, preventing 1.4 TWh of potential energy transmission, or 1.5 % of the total technical capacity (Emax). In addition, maintenance outages amounted to 2.8 TWh, or 3 % of the total technical capacity (Emax), and other limitations reduced the transmission capacity by an additional 2.9 TWh or 3.2 %. This amounts to about 8 % reduction in the total transmission capacity.

This lack of reliability in long-term operation of HVDC networks is leading to increased scepticism and delay in the arrival of the new technology. Currently, the International Electrotechnical Committee (IEC) that defines standards for test and qualification of high voltage components and regulates the quality of manufacturing, specifies a particular dielectric test called Partial Discharges (PD) test among several others. It is defined as a means of quality assurance for both AC and DC systems. The partial discharge test is a unique test that does not just potentially indicate the insulation quality in terms of value but also potentially provides information on the location and the nature of the defect in the insulation. So far, PD tests on AC components have proven to be a very powerful tool for defect identification, pre-emptive maintenance, monitoring and diagnostics. Well above 80 % of the insulation failures in rotating machines could be isolated and prevented through regular PD testing [3]. Different dielectric defects can be recognized based on their

characteristic fingerprint patterns that arise due to the phase relationship of the defect behaviour to the AC sine wave. Given the remarkable success of partial discharge measurements in defect isolation under AC, mounting expectations for a similar prospect under DC conditions has become a thriving notion.

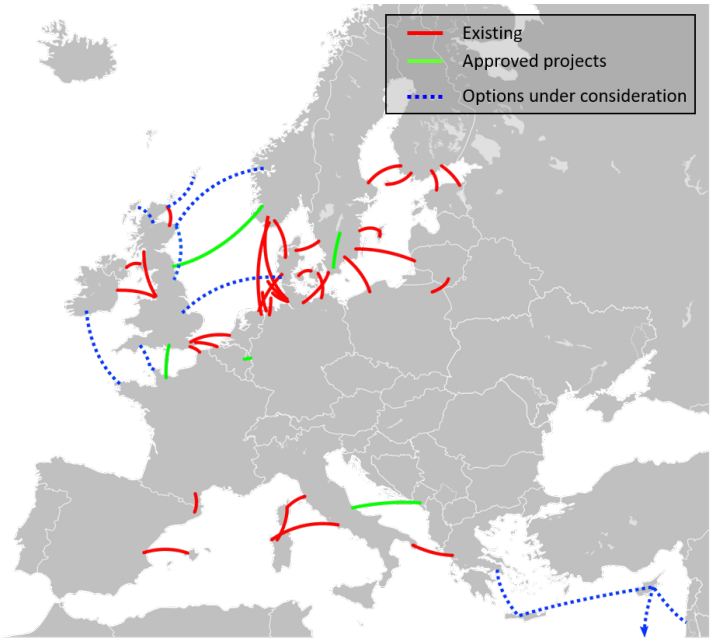

By J JMesserly and those stated in source. - Blank map of Europe.svg by Maix, which is based on Europe countries.svg by Tintazul, CC BY-SA 3.0, https://commons.wikimedia.org/w/index.php?curid=5553728

Figure 1.1: The map of Europe showing the active, ongoing and planned HVDC connections [4].

1.2. Scope of the thesis

Partial discharge is a particularly wide subject area, it deals with concepts beginning from electrotechnic to aspects of material science. Researchers in the past decades have extensively studied PD both as a dielectric phenomenon as well as an application. Today, the measurement of PD under AC is used as a means of defect detection, identification and localization for insulation damage. Though the concept of PD measurement under AC and DC is the same, the process of defect identification differs significantly. This is because the characteristic fingerprints or patterns that are used to differentiate the various common defect types under AC are based on the relationship of the defect/ discharge behaviour to periodicity of the AC waveform. Some typical examples of PD fingerprints for common defect types are shown in Figure 1.2. These patterns are popularly referred to as Phase Resolved PD patterns or PRPD patterns in short. These diagrams show the repet-

itive charge magnitude with respective to the voltage phase of occurrence. They are viewed either in unipolar or bipolar format as shown in Figure 1.2. The partial discharge analysis under DC however, does not permit the creation of such patterns due to the lack of alternating polarity. Therefore, this particular research sets its focus upon the possibilities of defect identification through partial discharge testing, specially under DC stress conditions.

In order to understand the complete and unaltered discharge behaviour of various defects, the research will involve the study of artificially created defects in a laboratory test arrangement. Some of the most common defect types namely, corona from sharp objects, floating electrode and surface discharge fall under the scope of this thesis. The research will not involve the development of any special hardware or software for direct implementation of the PD measurement application under DC.

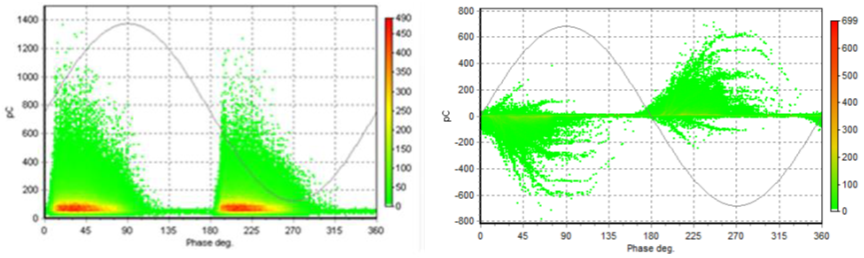

(a) (b)

Figure 1.2: Typical PRPD patterns recorded under AC voltage stress (a) for slot discharges in a medium sized rotating machine and (b) Voids in resin-based insulation material.

1.3. State of the art

1.3.1. Defect identification under AC voltage stress

Partial discharge measurement under AC voltage has now become exceedingly popular and accepted in laboratories and industries as a tool to inspect insulation quality. Partial discharge tests are feasible on a wide range of test objects including, power transformers, instrument transformers, cables, Gas Insulated Switchgears (GIS), rotating machines, bushings, capacitor banks etc. Partial discharges are not limited by the range of applied voltages. A PD test can be made on DUTs (Device Under Test) operating at 400 V to those over a few MV. This is because PD inception is related to the critical electrical field stress within or along the insulation and does not directly depend on the value of applied voltage. This makes the PD test highly pervasive among the various international standards concerning the test and qualification of electrical components.

Though the application of a PD test as a tool for quality assurance has become

indispensable in the past years, the precedence of its application as a diagnostic and monitoring tool has steadily gained momentum. Partial discharge is no more seen as a scalar value in terms of charge (or voltage in mV) but a comprehensive bundle of information regarding trends in magnitude over time and variation in magnitude with location of sensors, and several other estimates. It has evolved from a PD detection test that reads a simple pass/fail value to a complex analysis to additionally identify the nature and the location of the defect. Therefore, defect detection, identification and localization can be referred to as the three major elements or aspects of a PD measurement as shown in Figure 1.3.

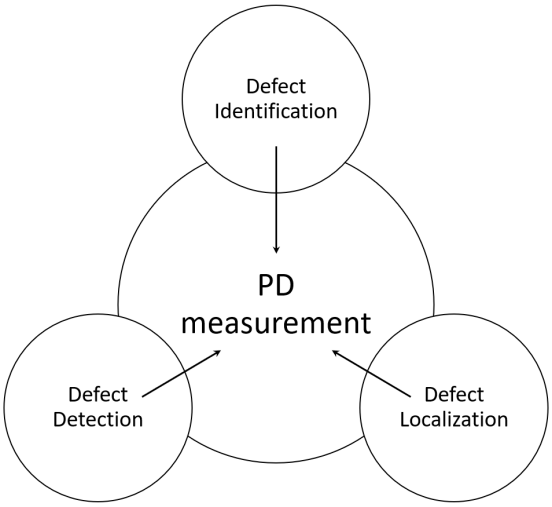

Figure 1.3: The three major elements or aspects of a PD measurement.

In straightforward test cases, with test objects with one defect, the PD identification can be done predominantly with the aid of PRPD plots. In certain specific cases, additional plots such as the plot of charge versus voltage (Q(V)), supply the user with useful information in order to determine the nature of the defect. Some typical examples of Q(V) plots are shown in Figure 1.4 [5]. In other complex test cases, with DUTs with multiple defects discharging simultaneously,the PRPD plot is rendered almost futile since the clusters that denote individual defects start to overlap. Alternatively, the discharge cluster could also be embedded within the noise cluster. For these scenarios, de-clustering or de-noising algorithms are employed to separate the various clusters and identify the nature of the individual defects. Some of the commercially available de-noising approaches include antenna gating, dynamic noise gating, real-time pulse waveform analysis and synchronous multi-terminal PD measurements [6]. Other less commonly used methods include pulse feature extraction [7], TF (Time-Frequency) maps [8], pulse clustering based on waveform parameters/pulse envelopes [9] and based on pulse energy calculations [10]. The possibility to automate the process of defect recognition has also been explored by many. For example, in [11], the statistical analysis of the basic dis-

charge parameters such as pulse count and magnitude have been studied. In [12], digital detection and fuzzy classification of the occurring partial discharge signals has been developed. Others have used advanced image features derived from two-dimensional PRPD patterns to automate PD pattern recognition [13].

The final element of PD measurement is defect localization. Defect localization is a concept within the PD measurement procedure that is increasingly object/DUT specific unlike the rest of the procedure. This feature of a PD test makes it a very unique and powerful tool amongst the other dielectric tests such as $\tan\delta$. A $\tan\delta$ test only provides information on the quality of the bulk insulation. Whereas, a PD test can pin-point towards the location of the defect within the insulation with a certain level of accuracy (depends on several influencing factors such as type of DUT, nature of PD measurement, accuracy and sensitivity of measurement, etc.). For instance, defect localization is done in power cables applying the concepts of Time Domain Reflectometry (TDR) [14]. Localization accuracies up to 1 % of full cable length are achievable in most cases. When it comes to power transformers, defect localization through non-conventional PD measurement techniques (all other techniques such as acoustic, UHF, electromagnetic etc.) through the process of triangulation is more common [15]. These features of a partial discharge test have placed great reliance on the measurement and its respective analysis.

1.3.2. Defect identification under DC voltage stress

The three major elements of a PD measurement that were discussed in the previous section, namely PD detection, identification and localisation still remain unaccomplished when it comes to PD testing under DC. The overall concept of PD measurement, including the use of a capacitive shunt across the DUT, and the application of a measuring impedance to decouple the high frequency (HF) signal remain same as AC-PD measurement. But, the means of analysis of the detected PD pulses has known to be very diverse from the AC case. This majorly stems from the lack of alternating voltage, phase angle and the slow repetitive pulse occurrence under DC.

It is clear that the lack of voltage phase angle has rendered the PRPD diagram ineffective by all means for analysis of partial discharges under DC. But this does not exclude the application of an analysis of a different kind through diverse patterns. The very low pulse rates certainly pose a greater problem to the DC-PD analysis as the study of any defect type would require a certain amount of minimum data points. Especially with defects embedded inside the insulation, such as internal voids which have a very low discharge rate [16] could become a hindrance to the research process.

One of the early researches on DC-PD comes from the Delft University of Technology by Udo Fromm [17], as early as 1995. Fromm studied three kind of defects, internal, surface and corona discharge. The research employed statistical analysis of the discharge data. However, with the limited computational resources for post-processing (a 3 MByte extended memory over a 386 PC) and an acquisition system with limited capabilities (triggered with 1 MHz intervals), the research was clearly ahead of its time. The research showed promise but no conclusive remarks and

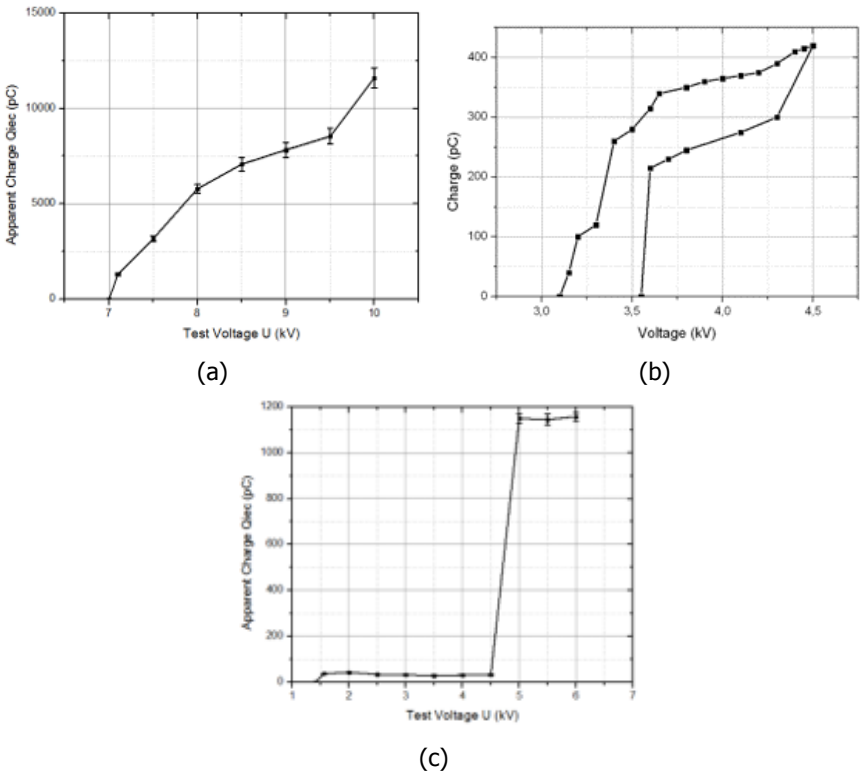

Figure 1.4: Typical charge-voltage dependence or Q(V) plots obtained during AC-PD tests for (a) a surface discharge defect (b) discharge from voids and (c) corona from sharp points [5].

recommendations on the means of PD defect identification under DC.

One of the DC discharge patterns that gained a lot of popularity is the 'Pulse Sequence Analysis' or PSA that was first introduced in 1995 by the researchers Hoof and Patsch [18]. The concept of PSA as its name indicates, is to study the sequence of the discharge pulses. PSA uses the measured magnitude of charge and its time stamp to derive specific plots to study the discharge trends. For instance, information on causality and correlation can be obtained from these plots. However, the randomness of these plots was so high that they were not reliable enough to be employed in real-time defect identification.

DC-PD has been studied based on pulse shape analysis in [19]. Pulse parameters such as rise time and amplitude of the pulse in mV have been used for the study. However, the discharge pulse shape changes based on the location of the defect and the propagation path and therefore, a method of defect classification based on pulse shape analysis could not serve in PD defect identification. The paper itself concluded by stating that comparison of PD signal values on different measuring setups can be very difficult and hence not feasible. Similar proposals of DC-PD defect identification

based on a pulse shape analysis strategy have been proposed also in [20][21]. Other methods such as modified PSA have also been explored in [19]. However, in this case the paper focuses on the data processing methodology more than the data acquisition. The acquisition of the discharge data is done using a PD detector and therefore, the discharge data is limited by the detectors technical limitations on pulse count and dynamic pulse rating. In addition to the PD magnitude,[22] recommends the measurement of average discharge current over the testing time as this both the amplitude of the discharge as well as the PD pulse repetition rate (pulse count). Though the measurement of the average discharge current provides a good indication of the presence of the defect, it does not necessarily aid in its identification.

The other most common methodology adopted for the analysis of DC-PD is a statistical study of the discharge parameters. Histograms of discharge parameters such as pulse count, pulse charge and time between pulses are plotted and the shape parameters of the distribution fitting the empirical PD distribution is derived [23][24][25][26]. Additional PD parameters such as the correlation between a discharge pulse and its successive and preceding discharge pulse in terms of discharge magnitude have been studied in [25]. In case of study of DC-PD based on visual patterns, derived patterns such as TF maps, similar to the ones employed in the analysis of AC-PD are also employed [27][28]. The original PSA plots developed by Hoof and Patsch with several modifications are also commonly used for the study of DC partial discharges. These either use an electrical PD measurement for the HF input raw data, such as in [29] or other non-conventional PD measurement techniques, namely UHF as used in [30]. One limitation that all these approaches share in common is the direct use of a commercial partial discharge detector that provides the values of charge and time of occurrence of the pulses. The PD detector however does not provide raw data in terms of pulse stream where the pulse shape and pulse sequence can be studied and analysed. Based on the hardware, firmware and software limitations of the PD detector, discharge pulses might either be missed or wrongly recognised. It is also probable that the discharge pulses may be recognized with the wrong polarity information. Due to these above stated reasons, the sole use of a PD detector for scientific research purposes is not recommended.

Further, the lack of voltage phase angle has been tackled by several researchers by studying the discharge characteristics based on the ripple on the DC voltage [31][32][33]. The partial discharge behavior under DC is analysed based on the same PRPD pattern that is used for AC-PD analysis. Nevertheless, the levels of ripple used to arrive at distinguishable patterns exceed the maximum 3 % ripple requirements as specified in the standard IEC 60060-1 [34]. Therefore, the direct application of the PRPD visual patterns to identify PD defects under DC still seems improbable. It is to be noted that , other modified voltage waveforms with a defined ripple have also been proposed for partial discharge tests under DC and are under investigation [35].

Several other advanced approaches based on complex mathematical tools for the analysis of DC partial discharges have been studied in the recent years. Feature optimization and dimension reduction [13], study of singular pulse spectral density

[36] and pattern recognition through deep learning [37] are a few of the namely methods that have been explored.

To improve the standard test requirements and technical requirements related to DC-PD, the reproducibility of the DC partial discharge behavior has also been studied. The study is focussed on the reproducibility of the discharge behaviour based on the IEC guidelines IEC 60270 [38] in comparison with the AC partial discharge behavior [39][40]. Some of the results presented in [39] for the reproducibility of a corona defect over AC and DC voltage stresses are improperly analysed. Wrong detector settings and failure to understand the acquisition system settings is the reason for the erroneous results. Nonetheless, improving the analysis methodology to study the reproducibility of DC-PD measurements over different instruments and laboratories is important towards the standardization of the DC-PD measurement technique.

Researchers so far have studied the discharge data under DC using various statistical tools and innovative discharge patterns but few have coupled it along with the physical understanding of the discharge process [26][29][41]. Even so, the lack of focus on the pulse acquisition methodology and a failure to evaluate the limitation of the acquisition system have resulted in conclusions that are heavily influenced by the system parameters and dependant on the acquisition system's hardware and firmware capabilities.

Currently, there is no agreed upon methodology to diagnose a DC system for partial discharges. PD defect identification under DC voltage still happens to be in its elementary form. With this research we will once again explore the possibilities of PD defect identification under DC with the increased computational and pulse acquisition capabilities we have available today.

1.4. Research goals

Currently, there exists no robust methodology to characterize partial discharge sources under DC stress. Therefore, the overreaching goal of this research is to develop a tool or a methodology for the classification/identification of various common insulation defects through electrical PD measurement under DC voltage stress. The research will work in the direction of extending the existing physical understanding of the partial discharge phenomena of specific defects under DC voltage stress through in-depth studies of the discharge process.

In order to fulfil the main research objective, a list of fundamental tasks that can be considered as ancillary to the final goal are identified in listed below. The fulfilment of these tasks prior to embarking on the principal scientific study of the discharge scenarios is essential as it provides crucial information by defining system limitations and boundaries which in turn influence the overall research outcome. The tasks are as follows:

(i) Development of artificial PD defect sources.

(ii) Testing and validation of the defect sources under AC.

(iii) Study and identification of the system limitations of the PD measurement setup.

(iv) Definition of the PD acquisition procedure.

The main research objective can be broken down into the following sub-objectives:

1. In-depth study of PD characteristics of various defect sources under DC stress.
2. Development of an optimal post-processing strategy for the analysis of the acquired PD data.
3. Evaluation of the PD defect characteristics to find a defect identification methodology.

It is vital to identify and further understand the influence of various parameters on the measurements, as these could possibly influence the resultant conclusions. A general overview of the research objective and its associated sub-objectives is shown in Figure 1.5. Each of the above mentioned objectives are dealt with in the forthcoming chapters of the thesis.

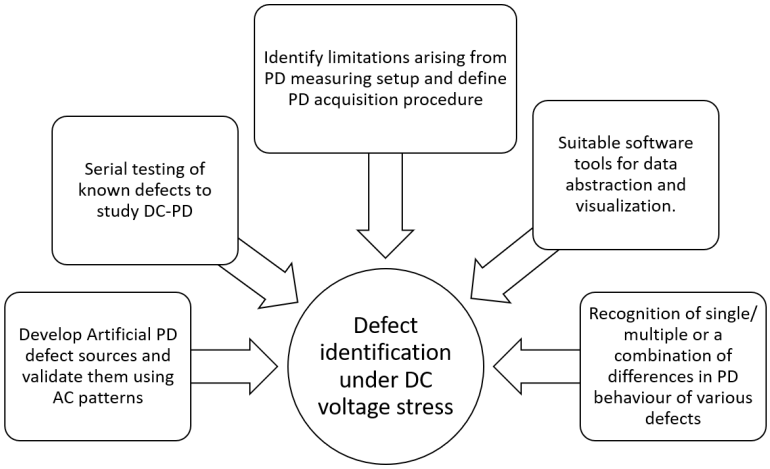

Figure 1.5: The overall research objective and the branching sub-objectives.

The major contributions of this thesis to the research community and the industry could be defined as follows:

(i) To forward the existing knowledge in the field of DC partial discharges.

(ii) Provide a means of defect identification for PD under DC stress.

(iii) Deep understanding of the defect behaviour and its respective patterns.

(iv) Future possibility to define system requirements for PD analysis under DC and accompanying modifications on the relevant international standards.

1.5. Research approach and thesis outline

This thesis adopts a sequential approach of studying individual defect sources with focus on understanding their inherent discharge behaviour under DC. A brief outline of the research process is also depicted in Figure 1.6. The discharge sources are studied in a well designed test setup with no or low level of influence from either the measuring circuitry or the acquisition process. The defect behaviour is studied over variable time and voltage steps. The raw data of the discharge process is recorded in time-domain using a suitable acquisition device and the data is exported in digital format to be post-processed. Based on the study of the recorded discharge process, several discharge parameters are derived and analysed by several different means. The two methods of analysis mentioned on Figure 1.6 are visual patterns and statistical trends in the data. The detailed study of the discharge process gives an added advantage of identifying unique behavioural features of different defects that might have been missed if the study involved merely the processing of raw data acquired over a fixed and short period of time.

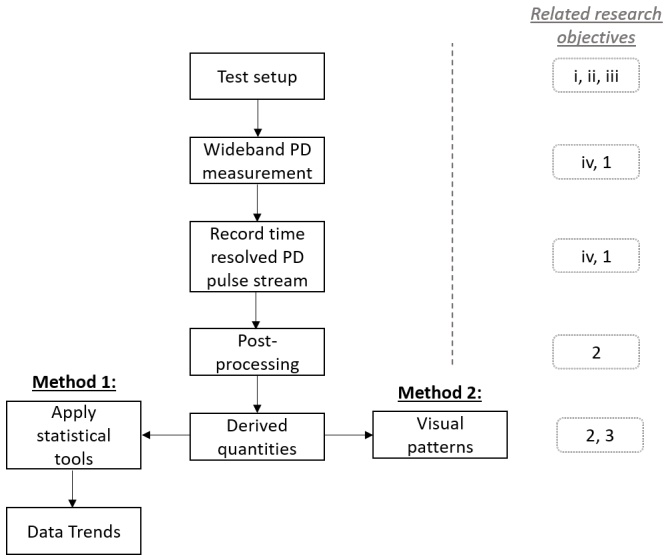

Figure 1.6: The steps in research approach adopted in this thesis.

The thesis outline is as follows, chapter 2, gives the required background for the readers with respect to PD in general. Topics such as origin and types of PD, its equivalent circuit representations, PD as a physical phenomenon and standardization in PD testing are addressed here. Chapter 3 enumerates all the pre-requisites of the research. For instance, details of the PD defect sources that were developed, their validation, the PD measuring circuit and the details of the data acquisition procedure are all described in this chapter.

This thesis is designed such that three individual chapters, namely chapters 4, 5 and 6 are dedicated to explain the study of the three typical defects namely corona,

floating electrode and surface discharge defect, that were researched in this project. These chapters follow a similar outline, starting with a chapter specific introduction, details of the study, results and observations of the PD tests followed by specific conclusions or inferences. The next chapter following them, chapter 7, combines the results obtained in these chapters. It describes the final analysis process involving the results and observations of all three PD defects. This chapter explores the various defect discrimination methodologies while weighing the advantages and disadvantages of each. The final chapter of the thesis is an overall conclusion that sums up the research while providing recommendations for future work.

references

[1] Market Research Report. *HVDC transmission marlet by component, project type, technology, application and geography- Global Forecast to 2024*. Markets and Markets, 2019. url: https://www.marketsandmarkets.com/Market-Reports/hvdc-grid-market-1225.html.

[2] European Network of Transmission system Operators for Electricity. *Nordic and Baltic HVDC utility station and Unavailability statistics*. Entsoe, 2016.

[3] Cigre. *Cigre Brochure WG A1.10: Survey of Hydrogenerator Failures*. 2009, p. 22.

[4] J. Messerly. *HVDC Europe.svg*. 2008. url: https://commons.wikimedia.org/w/index.php?curid=5553728.

[5] P. Mraz. *Aspects of partial discharge activity evaluation*. University of West Bohemia in Pilsen, 2014.

[6] A. Kraetge, S. Hoek, R. Hummel, M. Krüger, O. Kessler, and S. Hong. "Denoising approaches for partial discharge measurements — A comparison of methods and their practical application". In: *2012 IEEE International Conference on Condition Monitoring and Diagnosis*. 2012, pp. 538–541. doi: 10.1109/CMD.2012.6416198.

[7] A. Cavallini, M. Conti, A. Contin, and G. C. Montanari. "Advanced PD inference in on-field measurements. Part 2: Identification of defects in solid insulation systems". In: *IEEE Transactions on Dielectrics and Electrical Insulation* 10.3 (2003), pp. 528–538. issn: 10709878. doi: 10.1109/TDEI.2003.1207481.

[8] J. C. Chan, H. Ma, and T. K. Saha. "Time-frequency sparsity map on automatic partial discharge sources separation for power transformer condition assessment". In: *IEEE Transactions on Dielectrics and Electrical Insulation* 22.4 (2015), pp. 2271–2283. issn: 10709878. doi: 10.1109/TDEI.2015.004836.

[9] F. Alvarez, J. Ortego, F. Garnacho, and M. A. Sanchez-Uran. "A clustering technique for partial discharge and noise sources identification in power cables by means of waveform parameters". In: *IEEE Transactions on Dielectrics and Electrical Insulation* 23.1 (2016), pp. 469–481. issn: 10709878. doi: 10.1109/TDEI.2015.005037.

[10] A. Rodrigo Mor, L. C. Castro Heredia, and F. A. Munoz. "New clustering techniques based on current peak value, charge and energy calculations for separation of partial discharge sources". In: *IEEE Transactions on Dielectrics and Electrical Insulation* 24.1 (2017), pp. 340–348. issn: 10709878. doi: 10.1109/TDEI.2016.006352.

[11] E. Gulski. "Digital analysis of partial discharges". In: *IEEE Transactions on Dielectrics and Electrical Insulation* 2.5 (1995), pp. 822–837. doi: 10.1109/94.469977.

[12] A. Contin, A. Cavallini, G. C. Montanari, G. Pasini, and F. Puletti. "Digital detection and fuzzy classification of partial discharge signals". In: *IEEE Transactions on Dielectrics and Electrical Insulation* 9.3 (2002), pp. 335–348. doi: 10.1109/TDEI.2002.1007695.

[13] K. Wang, J. Li, Shuqi Zhang, F. Gao, Xiaoyu Zhao, R. Liao, and Guoping Zou. "A new group of image features derived from two-dimensional linear discriminant analysis for partial discharge pattern recognition". In: *2016 International Conference on Condition Monitoring and Diagnosis (CMD)*. 2016, pp. 823–827. doi: 10.1109/CMD.2016.7757967.

[14] P. Mraz, P. Treyer, and U. Hammer. "Innovative PD site location optimized for FAT in the cable industry". In: *10th International Conference on Insulated Power Cables*. Paris, Versailles, 2019.

[15] S. M. Markalous, S. Tenbohlen, and K. Feser. "Detection and location of partial discharges in power transformers using acoustic and electromagnetic signals". In: *IEEE Transactions on Dielectrics and Electrical Insulation* 15.6 (2008), pp. 1576–1583.

[16] M. S. Siregar, U. Schichler, R. Woschitz, A. Pirker, and Suwarno. "Partial Discharge Patterns on Cross-Linked Polyethylene DC Power Cables". In: *3rd IEEE Conference on Power Engineering and Renewable Energy* (2016), pp. 119–123.

[17] U. Fromm. *Partial Discharge and Breakdown Testing at High DC Voltage*. Delft University of Technology, 1995. isbn: 90-407-1155-0.

[18] M. Hoof and R. Patsch. "Pulse-sequence analysis: a new method for investigating the physics of PD-induced ageing". In: *IEE Proceedings-Science, Measurement and Technology* 142.1 (1995), pp. 95–101.

[19] J. Pihera, J. Hornak, A. Vobornik, L. Kupka, S. Chladek, and R. Haller. "Partial Discharges Pulse Shape Analysis at AC and DC". In: *Proceedings of the 21st International Symposium on High Voltage Engineering*. Ed. by B. Németh. Springer International Publishing, 2020, pp. 549–559. isbn: 978-3-030-31676-1.

[20] Xiaohua Li, Guangning Wu, Xueqin Zhang, and Shanshan Bian. "Partial discharge pulse shape detection and analysis under DC condition in typical defect models". In: *2007 Annual Report - Conference on Electrical Insulation and Dielectric Phenomena*. 2007, pp. 188–191. doi: 10.1109/CEIDP.2007.4451593.

[21] M. A. Sanchez-Uran, F. Garnacho, F. Alvarez, G. Donoso, and J. Ortego. "Cigre 2016". In: *Signal processing and study of the ripple influence in PD patterns for measurements under HVDC stress*. 2016, pp. 1–6.

[22] J. Pihera, R. Haller, and P. Mráz. "Partial discharges evaluation at DC voltage". In: *Proceedings of the 2014 15th International Scientific Conference on Electric Power Engineering (EPE)*. 2014, pp. 441–445. doi: 10.1109/EPE.2014.6839436.

[23] E. Corr, W. H. Siew, and Weijia Zhao. "PD activity in void type dielectric samples for varied DC polarity". In: *2016 IEEE Conference on Electrical Insulation and Dielectric Phenomena (CEIDP)*. 2016, pp. 510–513. doi: 10.1109/CEIDP.2016.7785616.

[24] H. Q. Niu, A. Cavallini, and G. C. Montanari. "Identification of Partial Discharge Phenomena in HVDC Apparatus". In: *Conference Record of the 2008 IEEE International Symposium on Electrical Insulation*. 2008, pp. 373–376. doi: 10.1109/ELINSL.2008.4570352.

[25] R. Piccin, A. Rodrigo Mor, P. Morshuis, G. C. Montanari, and A. Girodet. "Partial discharge analysis and monitoring in HVDC gas insulated substations". In: *2014 IEEE Electrical Insulation Conference (EIC)*. 2014, pp. 488–492. doi: 10.1109/EIC.2014.6869436.

[26] P. H. Morshuis and J. J. Smit. "Partial discharges at dc voltage: Their mechanism, detection and analysis". In: *IEEE Transactions on Dielectrics and Electrical Insulation* 12.2 (2005), pp. 328–340. issn: 10709878. doi: 10.1109/TDEI.2005.1430401.

[27] M. R. Rahimi, R. Javadinezhad, and M. Vakilian. "DC partial discharge characteristics for corona, surface and void discharges". In: *2015 IEEE 11th International Conference on the Properties and Applications of Dielectric Materials (ICPADM)*. 2015, pp. 260–263. doi: 10.1109/ICPADM.2015.7295258.

[28] R. Aldrian, G. C. Montanari, A. Cavallini, and Suwarno. "Signal separation and identification of partial discharge in XLPE insulation under DC voltage". In: *2017 1st International Conference on Electrical Materials and Power Equipment (ICEMPE)*. 2017, pp. 53–56. doi: 10.1109/ICEMPE.2017.7982098.

[29] A. Pirker and U. Schichler. "Partial discharge measurement at DC voltage - Evaluation and characterization by NoDi∗ pattern". In: *IEEE Transactions on Dielectrics and Electrical Insulation* 25.3 (2018), pp. 883–891. issn: 10709878. doi: 10.1109/TDEI.2018.006742.

[30] M. Geske, C. Neumann, T. Berg, and R. Plath. "Assessment of typical defects in gas-insulated DC systems by means of Pulse Sequence Analysis based on UHF partial discharge measurements". In: *VDE High Voltage Technology 2020; ETG-Symposium*. 2020, pp. 1–8.

[31] T. Dezenzo, T. Betz, and A. T. Schwarzbacher. "A new method for the evaluation and recognition of corona under direct voltage stress". In: *2015 26th Irish Signals and Systems Conference (ISSC)*. 2015, pp. 1–6. doi: 10.1109/ISSC.2015.7163750.

[32] T. Dezenzo, T. Betz, and A. Schwarzbacher. "Transfer and evaluation of the AC PRPD representation for internal PD at DC voltage". In: *2016 IEEE International Conference on Dielectrics (ICD)*. Vol. 1. 2016, pp. 528–531. doi: 10.1109/ICD.2016.7547658.

[33] T. Dezenzo, T. Betz, and A. Schwarzbacher. "Phase resolved partial discharge measurement at dc voltage obtained by half wave rectification". In: *VDE-Fachtagung Hochspannungstechnik 2018*. 2018, pp. 4–9. isbn: 9783800748075.

[34] Standard IEC 60060-1. *High-voltage test techniques– Part 1: General definitions and test requirements*. International Electrotechnical Commission (IEC), 2010.

[35] P. Romano, G. Presti, A. Imburgia, and R. Candela. "A new approach to partial discharge detection under DC voltage". In: *IEEE Electrical Insulation Magazine* 34.4 (2018), pp. 32–41. doi: 10.1109/MEI.2018.8430041.

[36] F. Yang, H. Song, G. Sheng, Z. Gao, and Y. Sun. "Partial discharge pattern recognition based on adaptive multi-resolution analysis of higher-order Singular Spectrum Entropy". In: *2016 International Conference on Condition Monitoring and Diagnosis (CMD)*. 2016, pp. 829–832. doi: 10.1109/CMD.2016.7757978.

[37] Z. Li, Y. Xu, and X. Jiang. "Pattern Recognition of DC Partial Discharge on XLPE Cable Based on ADAM-DBN". In: *Energies* 13.17 (2020). issn: 1996-1073. doi: 10.3390/en13174566. url: https://www.mdpi.com/1996-1073/13/17/4566.

[38] Standard IEC 60270. *High-voltage test techniques–Partial discharge measurements*. International Electrotechnical Commission (IEC), 2000.

[39] M. Hartje, A. Pirker, B. Schober, U. Schichler, H. Saadati, and P. Werle. "Comparison and Analysis of PD Measurements Under DC Voltage in Different HV Laboratories". In: *21st International Symposium on High Voltage Engineering, 2019*. Budapest, 2019, pp. 2–7.

[40] P. M. Hartje, D. B. Schober, P. U. Schichler, and M. S. J. Torres. "Reproducibility of Partial Discharge Measurements of Surface Dis- charges according to IEC 60270 at DC and AC". In: *VDE-Fachtagung Hochspannungstechnik 2020*. 2020, pp. 424–429. isbn: 9783800753536.

[41] E. Ouss, L. Zavattoni, A. Beroual, A. Girodet, and P. Vinson. "Measurement and analysis of Partial Discharges in HVDC gas insulated substations". In: *Cigre Science & Engineering* 11.62-69 (June 2018).

2

Partial Discharge Basics

Partial discharge is a complex subject and its application requires a great deal of understanding of other parallel subject areas such as radio frequency transmission, material science and electron physics, apart from the field of electrotechnic. In order to facilitate the reader in understanding the advanced concepts of PD defect identification under DC that are described in the forthcoming chapters, this chapter is dedicated to describing some of its fundamental relevant and vital concepts. The origin and types of partial discharges are briefly explained followed by its various equivalent circuit representations. In the next sections, the difference between PD phenomenon under AC and DC voltage is explained. In the final section of the chapter, the international standard, IEC 60270 that regulates the PD measurement procedure is briefly introduced.

Parts of this chapter have been published in the proceeds of the 21st International Symposium on High Voltage Engineering (ISH), Budapest, Hungary, August 26-30, 2019 [1]

2.1. Introduction

Partial discharges as the name suggests are discharges in the insulation system of electrical components that partially bridge the dielectric between the two terminals (conductors at different voltages). Partial discharges can be deemed both as the symptom of weakness within the insulation as well as the contributing factor towards its failure. Partial discharges are measured in terms of their charge value in pico Coulomb (pC). Though a partial discharge on its own holds very little energy and is harmless, continued PD activity in the insulation system often and most certainly results in failure and complete breakdown. Therefore, periodic maintenance checks including PD tests on crucial electrical components are considered a necessity. These tests help in keeping check on the health of the insulation that is reflected by the magnitude of discharge and the trend in measured values. In the past decades, partial discharge testing has come to become an indispensable tool in the qualification tests of various electrical components. The functionality of the PD tests is different to the other dielectric tests such as $\tan\delta$, which is a bulk measurement on the insulation system, as it provides additional advantages of defect identification and localization. The various applications covered by PD tests range from large rotating machines, power transformers, instrument transformers, Gas Insulated Switchgear, underground cables and its accessories, until small motor drives. Since the occurrence of PD is not directly related to the voltage level but to the critical electrical stress in the insulation, it is a part of qualification tests for applications over a wide range of voltages. In other words PD test is applicable both for test objects operating at 400 V or a few MV. This is excellently illustrated in Figure 2.1 with a large cylinder type cascade transformer rated for 1 MV, 10.5 m high versus a miniscule sized DC motor that seems to fit in ones palm. The application of PD tests are not limited to the field of electrotechnic, PD tests are now prevalent in the aviation industry to test flight components, in the booming photovoltaic (PV) industry as well as the industry with EV charging. Hence, this chapter provides background to the subject of PD as a physical phenomenon and PD as an application by describing important concepts that will navigate the reader through to the forthcoming advanced chapters on PD defect identification under DC stress.

2.2. Origin and types of partial discharges

The initial introduction of Partial Discharge in the mid 20th century, into the field of electrotechnic was as a measure of radio interference. Later investigation revealed more information on its ramifications on the electrical insulation in which it occurs. There are numerous reasons for the origin of partial discharges. Essentially, it is caused by the excessive electrical stressing of the dielectric medium. Poor design and manufacturing, damage during transportation, poor installation or workmanship and ageing or deterioration of the material could be some of the possible reasons. These in turn cause the formation of voids or air filled cavities in solid and liquid dielectrics, metal deposits or contaminants in fluid insulated systems such as transformers and GIS or irregularities on the electrode and insulation surfaces that

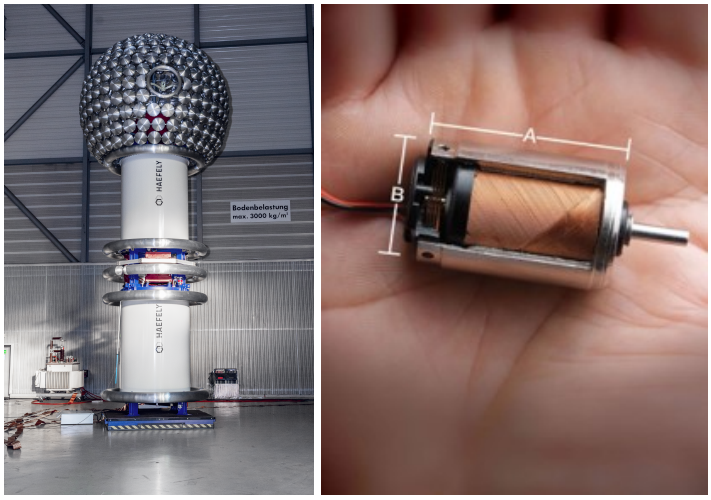

(a) (b)

Figure 2.1: The application of PD measurement ranges from (a) a cylinder type 1 MV cascade transformer (PSZ 1000, Haefely design) to (b) a DC motor that can fit in ones palm [2].

give rise to corona or surface discharges. Figure 2.2 gives the most common types of PD defects that are classified as corona, surface, floating metal/electrodes and internal void.

Partial discharges can be broadly classified as internal and external discharges.

- Internal discharges: Dielectric bounded cavities or voids, air bubbles in liquid dielectrics and non-homogeneities in gaseous insulations such as SF_6.
- External discharges: Corona discharge from sharp objects, mostly in air di-

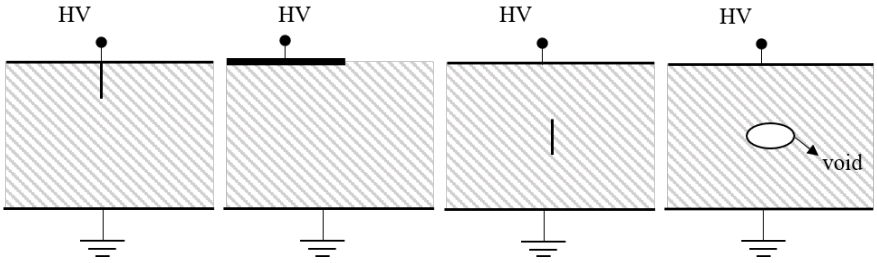

Figure 2.2: Some typical illustrations of PD defect configurations such as (a)corona, (b) surface discharge, (c). floating metal and (d) internal void.

electric and surface discharges, also referred to as gliding or creeping discharges over interfaces.

The most common external defects are corona from sharp objects and surface discharge at interfaces. Internal defects such as voids in insulation, cause permanent damage to the test object as they cannot be easily rectified and the consequences of long term PD activity deteriorates the insulation over time. Similar effects can also be observed with tracking discharges along interfaces.

2.3. Equivalent circuit for partial discharge

Since the 1930's several models have been developed to represent the partial discharge phenomenon accurately [3]. The most popular and widely accepted among them is the 3-capacitor model also referred to as the a-b-c model shown in Figure 2.3a. Its simplicity enables the easy comprehension of discharge scenarios by representing the defect as a lumped capacitor. Though several other models (more complex) were proposed through the years, namely the 5-capacitor model in the 1960's [4] and later the dipole model in the 1980's [5], the a-b-c model remained the most popular. Based on this model, IEC 60270 [6] defines the term 'Apparent charge' which is the charge measurable at the terminals of the test object. The message that the IEC conveys through the term apparent charge is that the value of the measured charge is smaller than or much smaller than the charge involved at the site of discharge. This can be explained as follows, in Figure 2.3a, if C_c is the capacitance of the defect, C_b is the capacitance of the healthy dielectric in series with the defect and q_c is the charge at the defect location then the charge measured at the terminals (q_a) is given by;

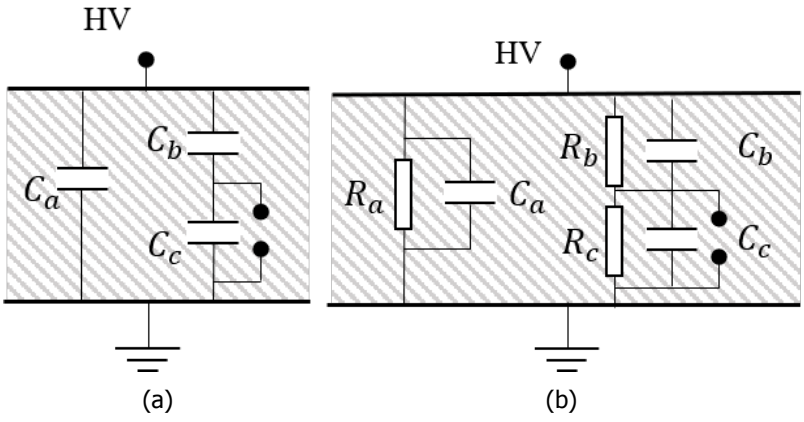

Figure 2.3: The 3-capacitive model for partial discharges for (a) AC voltages and (b) DC voltages.

$$q_a = q_c\,(C_b/C_c) \tag{2.1}$$

under the assumption that $C_c >> C_b$, $q_a << q_c$. Due to this reason this term has been misconstrued to be an arbitrary value which has no relation to the value of the real discharge. However, this is not true, the value of the measured charge is directly representative of the charge involved at the discharge site as confirmed by E. Lemke in the 2010's [7][8] based on Pedersen's Dipole model [5]. He introduced the term 'Induced charge' in an attempt to redefine the value of the measured PD at the test terminals and dismiss the delusion involved with the usage of the term apparent charge. According to this theory the measured charge is proportional to the real charge through a continuous dimensionless positive scalar function λ which differs based on the geometry and location of the defect;

$$dq = -\lambda\,.\,dQ \tag{2.2}$$

where *dq* is the measurable charge and *dQ* is the charge involved at the defect location. Henceforth, the charge value measured in pC as prescribed by the IEC is a quantity that is well correlated to the PD severity.

In case of DC partial discharge, the a-b-c model is slightly modified. The capacitance of the insulation is only effective during the transient phase of voltage change (either during switch on/off or polarity change). The leakage resistance of the insulation determines the partial discharge occurrence. This modified circuit is shown in Figure 2.3b. It also controls the charging time of the DUT as well as the defect, and in turn the discharge repetition rate. The charging voltage over the defect assuming that the leakage resistances are all linear is presented in [9] as;

$$v_c = \frac{R_c}{R_b + R_c}\,.\,(1 - e^{t/\tau})\,.\,V \tag{2.3}$$

$$\tau = \frac{R_b\,.\,R_c}{R_b + R_c}\,.\,(C_b + C_c)$$

where V is the applied DC voltage at the terminals of the test object and τ is the charging time constant that depends on the resistivity of the involved dielectric media and its capacitance.

2.4. PD phenomenon under AC vs. DC voltage

The cause of partial discharge under AC and DC voltage remains fundamentally the same. Which is, partial discharge is a result of overstressing of the insulation which leads to its partial breakdown. However, two identical test objects or samples when tested for PD under AC and DC voltage, produce different results. This stems from the underlying difference in the electrical field distribution in the two cases. The field distribution in the AC test case is a *capacitive* distribution, where the dielectric constants (ϵ_r) of the materials are directing the electrical fields. Figure 2.4a presents two illustrations from the book of Kreuger [9], showing the equipotential lines over an arrangement with two dielectric media. It can be noted that the

equipotential lines tend to concentrate in the region of low ϵ_r. This can be derived from the expression of electrical flux density (D) as follows;

$$D_1 = \epsilon_1 E_1 \ \& \ D_2 = \epsilon_2 E_2$$

$$D_1 = D_2$$

$$\epsilon_1 E_1 = \epsilon_2 E_2$$

$$\frac{\epsilon_1}{\epsilon_2} = \frac{E_2}{E_1}$$

In case of steady-state DC, the field distribution is dictated by the specific conductivities (σ) of the materials instead of the permittivity (ϵ_r). This is derived based on the Ohms law for conductive current (*j*) given by;

$$j = \sigma E$$

The same arrangement with resistive field has a completely different distribution as shown in Figure 2.4b. Similar to as was derived for the AC case, the ratios of electrical field intensity for the DC case can be derived to be;

$$\frac{\sigma_1}{\sigma_2} = \frac{E_2}{E_1}$$

This fundamental difference in the underlying physical distribution of the electrical field stress in the insulation gives rise to the difference in PD behavior. The AC-PD behaviour is repetitive in nature over the 50 Hz voltage cycle. However, the DC-PD pulse occurrence studied so far is both slow and low-repetitive, with a varying pulse interval. The research presented in [10] with the detailed study of the DC-PD mechanism in a gaseous void in solid dielectric highlights the innate complexity of operation of DC systems and its influence on the discharge behaviour of defects. The complexity has caused the PD behaviour of various defects to remain elusive.

To understand the PD measurement setup and the system requirements for data acquisition, it is necessary to be informed on the nature of a PD pulse. In terms of physics, a PD pulse is a fast pulse in time-domain and a high-frequency (HF) pulse in frequency domain. It is often described as a fast pulse with fixed rise and fall time in the order of a few ns (nanoseconds) with its corresponding frequency components extending into hundreds of MHz up to a few GHz at times. A representation of a typical PD pulse is shown in Figure 2.5. As the figure indicates the PD pulse in time domain can at times have pulse width up to a few μs depending on the type and location of the defect, as well as the propagation path of the PD pulse. These features of the PD pulse make the PD test very demanding in terms of resources. The short duration pulses in time-domain preferably need to be measured in real-time with the resolution of a few micro seconds. This requires high speed and high sensitive electronics for the measurement of a quantity in the range of a few mA, and its acquisition at a rate of a few MS/s or GS/s and processing it to acquire quantities of charge, time stamp and others over real-time. In addition, the minute

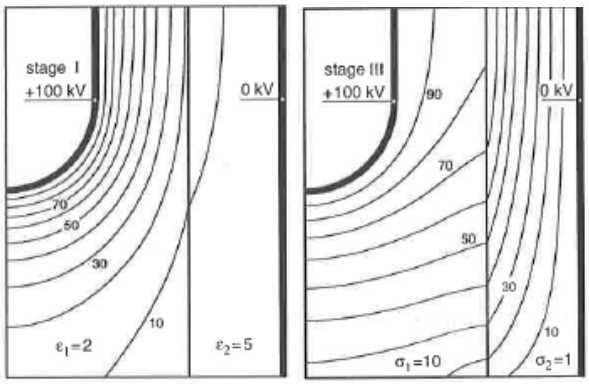

(a) (b)

Figure 2.4: The electrical field distribution plots showing the equipotential lines with (a) AC and (b) DC voltage stress [9].

physical quantity in the range of pC (or mA) is measured in electrical systems operating at high voltages and most commonly in industrial locations. This places high demand on the PD measurement hardware from the point of noise discrimination and measurement sensitivity.

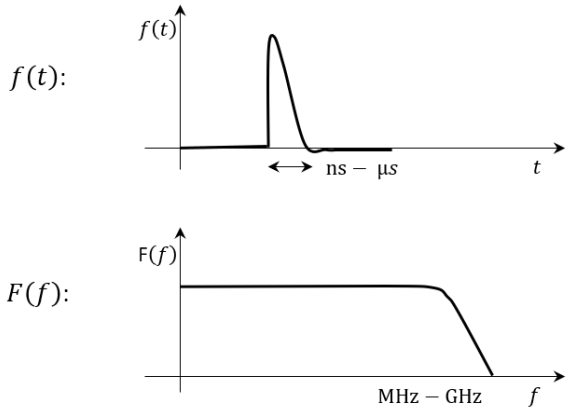

Figure 2.5: Graphical representation of a typical PD pulse in time domain (top) and frequency domain (below).

2.5. Standardization in PD measurement: IEC 60270

International standards such as IEC, IEEE and ANSI all have standards for PD measurement. The most widely accepted and overreaching standard when it comes to PD measurement is the IEC 60270. The IEC 60270 covers the PD measurement in electrical components and systems tested with AC voltage up to 400 Hz or DC voltage. It defines the requirements of the measurement system such as the measuring impedance (also known as the quadripole), PD detector and calibrator in an attempt to regulate the PD test procedure. A regulated PD test procedure ensures repeatability and inter-comparability between measurements made by different operators/measuring equipment at different locations on identical test objects.

The most noteworthy and important setting in a PD test is the selection of the frequency measurement band for the quantification of the charge value in pC. The IEC 60270 defines two different measuring bands for this purpose:

- Wide-band PD measurement: The fixed values for the lower (f_1) and upper limit (f_2) frequencies below which there is adequate attenuation and the measuring bandwidth (Δf) is defined as;

$$30\ kHz \leq f_1 \leq 100\ kHz$$

$$f_2 \leq 1\ MHz$$

$$100\ kHz \leq \Delta f \leq 900\ kHz$$

- Narrow-band PD measurement: In this case, the centre frequency or the midband frequency f_m and the bandwidth (Δf) is defined as;

$$9\ kHz \leq \Delta f \leq 30\ kHz$$

$$50\ kHz \leq f_m \leq 1\ MHz$$

Though the IEC was first introduced as a standard to cover lumped capacitive test objects, with decades of experience it has been found that it is beneficial also towards the test of distributed test objects like transformers and cables. The standard also defines a specialized term called the 'Q_{iec}' which is derived based on the pulse train response defined in section 4.3.3 of the standard. Apart from the standardization of the test procedure for PD measurement the IEC standard also defines various routine and performance tests to ensure the correct operation of the measuring device itself. The requirements of a calibration pulse for example are defined in detail in Annex A of the standard. The PD measurement circuit as described by the IEC 60270 has been shown in Figure 2.6. The two alternative positions of the coupling device/measuring impedance has also been shown in the figure. Measurement alternative 2 suffers from the drawback that the coupling device and the measuring instrument (detector) can be damaged in case of flashover of the test object. Moreover, in case of test objects which cannot be isolated from ground/ earth such as power transformers, measurement option 2 is not directly

possible. Therefore, the coupling device in such cases can be moved to the HV side. However, this is not preferred due to the direct galvanic connection to the HV terminals. Nevertheless, depending on the testing scenario, an optimal testing connection can be chosen.

A small portion of the IEC standard deals with the evaluation of PD test results with DC test voltage. The DC partial discharges are defined in terms of apparent charge instead of Q_{iec} and the standard defines the need to measure the time between successive PD pulses with a resolution of 2 ms. This time interval maybe considered as too long in certain cases where the PD pulse rate is faster and in others it can be considered as too short where the ringing of the pulse is longer. Further, it also specifies the need to measure additional quantities like the value of accumulated charge to gain insight into the PD behaviour. Due to the many inconsistencies and lack of detailed explanations or experience, there are many contradicting views on the IEC's standard for DC-PD. Nevertheless, this research follows the test requirements defined by the IEC towards the PD measurement setup but does not directly base the research on the IEC recommendations for PD evaluation.

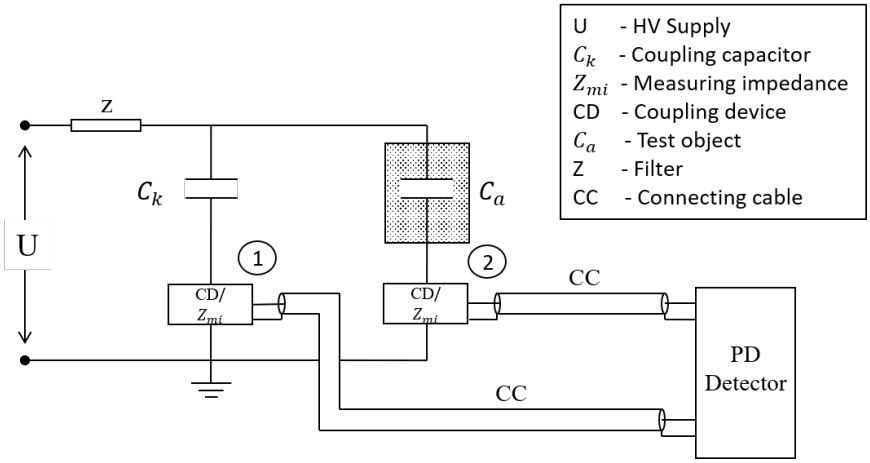

Figure 2.6: The PD measurement circuit as prescribed by the IEC 60270 [6] showing two alternative positions (1 and 2) for the connection of the coupling device.

references

[1] P. Mraz, **S. Abdul Madhar**, P. Treyer, and U. Hammer. "Guidelines for PD measurement according to IEC 60270". In: *The International Symposium on High Voltage Engineering*. Budapest, 2019.

[2] Tennessee Tech. *Transmission line robotics*. 2020. url: https://www.tntech.edu/engineering/research/cesr/wireless-power/robotics.php.

[3] A. Gemant and W. Philippoff. "Die Funkenstrecke mit Vorkondensator". In: *Zeitschrift für Technische Physik* 13.9 (1932), pp. 425–430.

[4] W. Böning. "Luftgehalt und Luftspaltverteilung geschichteter Dielektrika I. Untersuchung der Entladungen in einzelnen Luftspalten bei äußerem Wechselfeld". In: *Electrical Engineering, Archiv für Elektrotechnik* 48.1 (1963). issn: 0948-7921.

[5] A. Pedersen. "Partial discharges in voids in solid dielectrics. An alternative approach". In: *Conference on Electrical Insulation & Dielectric Phenomena*. Gaithersburg, MD, USA, 1987.

[6] Standard IEC 60270. *High-voltage test techniques–Partial discharge measurements*. International Electrotechnical Commission (IEC), 2000.

[7] E. Lemke. "A critical review of partial-discharge models". In: *IEEE Electrical Insulation Magazine* 28.6 (2012), pp. 11–16.

[8] E. Lemke. "Analysis of the partial discharge charge transfer in extruded power cables". In: *IEEE Electrical Insulation Magazine* 29.1 (2013), pp. 24–28.

[9] F. H. Kreuger. *Industrial High DC Voltage*. Delft University Press, 1995, p. 198. isbn: 90-407-1110-0.

[10] P. H. Morshuis and J. J. Smit. "Partial discharges at dc voltage: Their mechanism, detection and analysis". In: *IEEE Transactions on Dielectrics and Electrical Insulation* 12.2 (2005), pp. 328–340. issn: 10709878. doi: 10.1109/TDEI.2005.1430401.

3

Description of experimental setup

This chapter describes all the pre-requisites of the tests carried out in the forthcoming chapters. The artificial PD defect models that were developed for the study of each defect are described here. The measuring setup, its components and relevant details are also described. Though the research involves the study of PD defects under DC, in most cases the defect model is validated using AC tests. For this purpose, the chapter also describes the AC measuring setup. The last part of the chapter deals with data acquisition and evaluation. Various evaluation strategies are proposed based on which the derived data will be studied and analysed with the final goal of defect identification under DC conditions.

Parts of this chapter have been published in the author's journals with Elsevier's International Journal of Electrical Power and Energy Systems, ISSN 0142-0615, [1][2][3][4]

3.1. Introduction

This thesis relies on experimental data for its analysis. And therefore, well-designed experiments are crucial to the success of such a subject. In order to obtain good quality discharge data with low interference from any other phenomenon (external noise or additional discharge processes), it is important to build and develop PD defect models that only exhibit one kind of discharge process. Secondly, it is vital to understand the measuring principles, the influence of circuit components and connections and the limits of the system/ measuring arrangement. Several crucial decisions have to be made with regard to the means of data acquisition and processing in order to optimize the use of available resources.

This chapter outlines the entire preparatory process to the experimental phase of this project. It describes how each defect model was built and the conditions under which it was tested. It describes the PD measuring process that was employed and at last the post-processing of the obtained raw data and feature extraction for the final analysis phase. In the final section, possible methodologies that can be employed to study the discharge processes to identify different defect types are proposed.

3.2. Artificial PD defect models

Three common PD defect types, namely, corona (discharge from protrusion/sharp points), floating electrode and surface discharge are developed for this study. The following section describes the relevant details with respect to each model. All defect models are designed carefully to ensure there is no discharge from peripheral components that constitute the model such as flanges, connectors etc. The verification is commonly made by a preliminary AC-PD test by acquiring its corresponding PRPD pattern. A corona camera is employed additionally to ensure there is no discharge coming from any other sources (other than the intended defect). These details of the measurement are described in greater detail in section 3.3.

3.2.1. Corona defect

The corona defect is typically created as a point-plane arrangement as shown in Figure 3.1. The distance between the needle and the plane is maintained at 25 mm with a needle tip diameter in the range of ϕ 50-900 µm. The needles used are either stainless steel or brass. The arrangement is placed in open air at atmospheric pressure of 1 atm. Other test conditions such as temperature and humidity (16° - 30^oC, up to 60 % RH) were variable in order to ensure that these conditions do not influence the final results. The corona tests were also repeated on different days at different locations. This holds relevance from the point of view that, uncertainties such as external radiated noise, ground coupled interference and other variable parameters such as temperature, humidity, etc. could be excluded. This will improve the reliability of the results obtained. The test was repeated using different voltage sources and circuit connections. The duration of the voltage steps

and the overall duration of the test was varied, in an effort to improve the reliability of the outcomes and to showcase that the results are not specific towards a certain needle shape or test configuration/procedure. The position of the needle is changed between the high voltage terminal and the ground terminal to study all the different configurations of corona.

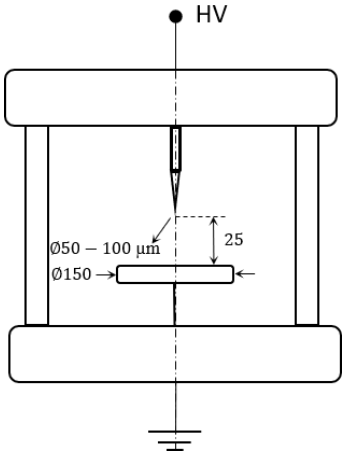

Figure 3.1: Schematic of the corona defect model in air; all dimensions are in *mm*.

3.2.2. Floating electrode defect

To reproduce a floating electrode defect, a set-up with a floating metallic electrode is constructed using a rod-plate arrangement (main electrodes) as shown in Figure 3.2. The electrode is held in a floating position with the help of an insulating mesh. The distance between the floating electrode and the rod electrode at HV is kept at 0.4 mm, while its distance to the ground electrode is maintained at 100 mm. The other dimensions are specified in Figure 3.2. The floating electrode has a small extension on the lower part to allow field enhancement which helps demonstrate the feature of corona from floating electrode. The defect arrangement is placed in open air at atmospheric pressure of 1 atm.

3.2.3. Surface discharge defect

The surface discharge model is implemented as a sandwich model with the dielectric sample (under test) held securely between two electrodes. The schematic of the defect arrangement is shown in Figure 3.3. Voltage is applied to the upper electrode while the lower electrode is at ground potential. In order to ensure there are no air gaps between the HV electrode (upper electrode) and the sample, a spring system is used on the upper suspender. The lower electrode is maintained to be of dimensions larger than the dielectric sample with the aim of creating a singular

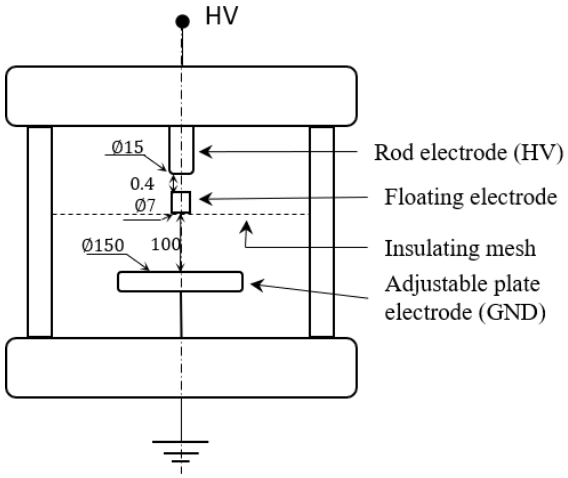

Figure 3.2: Schematic of the floating electrode defect model in air; all dimensions are in *mm*.

dielectric interface for the surface discharge activity. The dielectric samples are cleaned with alcohol and cellulose-free paper before testing. The dimensions relating to the thickness of the sample, mentioned to be 2 mm on Figure 3.3 is only an estimate. The actual thickness is variable for different dielectric samples and varies between 0.5-3 mm, the specifics of which are mentioned in the relevant chapters that describe the results of the surface PD tests.

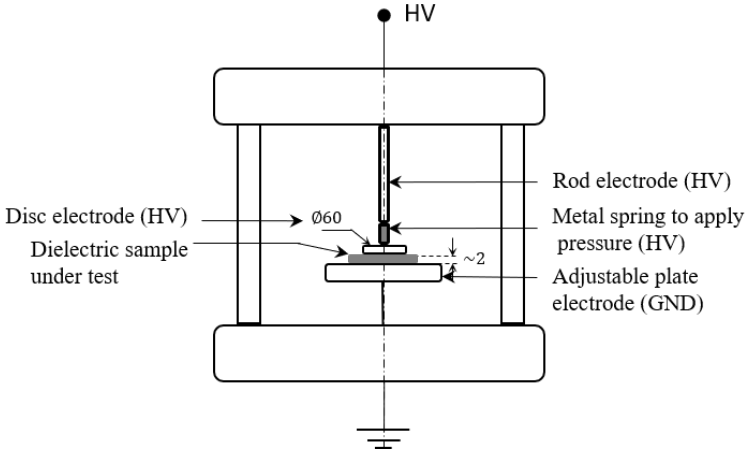

Figure 3.3: Schematic of the surface discharge defect model in air; all dimensions are in *mm*.

3.3. PD measurement

The AC measuring setup is built in accordance to the IEC 60270 requirements as shown in Figure 3.4. It comprises of an AC voltage source rated for 100 kV_{rms}, tested and certified PD-free, with a coupling capacitor (C_k), measuring impedance (Z_m) and a PD detector. The measuring impedance employed is in the form of a quadripole which in this case was the AKV 9310. It is incorporated in the current measuring loop to decouple the high frequency (HF) PD pulse. An additional HV filter is employed to improve the sensitivity and reliability of the measurements by blocking the interference coming from the HV source and preventing the PD pulse from flowing to the HV source. The requirements of each of these circuit components and the means to choose them are described in detail in [5]. The AC

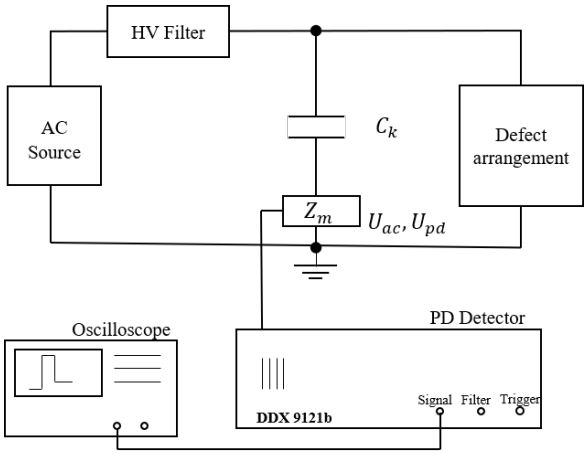

Figure 3.4: Schematic of the AC measuring setup built according to IEC 60270.

setup is modified by adding a half-wave rectifier stage rated for 140 kV_{dc} with a 20 nF smoothing capacitor after the AC source to generate a DC voltage. The direction of the diode determines the polarity of the rectified AC voltage. The setup includes a R||C voltage divider whose capacitor also serves as the coupling capacitor (280 MΩ || 1.2 nF) for PD measurement. As shown in the schematic of the measuring setup in Figure 3.5, in certain cases, a high frequency current transformer (HFCT) with a measuring bandwidth of 20 kHz to 100 MHz is connected under the defect arrangement for the possibility of supplementary measurement. In addition to the electrical measuring circuit, a corona camera from OFiL Luminar^{HD} systems that measures ultra violet (UV) radiation from the discharge site is used parallely to provide further insight into the discharge phenomenon. It measures highly sensitive UV discharges in the solar blind range of 250 to 280 nm. As a final check, the measuring setup/ construction is tested without the defect arrangement connected to ensure that it is PD free up to the maximum value of test voltage. The ripple on the output DC voltage has been measured to be below 0.4 % up to 30 kV_{dc} well within the maximum limit of 3 % defined by the IEC 60060-1 [6]. The results of the measurement are shown in Figure 3.6. Taking note of the ripple at the output

of the DC source is important to identify any influences on the DC-PD measurement from the 50 Hz AC cycle. Though its in-depth investigation is out of the scope of this thesis, awareness of such an influence might help refine the final conclusions. Before the start of each test (with a different defect arrangement), the setup is calibrated for charge measurements as prescribed by the IEC standards.

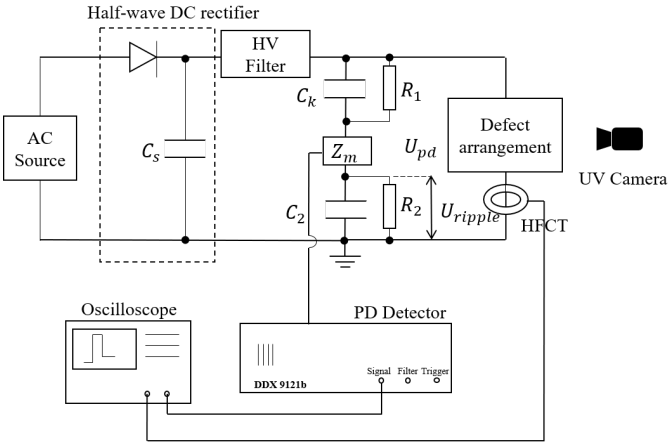

Figure 3.5: Schematic of the DC measuring setup built according to IEC 60270.

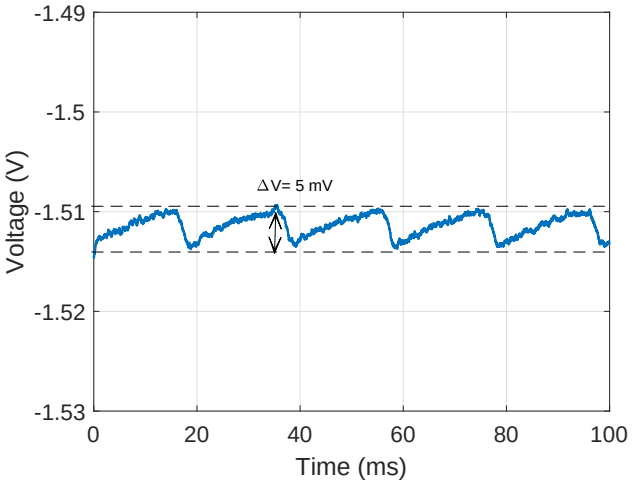

Figure 3.6: The measurement of the voltage ripple using an oscilloscope.

3.4. PD acquisition

The partial discharges are measured by two means. Firstly, through the PD detector (DDX 9121b) which serves as the front end of all PD measurements and logs the voltage, charge (pC), repetition rate and pulse polarity every second. And secondly, using an oscilloscope with a measuring bandwidth (BW) of 250 MHz that is fed through the 'signal' output channel on the PD detector (DDX 9121b). The oscilloscope is used to record a continuous data stream at the rate of 10 or 20 MS/s. The use of an oscilloscope to log the PD raw data, instead of using the measured output of the detector eliminates the errors at the detector stage that might arise due to limited BW and dynamic range that could possibly lead to wrong polarity recognition, double pulse recognition, pulse disappearance and so on. In addition, it is possible to eliminate interference and noise pulses from the acquired pulse stream in the case of raw data acquisition through data streaming by employing suitable post-processing algorithms for pulse recognition. The streamed raw data is independent of the IEC filter settings defined in the detector but is influenced by the detector's amplifier stage. In order to tackle this, the amplification level is set to a fixed value. The sampling rates for data acquisition were defined considering the influence from circuit parameters and other influences on the measured signal. In this case, The AKV 9310 (quadripole) together with the electrical measurement loop created by the 1.2 nF coupling unit has a measuring bandwidth of 8 MHz. The PD detector used has optional input analog filter stages (Low-Pass 2 MHz) to precondition the incoming pulse stream and discriminate them from external HF noise. These BW limitations create a complex interaction thereby influencing the resultant output pulse recorded by the oscilloscope. The lowered bandwidth influences the shape of the discharge pulse by making the pulse longer in time or slower in frequency. However, since the PD pulses that occur within an industrial HV component are almost always limited in BW, and the analysis made in this contribution does not aim at studying the discharges based on pulse shape parameters, this feature has not been optimized. The second major influence of the low BW is on the maximum PD pulse rate that can be recorded reliably. Ideally, with the 2 MHz Low-Pass (LP) analog filter a pulse rate given by the Nyquist criteria ($f_{max}=f_s/2$) approaches 1 MHz. Any limitations arising from this feature will be dealt with accordingly in the course of the study.

During the test, the voltage is ramped systematically and the raw data is logged in real-time at each stage. Depending on the presence/absence of the PD defect and its behavioural changes with increasing voltage, smaller or larger voltage steps are made. The final goal is to observe the defect's PD behavior as closely as possible in order to understand and derive useful feature information. The length of the acquisition depends on the repetition rate (longer acquisition for low repetition rates).

3.5. PD Evaluation

This section presents the steps after the acquisition of the PD signal. The post-processing of the data to extract useful information on the discharge process and the

possible methods of analysis of the discharge data using various tools are proposed.

3.5.1. Data processing

The acquired PD pulse stream is processed in MATLAB through a comprehensive set of algorithms that recognize the individual pulses from the data stream and assign them an equivalent charge value based on a calibration factor (quasi-integration) that is pre-programmed. The self-explanatory schematic shown in Figure 3.7 describes the process of quasi-integration, where the factor k_{cal} is referred to as the calibration factor. The pulse recognition algorithm is developed based on the equivalent energy threshold of the pulse as presented in [7] . Automated and flexible pulse width identification is used to recognize and count individual pulses. Desired exception handling is employed to ensure reliability of the output. An additional routine is used for polarity recognition, that is developed based on the steepness of slope [8]. The workflow diagram of the various algorithms that effect on the input data stream is shown in Figure 3.8. The post-processing of the pulse stream provides the resultant values of discharge along with polarity and the time stamp of the discharge events.

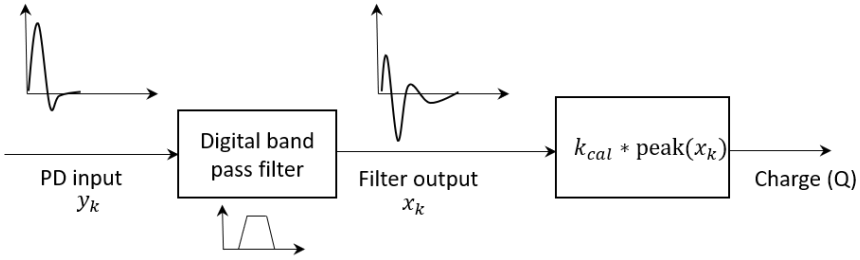

Figure 3.7: A schematic representation of the quasi-integration process for charge estimation.

3.5.2. Derived quantities

Based on the two basic quantities of discharge magnitude ($\pm Q_i$) and time stamp (t_i) several other discharge parameters can be derived. The derived quantities related to the magnitude of discharge (Q_i) are, charge of successive pulse (Q_{i+1}) and difference in charge of two successive pulses/ three pulses (ΔQ_i and ΔQ_{i+1}). The derived quantities related to the time of occurrence of the discharge (t_i) are time of occurrence of successive pulse (t_{i+1}) and time between two successive pulses/ three pulses (Δt_i and Δt_{i+1}). The graphical representation of all the derived quantities from the measured PD input signal is shown in Figure 3.9. Additionally, it is possible to deduce the repetition rate/density of pulses (N) either within a specific time frame (N vs. t) or within a specific discharge range (N vs. Q).

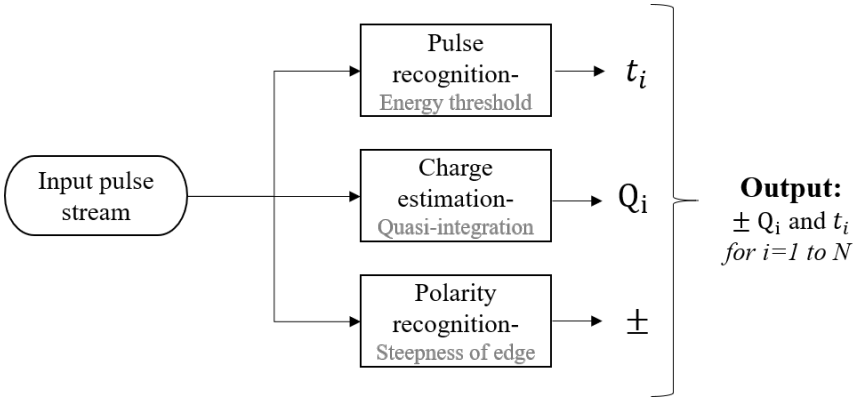

Figure 3.8: A workflow diagram of the various algorithms that effect on the input data stream.

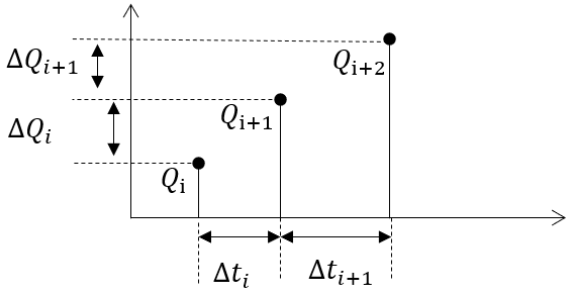

Figure 3.9: Graphical representation of the derived quantities from the measured PD raw data, where i= 1 to N-2.

3.5.3. Visual tools

The most straightforward method of defect identification is through the visual recognition of unique patterns on graphs/plots/diagrams. A good example of which are the Phase Resolved PD plots (PRPD) that are useful in the identification of different defect types under AC voltages. However, the PRPD diagrams cannot be directly implemented for DC defect identification due to the lack of voltage phase angle under DC. Hence, alternative diagrams are proposed based on the various derived quantities defined in the previous section. One of the most common ways of analysing PD pulse trends in DC is through Pulse Sequence Analysis (PSA) which was first presented in 1995 by Hoof and Patsch [9].

PSA is referred to a set of 3 plots namely;

(i) Plot of difference in time of occurrence and discharge magnitude of successive pulses, Δt vs. ΔQ

(ii) Plot of difference in discharge magnitude of successive pulses in a sequence

of three pulses, ΔQ_{i+1} vs. ΔQ_i

(iii) Plot of difference in time of occurrence of successive pulses in a sequence of three pulses, Δt_{i+1} vs. Δt_i

In addition to these, other combinations of the derived quantities could be used for the analysis. Some of the possible diagrams that could be used for visual defect identification are as listed below.

(i) Plot of discharge magnitude of successive pulses, Q_i vs. Q_{i+1}.

(ii) Plot of the discharge magnitude and time between the discharge event and the previous discharge event, Q_{i+1} vs. Δt_{i+1}.

(iii) Histogram of number of pulses/pulse rate over discharge magnitude, N vs. Q.

(iv) Plot of discharge magnitude over time to study defect progression with time, Q vs. t.

(v) Plot of discharge magnitude with increasing voltage, Q vs. V.

In order to enhance the contrast of the visual diagrams, most of them may be plotted as density plots with a colour scale. The axis of these plots is divided into a fixed number of bins and depending on the number of pulses in each bin, a colour is assigned. Therefore, in addition to the two dimensional axis that provides information on the shape/contour of the plot, the colour scale provides additional information on the distribution of the pulses over the plot's contour. Except for the diagrams of: N vs. Q, Q vs. t and Q vs. V. All other diagrams may be plotted as density plots.

3.5.4. Statistical tools

A second method of analysis that is possible for such a study is by studying the statistical distribution of the various discharge parameters in order to identify underlying trends and patterns. One such possibility is the generation of probability plots to study the discharge process/phenomenon of different defects. For instance, the probability plot of difference in charge magnitude (ΔQ) of the discharge events provides insight into the homogeneity of the discharge level or in other words the range of dispersion in the quantity of ΔQ. Similarly, the probability plot of time between discharge events (Δt) provides insight into the regularity of the discharge process. Likewise, the analysis needs to focus on finding the trends that the distribution of these quantities from each defect follows.

3.5.5. Discriminatory tools

The last proposed tool for the analysis of PD under DC is through reviewing the data of defect progression with time and voltage (plots of Q vs. t and Q vs. V) together with the possible features identified on the other diagrams. This would

result in the formulation of a discriminatory procedure in contrary to the stand-alone diagrams that the other two tools have proposed above. The procedure could be formulated in the form of a decision tree with branches leading to the discrimination of the various PD defects. Nevertheless, considering the possibility that the process of defect identification under DC may not be as simple as that under AC, the development of sound knowledge of the discharge progression of various defects can serve as a valuable tool in the process.

references

[1] **S. Abdul Madhar**, P. Mraz, A. Rodrigo Mor, and R. Ross. "Study of Corona Configurations under DC Conditions and Recommendations for an Identification Test Plan". In: *International Journal of Electrical Power and Energy Systems* 118 (June 2020), p. 105820. issn: 01420615. doi: 10.1016/j.ijepes.2020.105820.

[2] **S. Abdul Madhar**, P. Mraz, A. Rodrigo Mor, and R. Ross. "Physical interpretation of the floating electrode defect patterns under AC and DC stress conditions". In: *International Journal of Electrical Power and Energy Systems* 118 (June 2020), p. 105733. issn: 01420615. doi: 10.1016/j.ijepes.2019.105733.

[3] **S. Abdul Madhar**, A. Rodrigo Mor, P. Mraz, and R. Ross. "Study of DC partial discharge on dielectric surfaces: mechanism, patterns and similarities to AC". In: *International Journal of Electrical Power and Energy Systems* 126 (Mar. 2021), p. 106600. issn: 0142-0615. doi: 10.1016/j.ijepes.2020.106600.

[4] **S. Abdul Madhar**, P. Mraz, A. Rodrigo Mor, and R. Ross. "Empirical analysis of partial discharge data and innovative visualization tools for defect identification under DC stress". In: *International Journal of Electrical Power & Energy Systems* 123 (Dec. 2020), p. 106270. issn: 01420615. doi: 10.1016/j.ijepes.2020.106270.

[5] P. Mraz, **S. Abdul Madhar**, P. Treyer, and U. Hammer. "Guidelines for PD measurement according to IEC 60270". In: *The International Symposium on High Voltage Engineering*. Budapest, 2019.

[6] Standard IEC 60060-1. *High-voltage test techniques– Part 1: General definitions and test requirements*. International Electrotechnical Commission (IEC), 2010.

[7] P. Wagenaars, P. A. A. F. Wouters, P. C. J. M. van der Wielen, and E. F. Steennis. "Algorithms for Arrival Time Estimation of Partial Discharge Pulses in Cable Systems". In: *IEEE International Symposium on Electrical Insulation*. 2008, pp. 694–697.

[8] A. R. Mor, L. C. Castro Heredia, and F. A. Muñoz. "Estimation of charge, energy and polarity of noisy partial discharge pulses". In: *IEEE Transactions on Dielectrics and Electrical Insulation* 24.4 (2017), pp. 2511–2521. issn: 10709878. doi: 10.1109/TDEI.2017.006381.

[9] M. Hoof and R. Patsch. "Pulse-sequence analysis: a new method for investigating the physics of PD-induced ageing". In: *IEE Proceedings-Science, Measurement and Technology* 142.1 (1995), pp. 95–101.

4

Study of Corona Configurations under DC

Corona is one of the most common forms of partial discharge (PD) occurring in high voltage (HV) energy systems. The corona mechanism in air is not exclusive to the field of energy applications but has also been widely studied by physicists to theorize mechanisms of charge transfer during the different phases of gas discharge. The phases of the discharge and its corresponding behaviour with alternating voltage (AC) are well established and represented through various discharge trends, patterns and stages. This not only makes the identification of the PD defect possible but also helps evaluate the risk. This chapter investigates corona configurations under DC stress in an attempt to create a similar outline of the defect as exists under AC. The defect is studied in terms of the pulse sequence information. The measurement system requirements are kept within a realistic realm to preserve applicability to industrial measurements. Finally, it makes selective recommendations for the effective identification of the discharge condition under DC stress.

Parts of this chapter have been published in Elsevier's International Journal of Electrical Power and Energy Systems, **118**, (2020), 105820, ISSN 0142-0615, https://doi.org/10.1016/j.ijepes.2020.105820 [1]

4.1. Introduction

Corona is commonly referred to the discharges coming from sharp points at high electric field in air or other gaseous medium. It is caused by the ionization of the gas due to the excessive electric field stress and this mechanism is described by the nature of the dielectric and the availability of charge carriers. Several pointers exist for corona measurement under AC voltage, such as, the inception of corona on the negative half-cycle before the positive half-cycle, the concentration of the Trichel pulses over the peak of the sine wave, indication of increased risk after the inception of positive corona (positive streamer) among several others [2]. However, stable and comprehensive indicators of this nature are non-existent when it comes to corona measurement under DC conditions. A needle-plate corona arrangement is studied by this research in four different configurations based on the position of the needle and polarity of the DC voltage. The several minute differences in each of the four configurations permit the identification of the defect in its various forms. The final section makes recommendations towards an 'Identification Test Plan' to detect and recognize the configuration of corona coming from the device under test.

The principal difference between the measurement of AC and DC partial discharges (PD) remains in their evaluation, while the state-of-the-art measuring systems used in both cases remain alike. In case of AC-PD measurements, for each defect there is a unique variation of discharge magnitude over the AC voltage cycle referred to as the phase resolved PD (PRPD) pattern. And considering that discharge inception is defined by one pulse/cycle, the evaluation of the charge value (Q_{iec}) is less dependent of the repetition rate. A miscalculation of the pulse count by the PD evaluation system does not affect the outcomes of the test itself. However, in case of PD measurements under DC voltages, it becomes important to accurately count the number of discharges in a given time period [3]. This means that any outliners/interference, or miscalculation of the pulse count due to duplicate recognition or other means would negatively impact the outcomes of the test as described in [3]. At this moment, it is necessary to highlight an interesting view-point for the DC-PD evaluation, which is to distinguish partial discharges based on the source of the discharge. If one considers the discharges coming from a real geometrical/physical defect, the repetition rate of such PD should be proportional to the time constant of the defect arrangement. In reality, this may be tedious to deduce due to the complex configuration of the defect within the dielectric of the electrical component. However, strictly for laboratory measurements and specially keeping in mind the measurement of corona in air which this chapter discusses, pulses that may occur after the waiting period (time constant) could either be interference pulses from outside or due to effects of space charge, atmospheric influence, or random cosmic radiation. For example, consider the classical abc-circuit [4] as shown in Figure 4.1. Based on the DC model for PD the expression for the voltage over the defect is given by;

$$v_c = \frac{R_c}{R_b + R_c}.(1 - e^{-t/\tau}).V \tag{4.1}$$

Where τ is the time constant of the defect, R_b and R_c are the leakage resistances

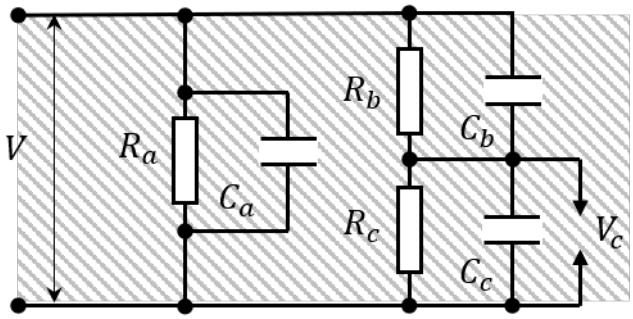

Figure 4.1: Classical abc-circuit with leakage resistances to accommodate DC PD [1].

across the test object and V is the applied DC voltage, same as Eq. 2.3. This model considers that the field across the defect, in this case a void, is purely due to the electrostatic field of the applied DC voltage.

However, in several cases the electric field due to the accumulated space charges may add to the local electric field stress establishing locally the temporary conditions for discharge inception. These discharges could be referred to as 'pseudo-discharges' since they neither have a stable repetition rate nor a pre-determined range (of PD magnitude). Figure 4.2a shows a void inside a bounded dielectric with homo-charge formation at the electrode junction. Figure 4.2b shows the HV electrode of a DC module stationed in air. Due to the electronegative nature of oxygen atoms the electrons attach to them, and in case of higher humidity they attach to water molecules [5], creating a momentary hetero-charge layer as shown. This enhances the electric field between the space charge region and the HV electrode causing erratic corona pulses due to the discharge from the electrode towards the region of the space charge. In order to incorporate this phenomenon, the value of V in Eq. 4.1 needs to be altered as follows;

$$V = \int_{l=0}^{x} (E_{dc} + E_{sp}(t,r)).dl \tag{4.2}$$

$$E_{sp}(r) = \frac{\rho(s)(r-s)}{|r-s|^3} d^3s \tag{4.3}$$

where E_{dc} is the electric field due to the applied DC voltage, E_{sp} is the electric field due to the space charge formation, ρ(s) is the charge density with respect to space, s is the unit vector perpendicular to the surface enclosing the charge and r is the point in space where the electric field is calculated. Thus, the volumetric integral of the charge density would equal the divergence of electric field, thereby following Gauss' law/Stroke's theorem. Therefore, based on Eq. 4.2, at applied voltage lower than inception, there is still a possibility of PD due to local field enhancement from space charge clouds. However, depending on the charge displacement in the dielectric medium (decay of the space charge) this condition may vary.

Theoretically, once the time constant of the charging circuit is surpassed without the inception of a partial discharge pulse, the voltage can be increased to the next step assuming the availability of an initiating electron. And practically, this is done by measuring the DC voltage immediately across the test object and determining if the voltage settles to the maximum DC value. Especially in the case of corona defect in air, as this research investigates, the waiting period should be minimum. Section 3.2.1 describes the defect arrangement and the test conditions. The study of the DC corona discharge was performed through recursive testing of the defect arrangement as mentioned in section 3.2.1. In the following chapters the PD measuring setup, procedure and post-processing tools are described followed by test results of various corona configurations. The observations presented in the next section belong to a certain specific test case, the values of voltages (inception/ extinction) and discharge magnitude correspond to this specific case.

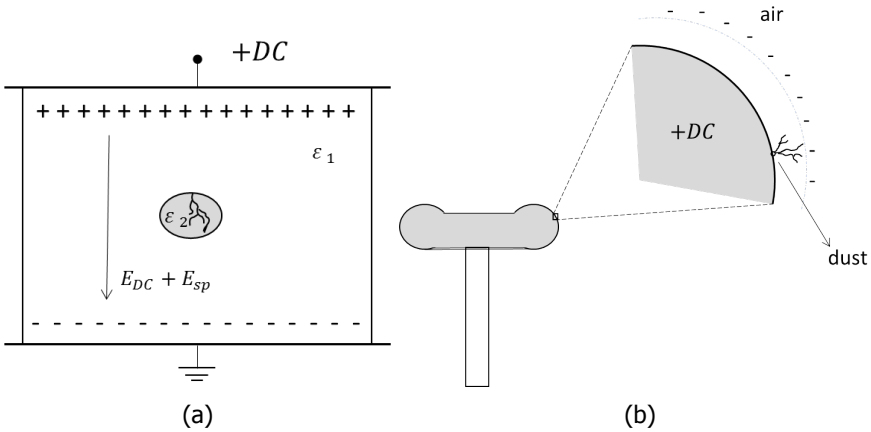

Figure 4.2: Pseudo-discharges (a) due to homo-charge formation and (b) hetero-charge formation [1].

4.2. Corona configurations

4.2.1. Configuration I: Negative DC with needle at HV

The first corona configuration investigated is with the needle at negative DC voltage. The detector's filter settings are fixed to the maximum BW of 1 MHz with a centre frequency at 600 kHz. The measurement noise floor is recorded as 0.03 pC. The progression of the defect configuration with increasing voltage steps is shown in Figure 4.3a. In this particular test case (described in the chapter 4) the corona incepts at -5.75 kV_{dc} (U_i) with a charge magnitude of 120 pC. The discharge stream remains stable in terms of amplitude at the given voltage level. The discharge rate is at 3370 pulses/s. With increasing voltage steps, the discharge rate increases exponentially while the discharge magnitude drops to ~50 pC. These trends are

presented graphically in Figure 4.3b. Given the 1 MHz measuring BW of the detector the pulses virtually disappear (virtual pulse-free zone) [2] at 15 kV_{dc} when the pulse repetition rate exceeds 1 pulse/µs. However, at this stage, it still remains possible to measure the pulses through direct pulse streaming using the oscilloscope. Close to 20 kV_{dc}, the pulses completely disappear from the electrical domain as shown in Figure 4.3b. The last value of repetition rates recorded are 800k-1M pulses/s.

The corona camera on the other hand can detect the corona around the needle in the pulse-free zone. The image recorded by the corona camera at 20.5 kV_{dc} is shown in Figure 4.4. This pulse-free zone extends from 20.5 kV_{dc} until gap breakdown at 45 kV_{dc}.

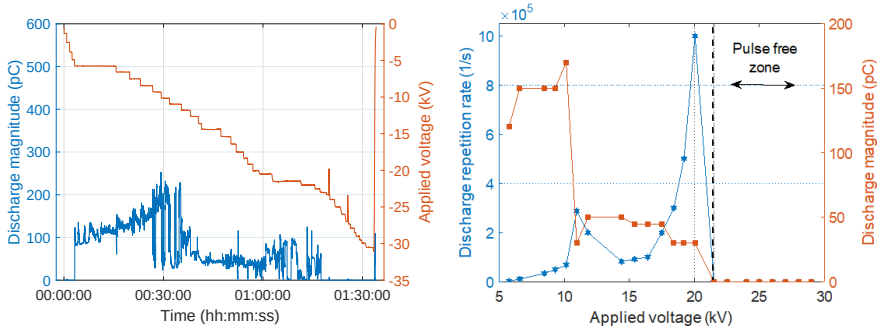

(a) (b)

Figure 4.3: (a) The defect progression with increasing voltage (kV_{dc}) as recorded by the PD detector and (b) discharge repetition rate and magnitude (in pC) as a function of voltage for the needle placed at negative DC voltage [1].

Discharge physics

The physics of the discharge under this configuration can be explained based on the physics of the 'Trichel pulse' [6]. Figure 4.5 pictorially depicts the discharge mechanism around the needle tip. The electronegative needle ionizes the air around it when the electric field stress around the tip exceeds the ionization field of air (~3 kV/mm). Trichel proposed that the formation of negative charges around the needle tip and its subsequent removal by the formation of a momentary positive space charge resulted in the repetitive discharges. There are primarily two competing mechanisms of discharge in this case; The electron attachment to the electronegative atoms such as oxygen and the electron detachment through excitation and photo ionization [7].

$$N_2 + e^- \rightarrow N_2^- + 2e^-; \Delta H = 104 kJ/mol \tag{4.4}$$

$$O_2 + e^- \rightarrow O_2^- + 2e^-; \Delta H = -125 kJ/mol \tag{4.5}$$

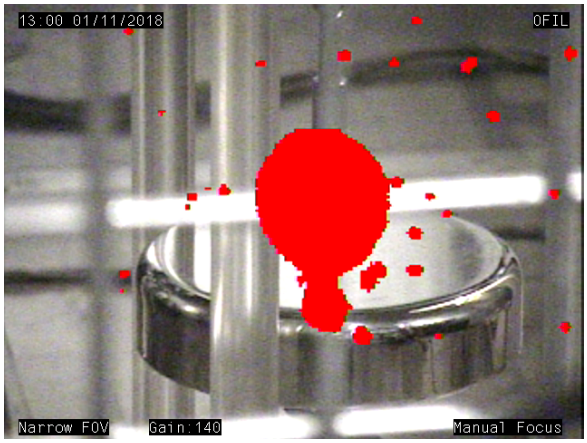

Figure 4.4: UV measurement by the corona camera with corona around the needle tip recorded at -20.5 kV_{dc} [1].

$$O_2 + N_2 + e^- \rightarrow O_2^- + N_2 \tag{4.6}$$

$$O_2^- + O_2 \rightarrow 2O_2 + e^- \tag{4.7}$$

$$O_2 + h\gamma \rightarrow 2O; \Delta H = 498kJ/mol \tag{4.8}$$

$$O_2 + O \rightarrow O_3 \tag{4.9}$$

Though nitrogen (N_2) is the most abundant (78%) gas in atmospheric air, as shown from Eq.4.4 , the energy for its ionization is higher than for oxygen (O_2). Hence, Eq.4.5 is more dominant than Eq.4.4 at lower fields. The dissociated electron soon attaches to a neutral oxygen molecule as shown by the 3-body reaction in Eq.4.6 creating a negative space charge at a distance away from the needle tip (into the gap). With increasing electric field stress (voltage) the photo-ionization of oxygen given by Eq.4.7 and enhanced electron detachment additionally by Eq.4.4 take over [8]. Additionally, the photo-ionization process strips the oxygen molecule to atomic oxygen, paving the way for the production of ozone, Eq.4.8 and 4.9. In [9] Giao et all. theorize that the increased rate of removal of negative charges and the reduced rate of formation of negative ions due to detachment effect in high fields is responsible for the pulse-less region of corona sometimes referred to as 'noisy corona' which is characterized by a DC offset current. In addition, the reduced gas density at the needle vicinity due to elevated temperatures contribute to this phenomenon [5].

The breakdown voltage of this configuration on the other hand is slightly higher since the electrons are dispersed to lower field region and the pre-breakdown requires avalanches to be formed. These avalanches require an electron feedback

mechanism that is created by the accelerated positive ions striking the cathode, by the Townsend's mechanism [6].

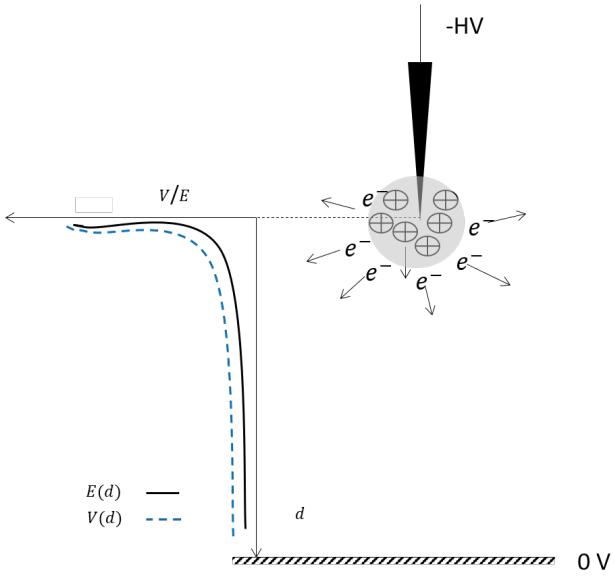

Figure 4.5: An illustration of the discharge mechanism around the needle tip at -DC voltage and the corresponding voltage and electric field graph over the gap distance, *d* [1].

Discharge patterns

The discharge raw data acquired was utilised to generate several plots based on the quantities mentioned in chapter 3, including the Pulse Sequence Analysis (PSA) plots that are revered by several researchers [10]. However, the most stable relationship (against increasing voltage level) was obtained for the plot of Charge (Q_{i+1}) vs Time to discharge (Δt_{i+1}) as shown in Figure 4.6. This plot represents a unique characteristic of negative corona where the magnitude of discharge is determined by the time elapsed since the previous discharge.

4.2.2. Configuration II: Positive DC with needle at HV

The needle on positive DC voltage incepts at 6.3 kV_{dc} with a discharge magnitude of 0.5-2 pC. The discharge is highly challenging to detect due to the low signal to noise ratio (SNR). Sufficient amplification and filtering stages are required for this measurement. Figure 4.7 shows the recorded pulse stream with the high repetition rate which could be mistaken for background noise. This stage of the corona is still possible to be recorded using the corona camera with the discharge concentrated around the needle tip. Figure 4.8 shows the test data log of the charge and voltage

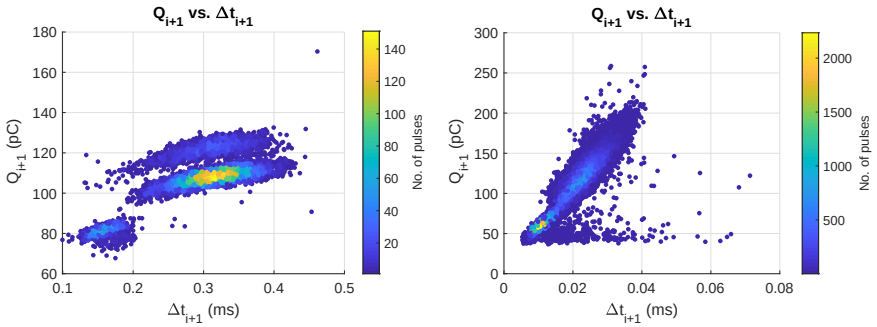

Figure 4.6: Discharge pattern of configuration I, Charge (Q_{i+1}) vs Time to discharge (Δt_{i+1}) (a) at inception voltage (U_i) of 5.75 kV_{dc} and (b) at 1.6U_i [1].

over time. It can be noted that at a specific voltage window, 6.4-6.6 kV_{dc} in this case, a stable pulse stream with a discharge magnitude of 400-450 pC incepts. This phenomenon is referred to as 'self-sustaining corona'. It occasionally incepts when the voltage is ramped downwards to this value than by rising the voltage upwards. The 0.5-2 pC (intermittent corona) pulses persist with increasing voltage, getting more repetitive in nature. The UV image captured by the corona-camera increases in intensity and girth. At 18.6 kV_{dc}, larger discharges in excess of a nC begin to incept repetitively indicating a pre-breakdown state.

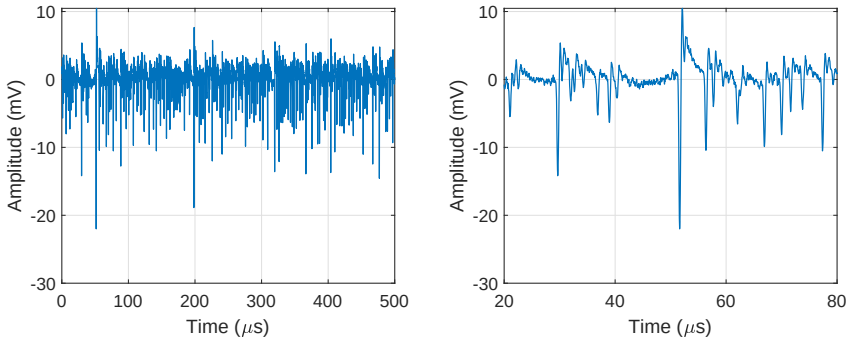

Figure 4.7: Discharge pulse stream observed at 6.3 kV_{dc} (a) 0.5 ms acquisition (b) zoomed in to show individual pulses [1].

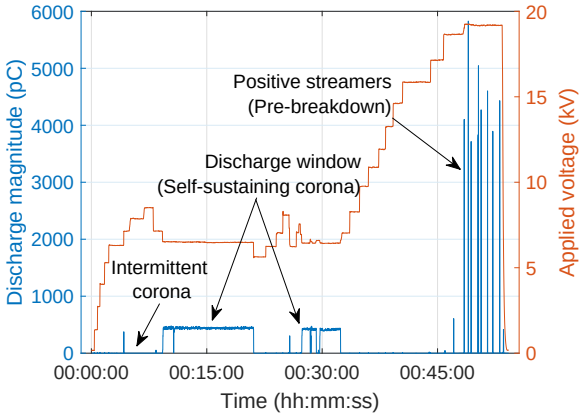

Figure 4.8: The progression of the defect (needle at +DC) with increasing voltage (kV_{dc}) as recorded by the PD detector [1].

Discharge physics

Positive corona is described in [11] to occur in three different forms: burst corona, streamer corona and glow corona. The first stage of corona observed with intermittent pulses has also been reported by Trichel [12]. He describes this phase of corona as being made up with 'imperfectly resolved current impulses of extremely high frequency'. However, he was never able to precisely measure them due to their low energy. This stage of 'intermittent corona' possibly arises from the ionization of the neutral molecules in air, either by impact ionization or photo-ionization around the needle tip giving rise to a small discharge current as shown by Figure 4.9a. The electric field is maximum at the maxima of the voltage over the needle tip. The self-sustaining corona that incepts at a specific voltage range is due to a large number of individual current-pulses distributed over the surface of the point in regions of adequate field strength [12]. As depicted in Figure 4.9b the positive space charge displaced at a distance 'x' from the needle tip with sufficient field strength sustains the Townsend's mechanism of discharge through electron avalanche. Once enough electrons are produced by ionization such that the current is taken care of by the electron avalanche alone, the pulses cease. At the last stage of the discharge large streamer pulses are observed. These are once again confirmed by Trichel [12]. At higher field strengths the discharge penetrates into the gap and as Trichel describes the appearance of these streamers is relatively sudden. They are believed to be incited by energetic α-rays or properly timed ions. Therefore, the streamers appear to be bursts propagating under 'favourable field conditions'.

Discharge patterns

The intermittent corona stage at inception is challenging to detect correctly and resolve into individual pulses as their occurrence is quite random. They do not

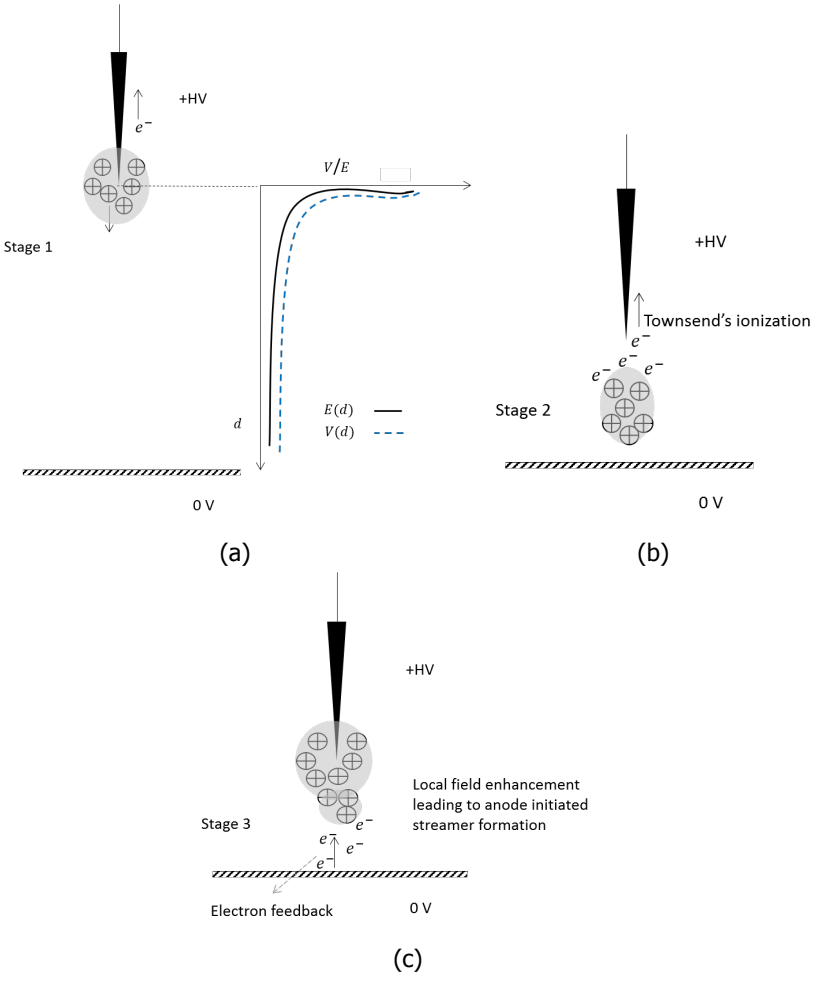

Figure 4.9: The mechanism of discharge at the needle tip at +DC voltage (a) intermittent corona at inception and the corresponding voltage and electric field distribution across the gap distance, *d* (c) self-sustaining corona and (d) streamer corona [1].

create any consistent pattern. The self-sustaining corona pulses with a charge magnitude of 400 pC occur quite repetitively with a stable rate. A 2.5 s pulse sequence is shown in Figure 4.10. Figure 4.11 with its PSA plot,ΔQ_i and ΔQ_{i+1} shows a vague star pattern, however, the plot of Charge (ΔQ_{i+1}) vs Time to discharge (ΔQ_{i+1}) shows no relationship indicating that this is unlike the negative corona in configuration I.

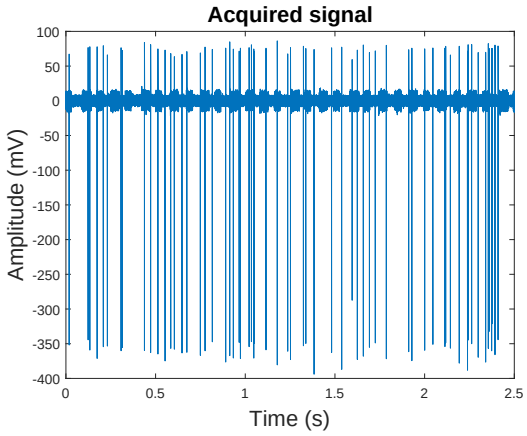

Figure 4.10: The discharge pulse sequence at +6.6 kV_{dc} [1].

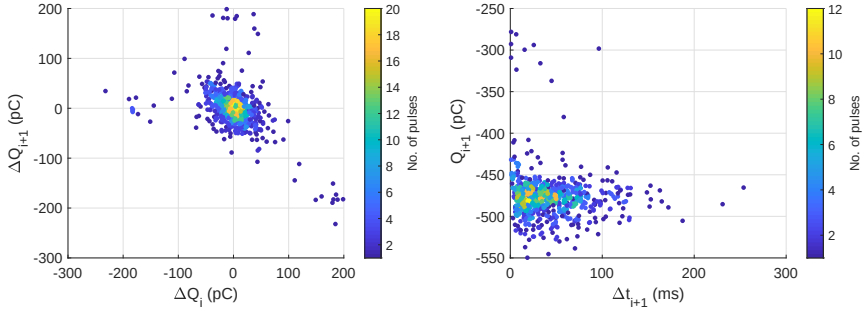

(a) (b)

Figure 4.11: Discharge patterns of configuration II (a) ΔQ_i and ΔQ_{i+1} (PSA) and (b) Charge (Q_{i+1}) vs Time to discharge (Δt_{i+1}) at 6.6 kV_{dc} [1].

4.2.3. Configuration III: Negative DC with needle at ground

Configurations III and IV of the corona arrangements presented in this chapter, with the needle placed at ground potential are often not studied, presuming that configurations I and II sufficiently represent III and IV. The mechanism of discharge may be similar; however, several differences exist among them. These are explained in the following sections.

The third corona configuration with the needle placed at ground potential and applying -DC to the plate electrode incepts similar to configuration II (needle at +DC) with a 0.5-2 pC stream but at a slightly higher voltage of 7.75 kV_{dc}. The small discharge with intermittent corona persists, while at 11.6 kV_{dc} the first large pulse with a recorded amplitude of 60 pC occurs. As can be seen from Figure 4.12 with increasing voltage the magnitude of discharge increases almost linearly. At

19.2 kV_{dc} repeated discharges in the order of 5 nC occur indicating a unstable pre-breakdown state. The larger discharges are accompanied with a hissing or whistling sound.

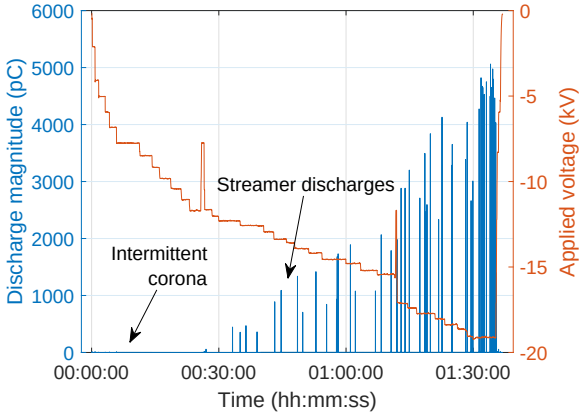

Figure 4.12: The progression of the defect (needle at ground; -DC) with increasing voltage (kV_{dc}) as recorded by the PD detector [1].

Discharge physics

The physics of the discharge in this configuration is similar to the one described in Section 4.2.2. The needle placed at ground potential is now the anode. The discharge incepts with the intermittent corona creating a small positive charge cloud around the needle. However, the second stage of discharge with the self-sustaining corona is absent in this configuration. This is because of the presence of a cathode in the vicinity of the needle that can provide free electrons via ion-impact on the cathode surface (at HV). Figure 4.13 shows the schematic of the discharge mechanism alongside the distribution of voltage and electric field across the gap. These free electrons constantly neutralize the positive space charge. However, at increasing voltages, the streamer corona sets-in similar to the pre-breakdown stage described in Section 4.2.2. This configuration of corona remains the most dangerous as the streamers incepts at low values of voltage with a large discharge magnitude and soon escalates to the unstable-breakdown state if left undetected. Therefore, attention needs to be paid to the ground electrode of DC electrical components, since any damage leading to sharp edges can have severe consequences.

4.2.4. Configuration IV: Positive DC with needle at ground

The final configuration of corona with the needle placed at GND potential and +DC applied to the plate behaves similar to configuration I with needle at -DC. Figure 4.14 shows the progression of the corona stages with increasing voltage. The defect

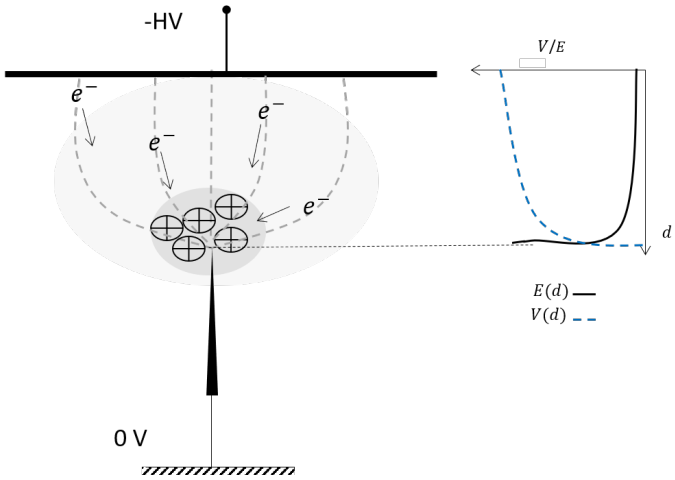

Figure 4.13: The mechanism of discharge in configuration III and the corresponding voltage and electric field graph across the gap distance, d [1].

incepts at 6.22 kV_{dc} with a discharge magnitude of 12 pC. The discharge repetition rate is 2620/s. With increasing voltage, the discharge magnitude rises from 12 pC at 6.22 kV_{dc} to 110 pC at 13.5 kV_{dc} with a discharge repetition rate of 170,000/s. With further increase in voltage to 14.55 kV_{dc} the repetition rate increases to up to 350,000/s while the discharge magnitude drops to 12-15 pC.

For voltages in excess of 16 kV_{dc}, the pulses disappear from the electrical measurements, denoting a real pulse-free zone as observed in Section 4.1. But until 23

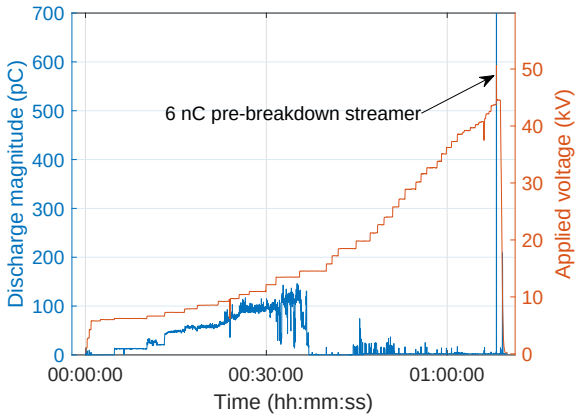

Figure 4.14: The progression of the defect (needle at ground; +DC) with increasing voltage (kV_{dc}) as recorded by the PD detector [1].

kV_{dc}, the pulse stream with reduced amplitude (12-15 pC) appears and disappears in flashes, denoting a transition phase between Trichel and glow discharge. The pulse-free zone with no discharges persists until a pre-breakdown pulse of 6 nC occurs at 43.6 kV_{dc}. In the pulse-free region (of configuration I and IV) of discharge a small violet glow slightly detached from the needle is observed. The corona camera when used in the pulse-free zone with reduced amplifier gain records a discharge ring around the violet glow as shown in Figure 4.15.

Discharge physics

The discharge physics of this configuration is similar to Section 4.2.1. The differences in inception voltage and discharge magnitude can be explained based on the differences in the electric field strength and voltage distribution of the gap at the same voltage levels. As shown in Figure 4.16 the electric voltage at the immediate vicinity of the needle tip is slightly reduced than when the needle is directly at HV. This subsequently reduces the resulting electric field stress and hence the reduced magnitude of discharge. Nevertheless, the defect progresses in the same fashion as the needle at -DC. The violet glow shown in Figure 4.15 which appears to be detached from the needle is analogous to the Crookes dark space [6]. The corona ring has also been reported in the past [13] and is due to the field distortion believed to have been caused by the negative space charges in the gap.



Figure 4.15: The UV measurement by the corona camera showing the corona ring around the needle tip recorded at 18.5 kV_{dc} [1].

Discharge patterns

The discharge patterns obtained in this configuration of corona are well-formed as shown in Figure 4.17. However, while comparing the robustness of the obtained diagrams, the discharge pattern of charge (ΔQ_{i+1}) vs time to discharge (Δt_{i+1}) shown in Figure 4.17a is highly stable and serves as a fingerprint for the identification of

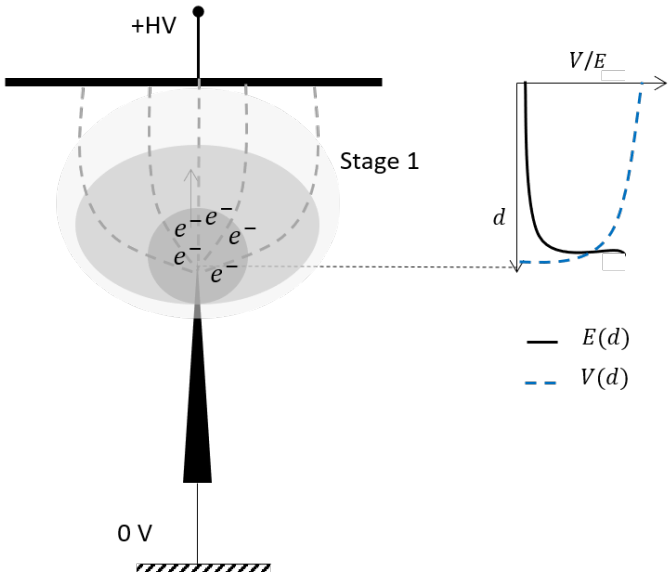

Figure 4.16: The mechanism of discharge around the needle tip at GND when +DC applied to the plate and the corresponding voltage and electric field graph across the gap distance *d* [1].

the corona/defect. The other patterns are highly sensitive to outliers and disturbances. For instance, in certain corona configurations a second luminous discharge appears at increased fields/voltages [6]. The discharge alternates between the two spots. Occasionally at still higher voltages, a third spot may appear. This is an inherent characteristic of the corona and depends on the dimensions of the needle tip. The PSA plots in the case of double corona source are completely distorted from the expected form shown in Figure 4.17. This is demonstrated through Figure 4.18. However, the plot of charge (ΔQ_{i+1}) vs time to discharge (Δt_{i+1}) preserves its unique relationship and even reveals information on the number of discharge sources through the number of clusters.

4.3. Discrimination of corona configuration under DC

Corona is by far the only defect that behaves the closest to its AC behaviour. The extremely high repetition rates found with corona are not found in any other defect. It also has a unique charge versus voltage (Q vs. V) characteristic for every configuration. Based on these behavioural characteristics of the corona defect it is possible to detect and localise the configuration of corona (either coming from the HV or GND terminal). It is possible that at the nominal test voltage, U_{nom}, the defect remains in the pulse-free zone or in the region of intermittent corona

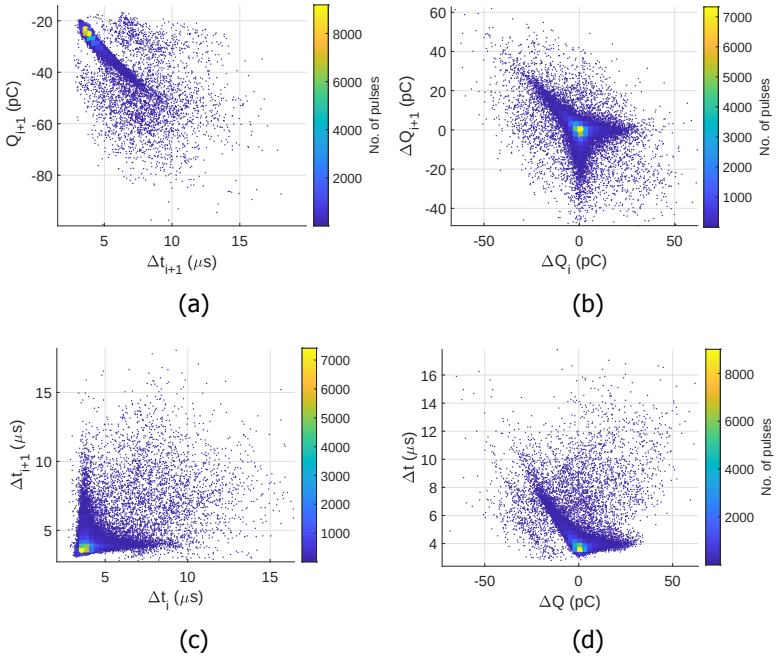

Figure 4.17: Discharge patterns of configuration IV (a) Charge (Q_{i+1}) and Time to discharge (Δt_{i+1}) (b) ΔQ_i and ΔQ_{i+1} (PSA), (c) Δt_i and Δt_{i+1} (PSA) and (d) ΔQ_i and Δt_i at 12.1 kV_{dc} [1].

(which is difficult to detect). This would lead to the defect going undetected. This is a risky scenario since the pulse-free zone is in reality an active plasma region which corrodes the metallic electrode, leaving behind unwanted residue such as sharp floating particles and poisonous gases. Similarly, if the region of intermittent corona goes undetected, it can lead to streamer discharges due to space charge build-up. Therefore, it is insufficient to do PD measurements on DC components at the value of nominal voltage alone.

Figure 4.19 shows a flow chart with a possible test plan that will allow the identification of the corona defect and its respective configuration. The component under test is first tested at its nominal testing voltage over positive polarity (+DC). If PD is measured, an analysis is made on whether the discharge stage has a stable repetition. A stable discharge rate would indicate towards self-sustaining stage of configuration II or negative corona or Trichel of configuration IV. To differentiate between the two configurations, the correlation between the parameters ΔQ_{i+1} and Δt_{i+1} is checked. If there exists a trend in the plot of ΔQ_{i+1} vs Δt_{i+1} as shown in Figure 4.17, it confirms that it is Trichel pulses and hence coming from a protrusion over ground terminal (configuration IV). If there is no correlation in the plot of ΔQ_{i+1} vs Δt_{i+1} but the pulses are stable and repetitive, this would indicate the self-sustaining corona stage of configuration II, indicating that the protrusion is

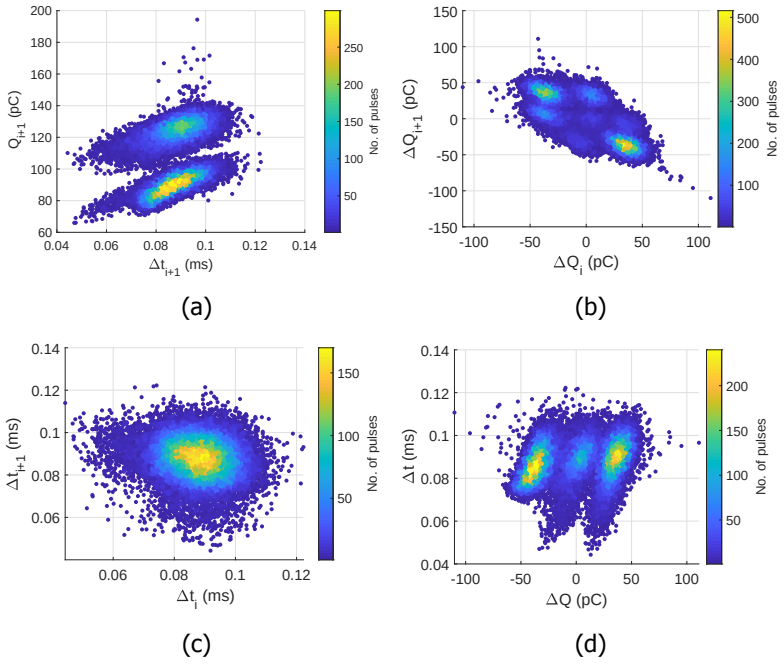

Figure 4.18: Discharge patterns of configuration I (a) Charge (Q_{i+1}) and Time to discharge (Δt_{i+1}) (b) ΔQ_i and ΔQ_{i+1} (PSA), (c) Δt_i and Δt_{i+1} (PSA) and (d) ΔQ_i and Δt_i at 6.6 kV_{dc} for needle at -DC voltage with 2 corona sources [1].

close to HV. In case discharge pulses are recorded but they occur randomly, one needs to rule out the possibility that these are streamer discharges of configuration II. Hence, the measurement is repeated at a reduced voltage to look for the self-sustaining or intermittent corona which would confirm that the protrusion is on HV (configuration II). In the event of no pulses being recorded at nominal voltage, one needs to rule out that the component is either under intermittent corona region or under the pulse-free zone. To do this, the measuring sensitivity is increased (by increasing the amplifier gain) to look for pulses close to the noise threshold. The presence of which would confirm that there is a protrusion close to HV (configuration II). However, if absolutely no PD is recorded, the measurement is repeated at reduced voltage until the possibility of pulse-free zone operation is completely ruled out. Similarly, when the component under test is tested at its nominal testing voltage over negative polarity (-DC), a similar process is followed. Due to the absence of self-sustaining corona stage in configuration III, any discharge with a stable rate would indicate towards the presence of protrusion over HV (configuration I). To rule-out the possibility of operation under pulse-free zone or streamer region, the measurements are repeated with reduced voltage similar to that described for positive DC. The DC components need to be tested at sub-multiples of the nominal

voltage to be completely certain of their fitness and quality.

Currently, this procedure has been designed to discriminate amongst the different configurations of corona under DC alone. This is based on the study presented in this chapter. However, the flow chart can be improved with the study of every new defect type.

4.4. Conclusion

Corona is one of the most highly documented and studied defect as it is a part of several beneficial industrial processes such as ozone generation, surface treatments, decontamination of gas streams, etc. The integration of available knowledge in diverse fields to further the understanding and interpretation in terms of PD pulse diagrams for corona characterization under High Voltage DC applications is what this research accomplishes. Several features such as the self-sustaining corona and noisy corona have been described in journals of applied physics and its applicability towards PD defect identification is exploited through this contribution. The following are the important concluding remarks:

1. There are four instead of two corona configurations based on the position of the protrusion and the polarity of voltage.

2. Each of these four configurations of corona behaves differently from the other. The greatest similarity amongst them is between configuration I and IV. They differ in terms of discharge inception voltage and discharge magnitude, the defect progression itself remains similar.

3. The plot of the discharge parameter, charge (Q_{i+1}) vs time to discharge (Δt_{i+1}) proves to hold the information towards the mechanism of discharge.

4. In comparison to the PSA plots (ΔQ_i and ΔQ_{i+1}, Δt_i and Δt_{i+1} and ΔQ_i and Δt_i) the plot of charge (Q_{i+1}) vs time to discharge (Δt_{i+1}) is shown to be more robust to outliners and other inherent effects such as double corona source over the protrusion at increased voltages.

5. Minute behavioral features such as the inception of intermittent corona under configuration II and III and the self-sustaining pulse stream of configuration II are pointers for the identification of the origin of the corona (whether from HV terminal or ground).

6. The riskiest configuration of corona is -DC applied with protrusion fixed on ground plane (Configuration III). The streamers in this configuration incept at a low voltage level and it subsequently breaks down at a reduced voltage. This has also been corroborated based on industrial testing experience where most often tests with negative DC voltages have faced problems due to corona coming from improper ground connections.

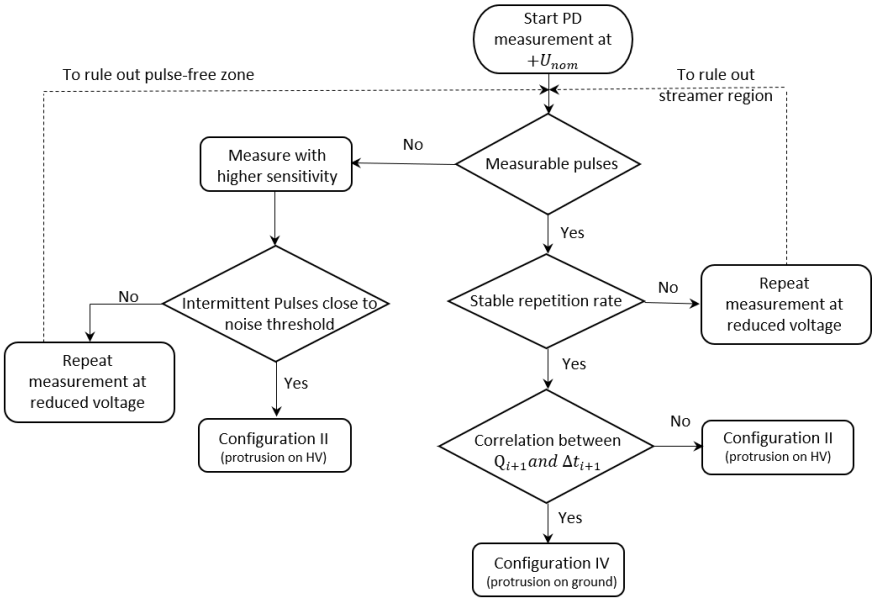

(a) PD test under positive DC voltage

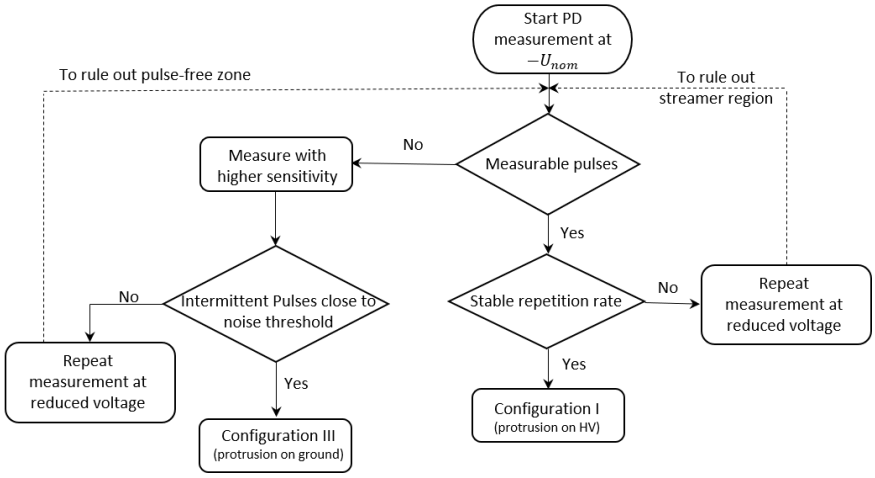

(b) PD test under negative DC voltage

Figure 4.19: Flow chart of the proposed test plan for identifying corona discharge and its configuration under a) positive DC voltage and b) negative DC voltage [1].

7. To ascertain the fitness and quality of DC components (currently, with respect to corona defects alone) the component has to be tested at nominal test voltage and its sub-multiples following the test schematic as described in Section

4.3.

8. The discriminatory procedure formulated in Figure 4.19 based on the investigation of the corona defect under DC voltage is a useful tool for the detection and identification of the corona defect.

references

[1] **S. Abdul Madhar**, P. Mraz, A. Rodrigo Mor, and R. Ross. "Study of Corona Configurations under DC Conditions and Recommendations for an Identification Test Plan". In: *International Journal of Electrical Power and Energy Systems* 118 (June 2020), p. 105820. issn: 01420615. doi: 10.1016/j.ijepes.2020.105820.

[2] P. Mraz, P. Treyer, and U. Hammer. "Evaluation and limitations of corona discharge measurements-an application point of view". In: *CMD 2016 - International Conference on Condition Monitoring and Diagnosis*. 2016, pp. 278–281. doi: 10.1109/CMD.2016.7757809.

[3] C. H. Stuckenholz, M. Gamlin, and P. Mraz. "PD Performance of UHV-DC Test Equipment". In: *ISH, Argentina*. 2015, pp. 23–28.

[4] F. H. Kreuger. *Industrial High DC Voltage*. Delft University Press, 1995, p. 198. isbn: 90-407-1110-0.

[5] S. Chen, F. Wang, and Q. Sun. "Branching Characteristics of Positive Streamers in Nitrogen-Oxygen Gas Mixtures". In: *IEEE Transactions on Dielectrics and Electrical Insulation* 25 (2018), pp. 1128–1134. doi: 10.1109/TDEI.2018.007043.

[6] G. W. Trichel. "The mechanism of the negative point to plane corona near onset". In: *Physical Review* 54.12 (1938), pp. 1078–1084. issn: 0031899X. doi: 10.1103/PhysRev.54.1078.

[7] B.H. Crichton. "Gas Discharge Physics". In: (1996), pp. 311–315.

[8] Y. Zhang, Q. Xia, Z. Jiang, and J. Ouyang. "Trichel pulse in various gases and the key factor for its formation". In: *Scientific Reports* August (2017). issn: 2045-2322. doi: 10.1038/s41598-017-10118-2. url: http://dx.doi.org/10.1038/s41598-017-10118-2.

[9] T. N. Giao and J. B. Jordan. "Modes of Corona Discharges in Air". In: *IEEE Transactions on Power Apparatus and Systems* PAS-87.5 (1968), pp. 1207–1215. issn: 00189510. doi: 10.1109/TPAS.1968.292211.

[10] A. Pirker and U. Schichler. "Partial discharge measurement at DC voltage - Evaluation and characterization by NoDi$*$ pattern". In: *IEEE Transactions on Dielectrics and Electrical Insulation* 25.3 (2018), pp. 883–891. issn: 10709878. doi: 10.1109/TDEI.2018.006742.

[11] J. S. Chang, P. A. Lawless, and T. Yamamoto. "Corona Discharge Processes". In: *IEEE Transactions on Plasma Science* 19.6 (1991), pp. 1152–1166. issn: 19399375. doi: 10.1109/27.125038.

[12] G. W. Trichel. "The Mechanism of the Positive Point-to-Plane Corona in Air at Atmospheric Pressure". In: *Phys. Rev.* 55 (4 Feb. 1939), pp. 382–390. doi: 10.1103/PhysRev.55.382. url: https://link.aps.org/doi/10.1103/PhysRev.55.382.

[13] A. Greenwood. "The Mechanism of the Ring Discharge in Negative Point-to-Plane Corona". In: *Journal of Applied Physics* 23.12 (1952), pp. 1316–1319. doi: 10.1063/1.1702066. eprint: https://doi.org/10.1063/1.1702066. url: https://doi.org/10.1063/1.1702066.

5

Study of the Floating Electrode Defect under DC

Partial discharge is a prevalent phenomenon under high voltage (HV) where the discharge partially bridges the gap between two electrodes. At increasing voltage levels, physical dimensions and distances between the electrical parts become critical. Designing electrical components for such high voltages and planning of high voltage laboratories/tests need to deliberate this aspect as it could lead to possible complications such as partial discharges (PD) from the floating metal components. Floating electrodes under AC voltages are associated with a distinctive PRPD pattern. However, there is a lack of literature on the physical interpretation of this pattern. Likewise, under DC voltages, no consistent explanation towards the defect behavior has been reported. Therefore, this chapter presents an in-depth study of the floating electrode defect configuration under AC and DC voltages. Subsequently, it provides the physical interpretation of the discharge patterns obtained through the stepwise description of the discharge stages under both conditions. By formulating criteria for repetitive discharges and presenting novel PD fingerprints for DC floating electrode configuration, the outcomes published in this chapter contribute towards prospective PD defect identification tools under HVDC.

Parts of this chapter have been published in Elsevier's International Journal of Electrical Power and Energy Systems, **118**, (2020), 105733, ISSN 0142-0615, https://doi.org/10.1016/j.ijepes.2020.105733 [1]

5.1. Introduction

Floating electrode at high voltages (HV) refers to a metallic object in the vicinity of an electric field that acquires a stray voltage depending on the level of capacitive and resistive coupling. If the resultant voltage on the metallic body is sufficient to cause a partial flashover (depending on the critical withstand strength of the surrounding dielectric medium)to the main electrode, ground or initiate corona around the body, then the partial discharge from the floating electrode appears. This phenomenon also occurs in nature in the event of a thunderstorm/lightning. The electric fields during a thunderstorm can induce charges on ungrounded metallic bodies, causing them to discharge. These aspects of floating body discharge in a lightning protection system have been studied in [2][3][4][5]. The risk involved with floating bodies in HV systems is manifest in one way through the possibility of shock and flashover. In certain cases, the floating body could also initiate treeing on the electrical components that it is a part of or those in its vicinity. The level of risk depends on the energy held across the floating body (capacitive energy). On account of this, HV installations always specify clearances, which are distances at which it is safe for personnel to operate other equipment [6]. A Floating PD, more specifically from an external source, can stall the quality inspection and qualification process in test laboratories. And an internal floating defect in the dielectric of the component risks the weakening of the dielectric depending the level/nature of discharge.

In AC tests, the modern-day partial discharge (PD) measuring equipment creates a Phase Resolved Partial Discharge (PRPD) pattern during the test which allows defect identification [7]. It is the unique shape of this PRPD pattern that helps in the identification of the defect as pattern holds the information on the defect's behaviour. Though the various trends of discharge progression with increasing voltage and time have been studied, little has been known so far on the actual interpretation on the pattern itself. This research aims at shedding light on the physical interpretation of the PRPD pattern of the floating electrode defect through the identification of key features of the defect behaviour. This is systematically done by plotting several discharge parameters. Following that, the chapter provides the detailed and stepwise description of the discharge behaviour. On the other hand, in the case of DC, several researchers have studied the discharge characteristics and presented the resultant patterns of floating particles or free-moving particles since this is of interest for Gas Insulated Systems (GIS) [8][9]. However, there is a lack of literature that describes the floating electrode defect similar to AC conditions. Hence, this contribution presents a detailed study of the discharge process from a floating electrode defect by identifying various discharge characteristics that represent the defect accurately. Further, the criteria for the repetitive stage of discharge from a floating electrode are defined and DC-PD fingerprints for the defect are presented. The contributions of the research could be subsequently utilized for defect identification under HVDC and an extension of the existing knowledge in the field of AC partial discharges.

5.2. Understanding floating discharge under AC stress

The floating electrode defect under AC voltages is most commonly associated with its distinctive PRPD pattern as shown in Figure 5.1 [10]. A stable, repetitive stage of discharge for the particular configuration under test (described in Chapter 3, section 3.2.2) is reached at 9.50 kV_{rms} establishing this as the PD inception voltage (U_i or PDIV). The discharge magnitude remains fairly constant over a given voltage and moves predominantly over the rising edge of the positive and negative half-cycle creating the straight lines over the PRPD pattern. When looking at the discharge pulse occurrence carefully one will notice the sliding of the pulse over the voltage phase towards and away from each other. This has been pictorially demonstrated through Figure 5.2 where the two pulses marked in grey are moving towards each other or the two pulses marked in blue are moving away from each other(denoting the pulse sliding that takes place). This phenomenon is a characteristic feature of a floating electrode defect and can alternatively be recognized or studied through the 3-pulse PSA (Pulse Sequence Analysis) plot of time between successive discharges as shown in Figure 5.3 [11].

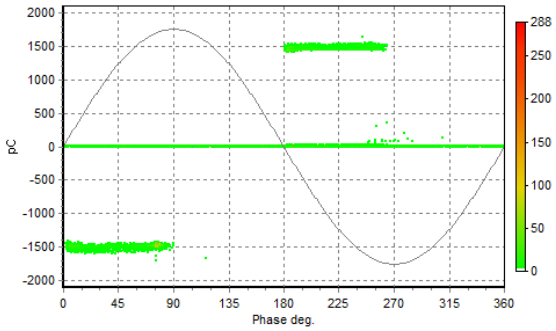

Figure 5.1: PRPD pattern of a typical floating electrode defect [1].

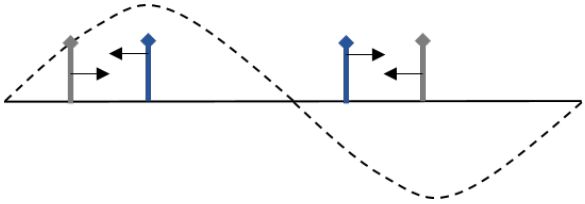

Figure 5.2: Pictorial representation of the moving pulse in a typical floating electrode defect [1].

The 3-pulse PSA plot of time between successive discharges shows a linear distribution that extends between the coordinates of (7,13) ms and (13,7) ms. This

illustrates that the time between the 2 discharges on the 2 half-cycle changes between 7 and 13 ms and follows a well-defined sequence. It also depicts that there are just 2 discharges per voltage cycle (20 ms or 50 Hz) as the sum of two successive Δt yields 20 ms, which is the time period of a 50 Hz cycle. For instance, the blue cluster seen in Figure 5.3 around 4 to 6 ms depicts the discharge period when there occur more than 2 pulses per cycle. To further understand the sequence in the change of time between successive discharges (Δt), the bar graph of the same is presented in Figure 5.4. This clearly shows the sequential increase (from 7 to 13 ms or 126° to 234°) and subsequent decrease (from 13 to 7 ms) of the time between discharges. Concurrently, one can also observe a region with Δt ranging from 4 to 6 ms. This is the period of discharge with 4 pulses per voltage cycle. Here, the sum of 4 successive Δt yields the time period of the 50 Hz cycle (20 ms). This region indicates that there are 2 discharges per half-cycle. Typically, in the case of floating electrode defects, with an increasing level of voltage above discharge inception, multiple pulses per half-cycle can be observed. Whereas the level of discharge magnitude remains constant. This is because the discharge magnitude is related to the gap withstand voltage and given that the floating body is fixed, the resultant PD magnitude remains constant. However, once the voltage exceeds the corona inception level for the curvature of the floating body, corona can also be observed. Section 5.2.2 is dedicated to the description of this phenomenon in more detail.

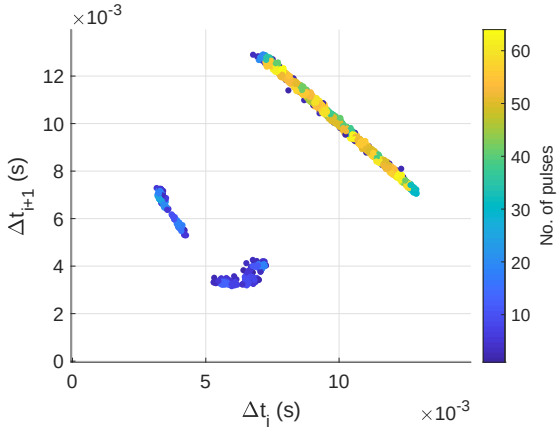

Figure 5.3: The plot of time between successive discharges of a 3-pulse sequence for a typical floating electrode defect [1].

5.2.1. Discharge behaviour

The reason for this unique feature of floating electrode discharge in which the pulses move towards and away from each other over the voltage phase lies in its physics. Therefore, the following section provides a theoretical background to the stepwise

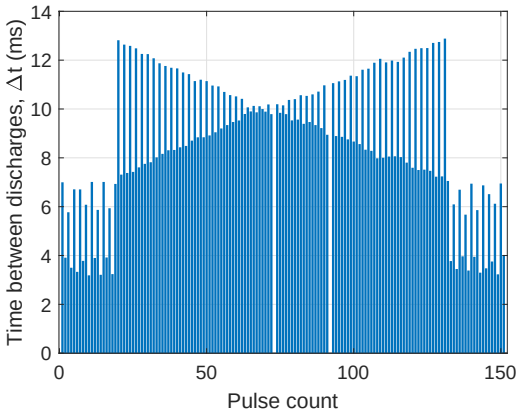

Figure 5.4: The plot of time between discharges for the floating electrode defect under AC voltage [1].

behaviour of a floating electrode defect under AC voltage cycle.

For illustration, let us consider a homogenous electric field distribution between two conducting plate electrodes with the floating electrode placed at a distance *l* from the electrode at HV, as shown in Figure 5.5a. Based on the capacitive coupling to the electrode arrangement the floating electrode is at a certain voltage that is equivalent to;

$$V(\omega) = E_f(\omega).l \tag{5.1}$$

where, E_f is the electric field intensity across the gap distance with length *l*, and is a sum of the electric field from the applied voltage ($E_{ext}(\omega)$) and the field from the induced charges on the floating electrode ($E_s(\omega)$). All the field and voltage values are a function of the angular frequency, ω of the power supply. Initially, the net charge on the metallic floating body remains zero (electrically neutral). Once the electric field exceeds the breakdown field value, over the positive half-cycle, the voltage across the gap *l* reaches the breakdown value thereby bridging the gap momentarily by a spark discharge or a current path. In terms of partial discharge measurements, it is represented as a current pulse with an integral equivalent to;

$$\Delta Q = \bar{i}.\Delta t \tag{5.2}$$

where $\bar{i}$ is the mean value of current over the transient time, Δt is the transient time of the discharge process and ΔQ is the value of charge. The discharge magnitude is a function of the electric field intensity (E_f) at the gap and the level of capacitive coupling of the floating electrode which in turn depends on the area of the floating electrode, the gap distance and the permittivity of the dielectric. The initial phase until and including the first breakdown can be described by the

following set of equations;

$$\begin{aligned} &\text{At } t = t_o, \\ &\qquad V_{ind} = \hat{V}_{ind} sin(\omega t_o + \phi) \\ &\qquad V_{ext} = \hat{V}_{ext} sin\omega t_o \\ &\qquad V_{bd} = V_{ext} + V_{ind} \end{aligned} \tag{5.3}$$

where, V_{ind} is the induced voltage on the floating electrode which follows the supply voltage, V_{ext} is the voltage drop across gap *l* due to the applied voltage, $\hat{V}_{\text{ind}}$ and $\hat{V}_{\text{ext}}$ are the absolute peak values of the voltage and V_{bd} is the breakdown voltage of the gap *l*, ϕ is the phase shift between the induced voltage, V_{ind} and the external voltage drop V_{ext} arising from the capacitive nature of the floating gap.

The transient phase of the discharge brings the floating electrode to the HV electrode's potential momentarily, charging it positively (due to the positive half-wave). Therefore, now the floating electrode is no more electrically neutral but possess a charge equivalent to *q* given in Eq.5.4. Based on the electrical field drawings shown in Figure 5.5b it can be observed that the applied electric field (E_{ext}) due to the supply voltage and the static electric field ($E_{s,+}$) due to the charge on the floating electrode now oppose one another in the gap *l*.Hence, the defect does not discharge again over the positive half-cycle given the voltage drop due to $E_{s,+}$ that compensates for the sinusoidal increase in the applied AC voltage. When the AC voltage polarity changes to the negative half-wave, the scenario Figure 5.5c occurs, where the applied electric field (E_{ext}) and the static electric field ($E_{s,+}$) add constructively once again to exceed the value of breakdown voltage of gap *l* initiating a discharge at $t=t_1$. The following equations describe the moment preceding the discharge event at $t=t_1$;

$$q = C.V_{bd}(t_o) \tag{5.4}$$

$$E_{s,+}(t_1) = \frac{k.q}{l^2} \tag{5.5}$$

$$V_{s,+}(t_1) = E_{s,+}(t_1).l \tag{5.6}$$

$$\begin{aligned} V_{bd}(t_1) &= V_{ext}(t_1) + V_{ind}(t_1) + V_{s,+}(t_1) \\ V_{bd}(t_1) &= \hat{V}_{ext} sin\ \omega t_1 + \hat{V}_{ind} sin(\omega t_1 + \phi) + \frac{kC}{l}[\hat{V}_{ext} sin\omega t_o + \hat{V}_{ind} sin(\omega t_o + \phi)] \end{aligned} \tag{5.7}$$

where, *q* is the charge on the floating electrode after restoration of the gap resistance following the first discharge, *C* is its capacitance to the HV electrode, $V_{bd}(t_o)$ is the instantaneous voltage during the breakdown at $t = t_o$, $E_{s,+}$ is the electrostatic field due to charge q, k is the electrostatic constant equal to $8.99 \times 10^9 Nm^2C^{-2}$ and $V_{s,+}$ is the resultant electrostatic voltage. From Eq.5.7 it can be

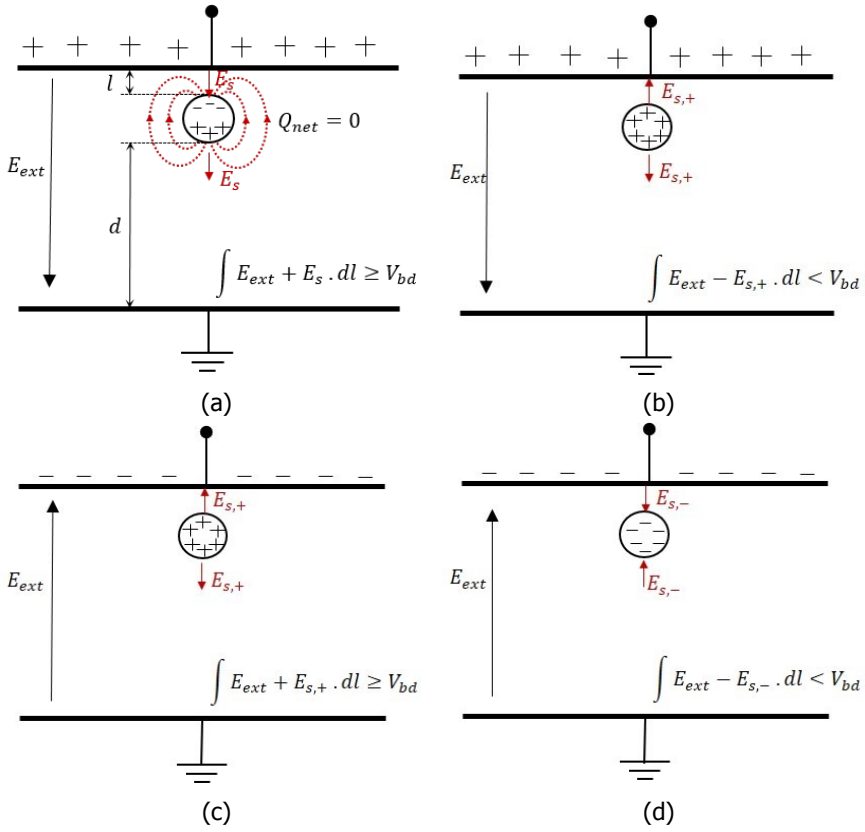

Figure 5.5: Schematic of the stepwise discharge process of a floating electrode defect under AC voltage (a) floating body before first breakdown of gap *l* during positive half-cycle (b) after first breakdown of gap *l* during positive half-cycle (c) before breakdown of gap *l* in the subsequent negative half-cycle and (d) after breakdown of gap *l* during the negative half-cycle [1].

resolved that the time (over half-cycle or phase position) t_1 at which discharge takes place depends on the voltage acquired as a result of the previous discharge at instance t_o. The discharge scenario based on Eq.5.7 has been simulated in MATLAB for the purpose of demonstration and is shown in Figure 5.6. It can be observed that since the breakdown at t_1 occurs at an increased voltage level (the corresponding external applied voltage during the breakdown at time instance t_1 is 0.84 V_{ext} as indicated on Figure 5.6) the discharge on the subsequent half-cycle at t_2 occurs at a lower level (0.30 V_{ext}). And this level of charge acquired at t_2 causes the discharge at t_3 to shift to a smaller voltage level (0.65 V_{ext} compared to the $0.84V_{ext}$ at t_1). Additionally, the sum of the subsequent values of Δt lie in the range of 19.05 and 20.50 ms which as in line with the observations presented in Section

5.2. One might otherwise also observe this time shifting of pulses over subsequent voltage-cycles as the sliding of the pulses away from each other (demonstrated through the arrows in Figure 5.6). In sum, this confirms that the phase angle at which the discharge takes place on one half-cycle determines the phase position of the subsequent discharge event on the next half-cycle. Thereby, leading to the moving/shifting pulses over the voltage phase angle as is observed with the AC floating discharge (reference to Figure 5.2).

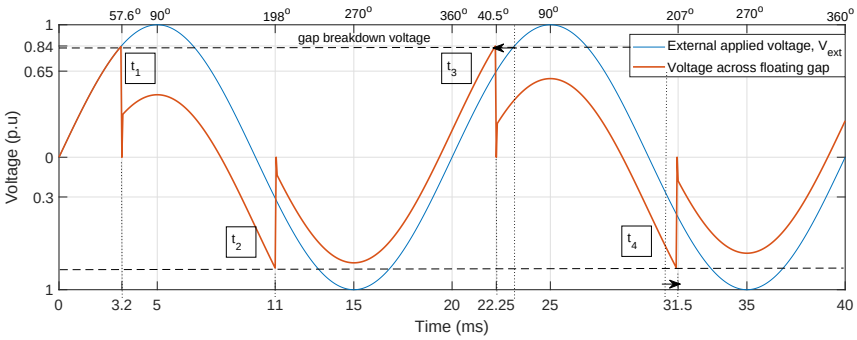

Figure 5.6: Simulation of the floating defect discharge scenario demonstrated based on Eq.5.7. The x-axis is given in terms of time in ms (below) and in terms of rotational phase in degrees (above) [1].

5.2.2. Corona from floating objects

Depending on the geometry and curvature of the floating electrode, corona may incept on it. However, the manifestation of the corona from the floating electrode can precede or follow the occurrence of floating discharge. This would depend on the geometry and positioning of the floating electrode in the gap. In the experimental case discussed in this chapter, the corona from the floating electrode incepts with increasing voltage (after the manifestation of the floating defect). The PRPD pattern of which is shown in Figure 5.7. The difference between corona from a needle plate arrangement with the needle at HV and the corona coming from a floating electrode is the difference in the energy source. In case of corona the energy for the discharge is directly supplied by the power supply. However, in case of the floating electrode, the energy on the floating electrode (W) is defined based on its net charge, Q and instantaneous voltage V, given by:

$$W = \frac{1}{2} Q.V \tag{5.8}$$

This cannot serve as a continuous discharge source such as in the case of the needle-plate corona arrangement connected to the power supply. Once the energy on the floating electrode is no more sufficient (depends on the resistance of the discharge channel) to incept the corona, the discharge ceases. To understand this

phenomenon better, consider the floating electrode arrangement given in Figure 5.5b, when the voltage is sufficiently high the positive charge acquired after breakdown by the floating electrode can incept positive corona (or streamers) over the gap *d*. As the floating electrode is electrically isolated, the positive corona charges the floating electrode negatively. With the floating electrode acquiring negative charge once again, the gap *l* breaks down making it positive again. And this process repeats itself, and the defect exhibits both patterns of floating and corona discharge. This process continues until polarity reversal. Similarly, at the negative half-cycle with increased voltage, negative corona incepts over gap *d*. The cluster shown in Figure 5.7 over the positive polarity of the positive half-cycle is due to the incorrect polarity recognition by the PD detector due to insufficient vertical bit resolution as the streamer discharges are well above a few 10s of nC.

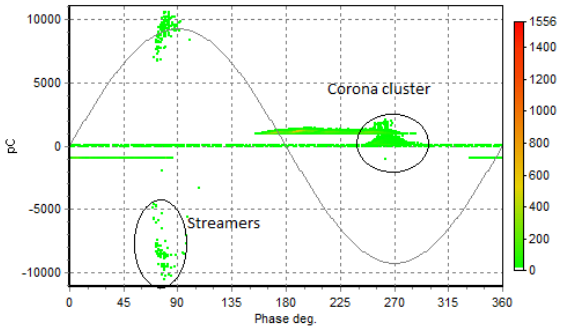

Figure 5.7: PRPD pattern of the corona from the floating electrode defect [1].

5.3. Floating electrode under negative DC

The floating electrode defect under DC voltage follows a completely different sequence as compared to the AC defect. The defect in this case does not have a stable discharge repetition rate once the breakdown voltage of the gap *l* is reached. The first discharge over the gap takes place when the resistive voltage drop over the gap *l* exceeds the value of breakdown voltage. However, after the first breakdown the floating electrode charges to a value of charge *q* that is determined based on the transient time of the discharge and the value of discharge current. Subsequently, this charge on the floating electrode as depicted in Figure 5.5d results in a local electric field, $E_{s,-}$, which is oriented opposite to the external electrical field, E_{ext}. Hence, no further discharge takes place at this voltage level ($\int E_{ext} - E_{s,-} \,.\, dl < V_{bd}$). The discharge over the gap recurs when the applied DC voltage increases, thereby compensating the opposing electrical field ($\int E_{ext} - E_{s,-} \,.\, dl = V_{bd}$).

With increasing voltage, the gap *l* breaks down at each voltage step charging the floating electrode each time to a higher value of charge. At a particular voltage level, the accumulated charge with its resultant static electric field ($E_{s,-}$) leads to

field enhancement over the gap *d* (scenario shown in Figure 5.5d). The field enhancement occurs as a result of the positive superposition of the two electrical field stress, $E_{s,-}$ and E_{ext}. This leads to inception of negative corona over the floating electrode. However, the negative corona diminishes the previously accumulated charge on the floating electrode. As the charge on the floating electrode reduces, the resulting electrical field $E_{s,-}$ which was opposing the external electrical field over gap *l* also reduces. And once the equation; $\int E_{ext} - E_{s,-} \, . \, dl = V_{bd}$ is satisfied, the gap *l* breaks down once again charging the floating electrode and the process repeats itself. To reach a stable discharge state the following two criteria need to be met:

- The constructive overlap of the applied electric field (E_{ext}) and the static electric field ($E_{s,-}$) produces corona over gap *d*.
- The corona discharge charges the floating electrode in the opposite direction, increasing the field across gap l to the breakdown value.

5

Once, these two criteria are satisfied, a stable discharge can be observed. The results of the experiments performed substantiate this theory. This phenomenon of discharge can be observed in Figure 5.8 where the pulses occur in blocks. The first pulse with larger amplitude is the breakdown of the gap *l*, while the successive pulses with small amplitude are due to negative corona. The larger discharge pulses seem to be bipolar due to the pulse undershoot which is an artefact of measurement generated due to the limited bandwidth of the oscilloscope used for recording. This stage of the floating electrode discharge yields very distinct discharge patterns.

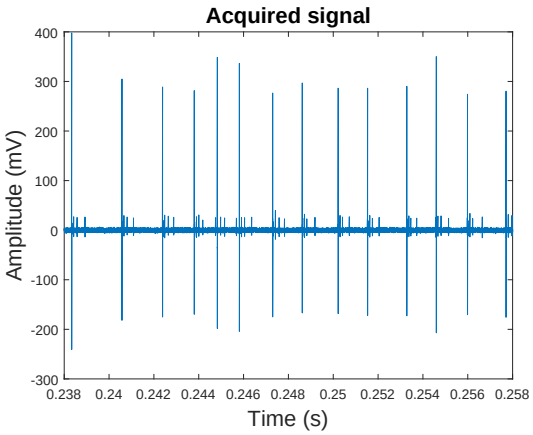

Figure 5.8: Discharge stream recorded at -29.5 kV_{dc} with the floating electrode defect [1].

Figure 5.9a shows the plot of difference in successive discharge magnitudes (ΔQ) vs. time between the successive discharges (Δt), Figure 5.9b gives the plot of difference in discharge magnitudes of 2 pulses in a 3 pulse sequence (ΔQ_i vs. ΔQ_{i+1}).

The distinct tri-star pattern arises from the nature of variation in the pulse magnitude in the discharge stream. This is explained through the example shown in Figure 5.10. In this figure, the various pulse clusters that occur during the floating discharge process under negative DC voltage are arranged in groups of 1 to 4 to show the formation of the indicidual clusters on Figure 5.9b. Figure 5.9c is a plot of time between successive discharges in a 3-pulse sequence (Δt_i vs. Δt_{i+1}). Figure 5.9d is the Figure 5.9c presented in logarithmic scaling of the axis and excluding the heat map function. It is synonymous to Figure 5.3 of the AC discharge pattern and shows a very distinct pattern similar to the one observed in the AC case. To further describe this pattern clearly, the bar graph of time between discharges of the floating electrode defect at the same voltage level is presented in Figure 5.11.

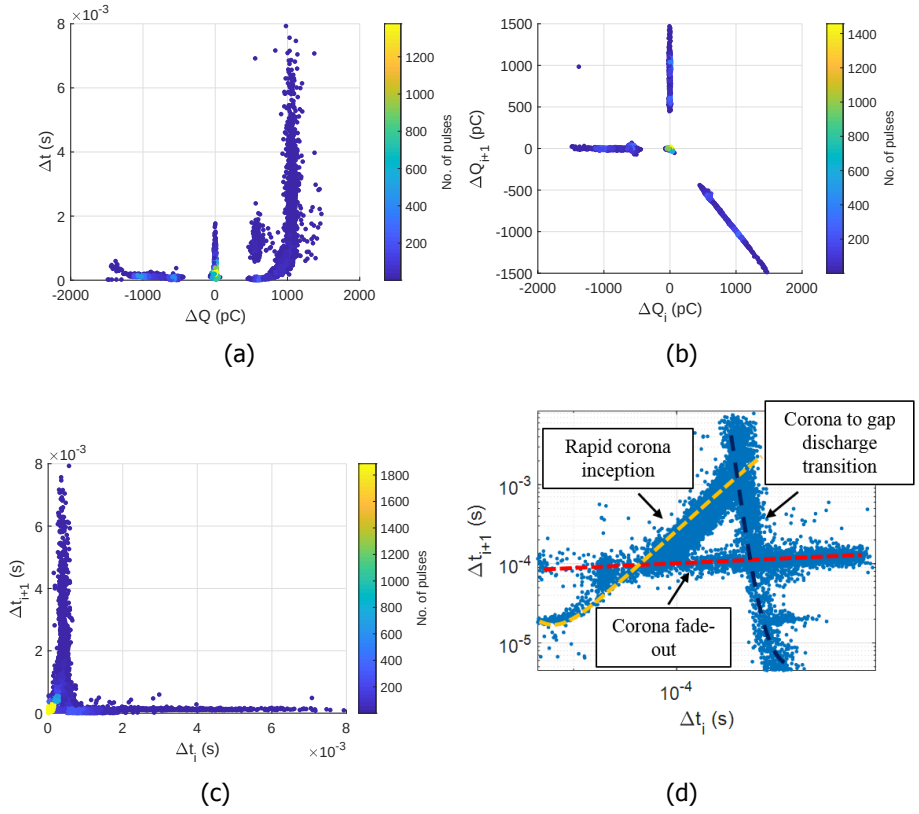

Figure 5.9: PSA patterns of the floating electrode defect under -29.5 kV_{dc} (a) plot of difference in successive charge (ΔQ) vs. time between the successive discharges (Δt), (b) plot of difference in charge of 2 pulses in a 3-pulse sequence (ΔQ_i vs. ΔQ_{i+1}), (c) a plot of time between successive discharges in a 3-pulse sequence (Δt_i vs. Δt_{i+1}) and (d) Figure 5.9c in logarithmic scaling [1].

From this it can be deduced that the time between discharges follows a very systematic scheme. The value of Δt increases exponentially from the discharge of gap *l* until the next discharge of gap *l*. The exponential curve shown by the yellow curve in Figure 5.9d indicate the corona inception over the floating electrode with small time between discharges. This can also be confirmed by the large density of pulses over this curve. The exponential decay curve shown by the black curve indicates the discontinuity or the shift from the corona stage to the next discharge of gap *l*. The third prominent curve creating a stable line highlighted through the red line in Figure 5.9d indicates the slow repetitive corona towards its termination (corona fade-out).

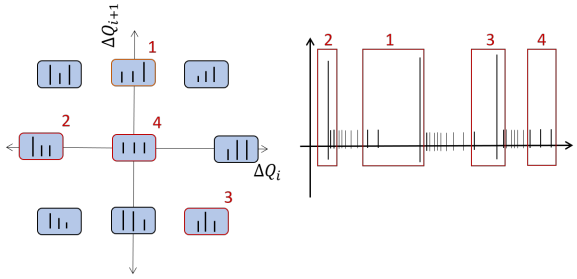

Figure 5.10: An illustration of the pulse stream occurrence and the formation of the tri-star pattern of Figure 5.9b [12].

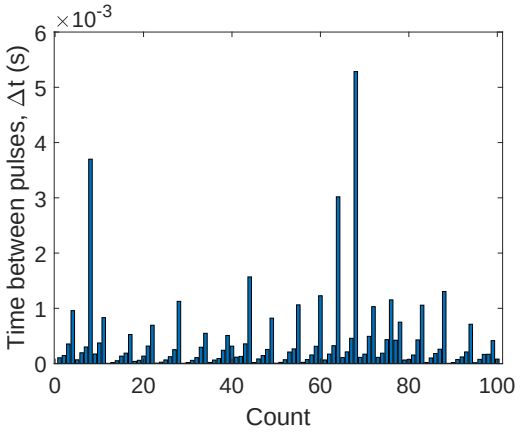

Figure 5.11: The plot of time between discharges for floating electrode defect under -DC voltage of -29.5 kV_{dc} [1].

5.4. Floating electrode under positive DC

Under the positive polarity of the DC voltage, the floating electrode follows the sequence of steps shown in Figure 5.5a and 5.5b. Once the gap breaks down and the floating electrode is charged positively, corona might incept on the floating body conditionally, when the criteria mentioned in section 5.3 are satisfied. However, positive corona incepts at higher voltages than negative corona due to the absence of an electron source. Hence, the inception voltage of the repetitive discharge state of a floating electrode under positive DC is slightly higher than that under negative DC. After the first breakdown of the gap *l*, several singular breakdowns can take place at increasing voltage steps given that the applied field E_{ext} increases sufficiently enough to compensate the previously accumulated positive charge.

Once the positive corona incepts over gap *d*, the floating electrode begins to get charged in the opposite direction (negatively). The drop in the positive charge over the floating electrode increases yet again the field stress across gap *l*, leading to the breakdown of the gap. Therefore, under the positive polarity there is a combination of streamer discharges and breakdown of the gap *l*.

The PSA plots associated with this configuration are shown in Figure 5.12. The absence of the negative corona with the repetitive pulses does not give rise to the unique pattern over the PSA plot of time between pulses such as the in the case of negative DC (Figure 5.9d). The discharge pulse stream recorded under this configuration is shown in Figure 5.13. From this, two types of pulses occurring alternatively can be observed, large and small. The discharge magnitude of the smaller pulses remains fairly constant while the larger pulses vary greatly. This feature of the discharge is reflected on the PSA plots of difference in discharge magnitude shown in Figure 5.12b. To study the formation of this plot further in detail, the difference in discharge magnitude of successive pulses is plotted in Figure 5.14a. The successive bars on the plot depict the difference in charge between two pulses. Observing from Figure 5.14a, the magnitude of ΔQ_i occurs in pairs. For instance, $\Delta Q_i(1) \approx -\Delta Q_i(2)$ and $\Delta Q_i(3) \approx -\Delta Q_i(4)$. This likeness in magnitudes within the pairs gives rise to the points in cluster 1, while the variation between pairs gives rise to the points over cluster 2 as shown in Figure 5.14b. To illustrate this process Figure 5.14c shows a sequence of pulses where the first 3 pulses deduce values of ΔQ_i and ΔQ_{i+1} that fall in cluster 1 while the consecutive 3, give rise to values that fall in cluster 2. Therefore, the constancy in the discharge magnitude of the smaller pulses and the wide variation in amplitude of the larger pulses forms two distinct clusters in the PSA plot of difference in discharge magnitudes (ΔQ_i vs. ΔQ_{i+1}) which could potentially serve in identification of the defect.

5.5. Conclusion

Floating defects are a rather familiar occurrence while performing HV test. They are identified readily based on their associated PRPD patterns. However, no literature so far has explained the origin of such a pattern. Therefore, this chapter illustrates the stepwise progression of the floating discharge defect under AC voltage conditions providing explanation for the pattern's origin. The following important conclusions

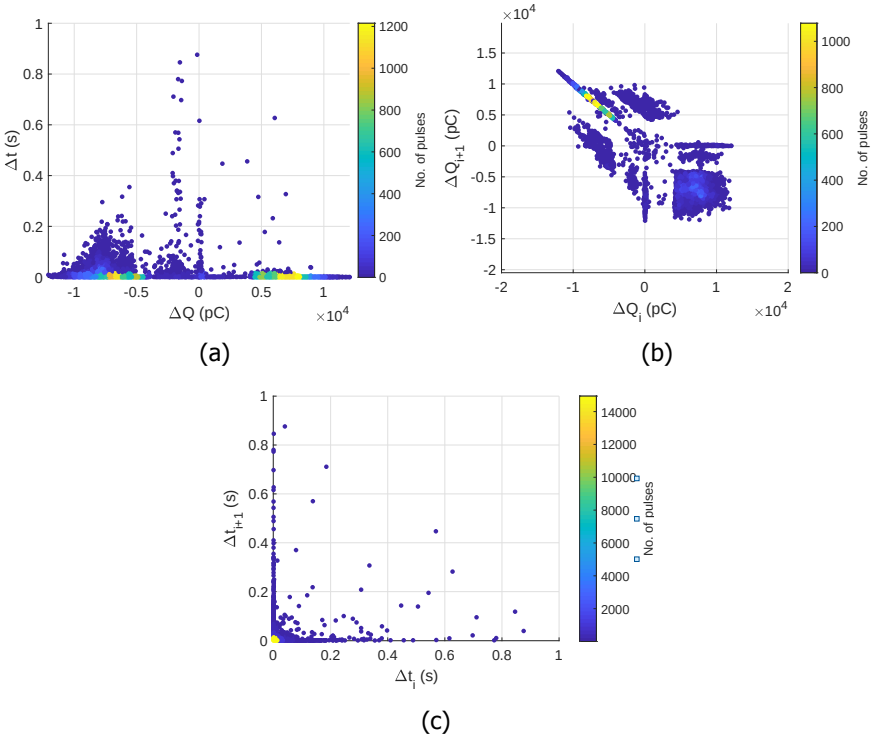

Figure 5.12: PSA patterns of the floating electrode defect under +DC voltage (a) plot of difference in successive charge (ΔQ) vs. time between the successive discharges (Δt), (b) plot of difference in charge of 2 pulses in a 3-pulse sequence (ΔQ_i vs. ΔQ_{i+1}), (c) a plot of time between successive discharges in a 3-pulse sequence (Δt_i vs. Δt_{i+1}) [1].

can be drawn from the study of floating electrode defect on AC stress conditions:

- The phase position of the discharge in one half-cycle of AC voltage is influenced by the phase position of the discharge from the previous half-cycle.
- The discharge from a floating electrode may also contain a corona pattern on the PRPD diagram depending on the geometry and radius of curvature of the floating object.
- In all cases of the floating electrode defect, on increase voltage, there is an onset of corona over the floating object, given that the healthy part of the dielectric gap does not break leading to complete breakdown/flashover.

In case of DC, though several potential partial discharge patterns had been proposed for PD identification, there has been a lack of knowledge on the discharge progression of a floating electrode defect under DC. This contribution therefore

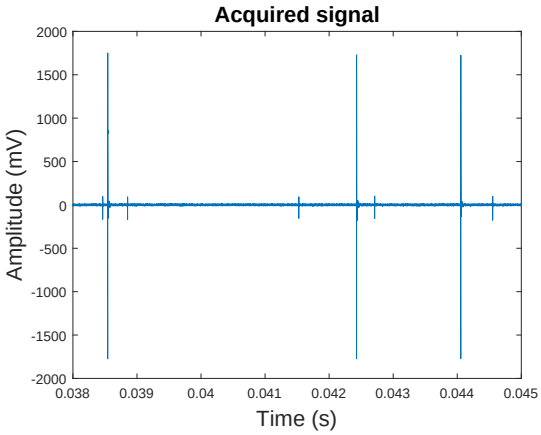

Figure 5.13: Discharge stream recorded with the floating electrode defect under positive DC voltage of +29.5kV$_{dc}$ [1].

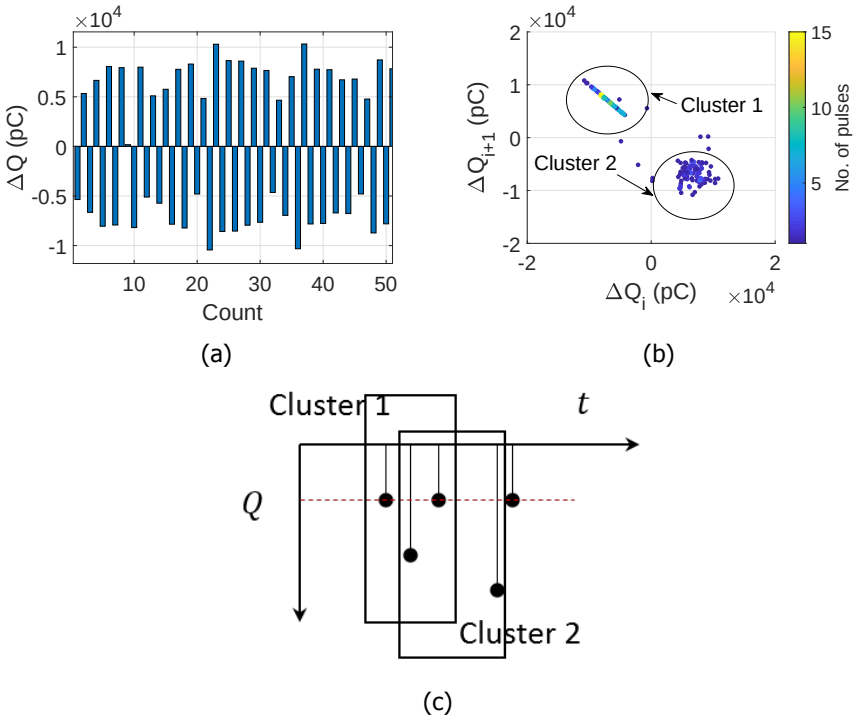

Figure 5.14: The formation of the 3 pulse PSA of ΔQ_i vs. ΔQ_{i_1}) (a) plot of difference in discharge magnitudes of consecutive pulses (b) cluster formation with first 200 pulses and (c) discharge occurrence over time [1].

describes in depth the process of discharge of a floating electrode defect and provides a physical interpretation to the derived Pulse Sequence Analysis (PSA) plots yielding some novel and interesting observations. The main contributions of the research derived based on the study of floating electrode configuration under DC is as follows:

- The discharge process from a floating electrode defect under DC stress differs from AC condition. For the repetitive discharge state, there needs to be alternative occurrence of corona and gap discharge as mentioned in Section 5.3. Otherwise, there is a risk that there is no discharge and the defect is not recognized.
- The results presented in this chapter such as the unique pattern in the PSA plot of time between successive discharges in a 3-pulse sequence (Δt_i vs. Δt_{i+1}) for the negative DC configuration could potentially serve in the defect's identification. Nevertheless, it provides an extension to the existing knowledge in the field of DC discharge patterns.

references

[1] **S. Abdul Madhar**, P. Mraz, A. Rodrigo Mor, and R. Ross. "Physical interpretation of the floating electrode defect patterns under AC and DC stress conditions". In: *International Journal of Electrical Power and Energy Systems* 118 (June 2020), p. 105733. issn: 01420615. doi: 10.1016/j.ijepes.2019.105733.

[2] F. Roman, V. Cooray, and V. Scuka. "Corona from floating electrodes". In: *Journal of electrostatics* 37.1-2 (1996), pp. 67–78.

[3] F. Román, E. Lötberg, R. Högberg, and V. Scuka. "Electrical characteristics of insulated metallic bodies in a lightning breakdown field". In: *22nd International Conference on Lightning Protection (ICLP), Budapest, Hungary*. 1994.

[4] F. Román. "The influence of a floating electrode on the breakdown voltage of a complex gap". In: (1995).

[5] F. Román, V. Cooray, and V. Scuka. "The corona onset voltage as a function of the radius of curvature of floating electrodes". In: *The 11th International Conference On Gas Discharges and Their Applications*. Chuo University Tokyo, Japan. 1995, pp. 192–195.

[6] N. Hylten-Cavallius. *High-voltage laboratory planning*. High Voltage Test Systems/ASEA Haefely, 1986.

[7] B. Fruth and L. Niemeyer. "The importance of statistical characteristics of partial discharge data". In: *IEEE Transactions on Electrical Insulation* 27.1 (1992), pp. 60–69.

[8] P. Wenger, M. Beltle, S. Tenbohlen, U. Riechert, and G. Behrmann. "Combined characterization of free-moving particles in HVDC-GIS using UHF PD, high-speed imaging, and pulse-sequence analysis". In: *IEEE Transactions on Power Delivery* 34.4 (2019), pp. 1540–1548.

[9] W. Gao, D. Ding, and W. Liu. "Research on the typical partial discharge using the UHF detection method for GIS". In: *IEEE transactions on power delivery* 26.4 (2011), pp. 2621–2629.

[10] A. R. Mor, L. C. Heredia, D. A. Harmsen, and F. Muñoz. "A new design of a test platform for testing multiple partial discharge sources". In: *International Journal of Electrical Power & Energy Systems* 94 (2018), pp. 374–384.

[11] M. Hoof and R. Patsch. "Pulse-sequence analysis: a new method for investigating the physics of PD-induced ageing". In: *IEE Proceedings-Science, Measurement and Technology* 142.1 (1995), pp. 95–101.

[12] **S. Abdul Madhar** and P. Wenger. "Simultaneous Electrical and UHF Measurement of DC-PD from Point-Plane Defect". In: *The International Symposium on High Voltage Engineering*. Springer, 2019, pp. 991–1003.

6

Study of Surface Discharges under DC

This chapter presents the investigation on surface discharge behaviour of various dielectric samples under DC. It sequentially develops the knowledge base for the study and analysis of the partial discharge (PD) defect with the goal of PD defect identification under DC. In order to facilitate this, the material properties of the dielectric are measured. Finite Element (FEM) simulation is used to obtain the preliminary estimates of the electric field and dielectric properties that concern partial discharge behaviour. The DC-PD tests performed on the surface dielectric samples demonstrate a plausible behaviour in line with the results of the simulation. There exists a disparity in the discharge magnitude under the DC positive and DC negative voltage polarities. It also displays a great degree of similarity towards the AC surface discharge behaviour. The chapter concludes by presenting novel partial discharge fingerprints for the surface PD defect that will aid in defect identification under HVDC.

Parts of this chapter have been published in Elsevier's International Journal of Electrical Power and Energy Systems, **126**, (2021), 106600, ISSN 0142-0615, https://doi.org/10.1016/j.ijepes.2020.106600 [1]

6.1. Introduction

As the power rating of the transmission network increases and the system moves from high voltage (HV) to extra high voltage (EHV) and ultra-high voltage (UHV), the criticality of the network elements also has been increasing. This has given rise to an expectation of increased level of reliability when it comes to asset quality. Each component of the power system, such as cables, bushings, transformers, Gas Insulated Switchgears (GIS) etc. are all tested for insulation defects during the design phase as well as before and after commissioning. With the traditional power grid designed for AC operation, partial discharge (PD) testing established itself as one of the most powerful and insightful tools in defect elimination and quality assurance. PD testing has become a vital tool in all stages of the asset life-cycle such as design, production, commissioning, monitoring/maintenance and diagnostics. However, the recent trends in HVDC with the introduction of long-haul DC lines along with its associated infrastructure have introduced additional concerns if not problems. The insulation system so far employed for AC is known to behave differently under DC stress conditions. The design of DC applications is a challenging process, the electric field calculations are made taking into account its dependence on operational temperature and changes in electrical conductivity of the respective insulating media [2]. Likewise, various other effects such as charge trapping, homo/hetero charge formation at interfaces and irregularities have made the realization of robust DC components a highly sophisticated process [3]. Due to these complexities, the partial discharge behavior of the insulation in the presence of various defects also remains highly elusive and distinct from the AC discharge behavior.

This particular chapter investigates the surface defect model, which is a common PD source in insulation systems, occurring over dielectric interfaces, sometimes also referred to as creeping discharge or tracking discharges (particularly if fluids are involved). These kinds of discharges occur on gas-solid interfaces and deteriorate the insulation over time. There are visual Phase Resolved PD (PRPD) patterns to recognize these kinds of defects under AC voltage stress. In this contribution, the discharge mechanism and patterns of a surface defect model under DC stress are studied and presented.

The chapter is organized in the following manner: Section 6.2 presents the relevant electrical properties of the dielectrics under study. In section 6.3, the simulation results of the surface discharge model under DC voltage are described. The results and observations of the AC and DC-PD tests, the obtained discharge patterns and inferences are discussed in Section 6.4. The last section is committed to presenting the striking similarities between the AC and DC discharge processes for these types of defects.

6.2. Measurement of electrical properties of the dielectric surface

The measurement of electrical properties of the dielectric samples is essential for the study of partial discharges in order to understand the underlying discharge mechanisms. The measured electrical properties also serve as a basis for the simulations performed in the following section. Therefore, this section presents the results of the measured electrical conductivity and dielectric constant of the samples investigated. The dielectric constants of the insulating samples are measured using the Tettex 2830 dielectric analyser together with the Tettex 2914 test cell for solid insulation material. The measurement of volumetric and surface dielectric properties is done according to the standard IEC 62631-3-1 and 62631-3-2 respectively [4][5], details of the measurement setup and technical specifications are presented in [6]. The measurement principle is based on a 3-electrode system consisting of namely, 1: main (HV) electrode, 2: measuring electrode and 3: guard electrode as shown in Figure 6.1. The relative permittivity (ϵ_r) is measured at AC power frequency (50 Hz) directly based on Eq.6.1.

$$C = \frac{\epsilon_r \epsilon_o S}{h} = C_o \epsilon_r \tag{6.1}$$

Where ε_o is the permittivity in free space and C is the measured capacitance of the sample, S is the effective surface area of the measuring electrode and h is the thickness of the sample.

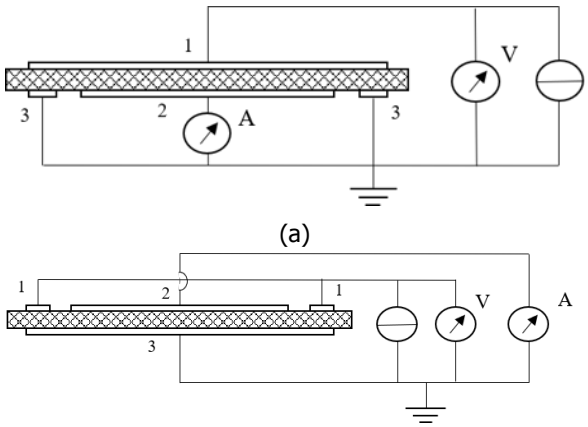

Figure 6.1: The circuit schematic for measurement of (a) volumetric dielectric properties based on IEC 62631-3-1[4] and (b) surface dielectric properties based on IEC 62631-3-2[5], [1].

The DC tests are carried out to measure the volume and surface resistivities of the dielectric samples. The volume resistivity (ρ_v) of the sample is measured in

the electrode arrangement shown in Figure 6.1a and derived from the value of measured resistance (R_s) using the relation shown in Eq.6.2.

$$\rho_v = \frac{R_s S}{h} \tag{6.2}$$

Where S is the effective surface area of the measuring electrode and h is the thickness of the sample. The surface resistance values of dielectric samples are measured using a similar 3-electrode setup as for measurement of volume properties, however, with the reversal of the HV and guard electrodes as shown in Figure 6.1b. The current flowing in the guard ring is measured and the surface resistivity, ρ_s, is deduced using the expression given by Eq.6.3.

$$\rho_s = \frac{d_2 + d_1}{d_2 - d_1}.\pi.R_s \tag{6.3}$$

Where R_s is the measured resistance, d_1 is the diameter of the inner electrode and d_2 is the inner diameter of the ring electrode. In order to get the absolute value of surface conductivity without the influence of the air gap, a special Teflon ring was manufactured and fitted in the gap. This explains the high values of surface resistivity presented in Table 6.1.

Four different samples were studied as a part of the surface discharge study. Samples A and B were dielectrics used in power cable application, sample A developed for high voltage applications and sample B for low voltage applications. Sample C was a high-grade Teflon commonly used in high voltage constructions and sample D a resin impregnated pressboard commonly used in transformer constructions. The results of the measurement are presented in Table 6.1. The dielectric constant of the samples A, B and C lie in the range of 1.5 – 2.2 which is commonly the expected range for Polyethylene and Teflon. The dielectric constant for sample D however is relatively high compared to the other samples. This is because the resin impregnated pressboard is designed for operation in oil and when not immersed in oil, the pressboard sample contains traces of moisture that results in a high value of ϵ_r. Based on the results of the measured volumetric electrical resistivity, the samples can be broadly classified into high and low resistive samples. While sample A and C are highly resistive with resistivities in the range of a few PΩm, Sample B and D are poorly/low resistive. Sample D has the lowest resistivity with a value of 2.14 GΩm while sample B has a resistivity of 24 TΩm.

The surface resistivity is associated with the resistance over surface tangent of the material. This measured value is extremely high for samples A and C where the maximum measuring limit of the device is reached. The other measured values for samples B and D are listed on Table 6.1. The implications of this variation in electrical properties is investigated through FEM simulation in the next section.

6.3. Simulation of the surface defect model

The use of simulation in this study was to derive the first estimates of the DC field stress and understand the influence of and the interaction between dielectric

Table 6.1: Results of the measurement of dielectric properties of the samples under study.

Sample identifier	Thickness h [mm]	Dielectric constant ϵ_r	Volume resistivity ρ_v $[T\Omega m]$	Surface resistivity ρ_s $[T\Omega m]$
A	0.58	2.18	2.98×10^{3}	6.91×10^{4}
B	2	1.57	2.40×10^{1}	1.04×10^{4}
C	0.60	1.95	6.40×10^{3}	6.91×10^{4}
D	3	8.0	2.14×10^{-3}	1.04

Table 6.2: Material properties used in the simulation.

Medium	Material properties	
Electrodes		
Surrounding medium	Air	(built-in)
	Electrical conductivity (S/m)	1×10^{-13} to 1×10^{-9}
Sample/ substrate	Dielectric sample	
	Relative permittivity	2.3
	Electrical conductivity (S/m)	$\sigma(T,E)$

properties of interfacial media. This was done using the COMSOL® Multiphysics user software which works based on Finite element method (FEM) by solving Partial Differential Equations (PDE). The following sections describe the setup, results and observations in greater detail.

6.3.1. Model setup

A concentric electrode arrangement is used for the simulation model with high voltage applied to the center electrode and the peripheral electrode at ground potential. The lower electrode on which the dielectric sample is placed is also at ground potential. This arrangement is chosen in order to enhance the tangential field stress over the dielectric surface that causes the surface discharges. The arrangement is placed in infinite medium of air using the infinite element domain available on COMSOL. The properties of the different media are listed in Table 6.2. A dielectric constant of 2.3 which is in the range of the dielectric constant of organic dielectrics like polyethylene and Teflon is used in the simulation. In case of DC simulations, the electrical conductivity of the sample is specially modelled as a function of temperature and electrical field stress, $\sigma(T,E)$. The dimensions of the arrangement can be estimated from Figure 6.2. A dielectric sample with thickness 1 mm is used for the purpose of simulation.

The model is studied under both AC and DC electrical stresses. The AC simulation is accomplished through the electrostatic physics and a steady-state study. An

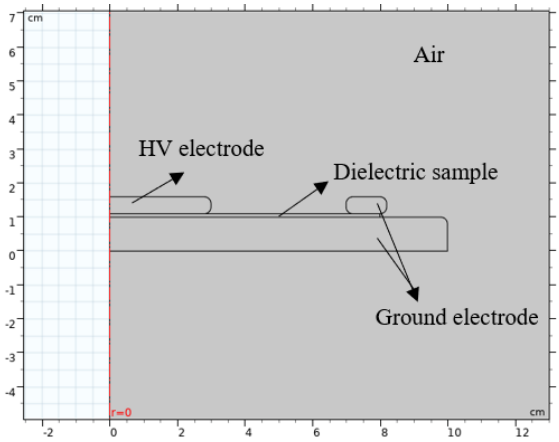

Figure 6.2: Geometry of the surface discharge model setup in COMSOL Multiphysics [1].

electric potential of 10 kV is applied to the HV electrode. This value represents the maximum value of AC voltage and not the RMS (root mean square). The DC simulations are implemented using the electrical currents physics interface and a time dependent study. An electrical potential of the same 10 kV is applied to the HV electrode. The time dependent study is solved for steps of 10 ms, starting from 10 ms until 1 s. The major difference between the AC simulation implemented using the electrostatics physics interface and the DC simulation using the electrical current interface is the manner in which the electrical fields are deduced. In the AC case, the electrical fields are solved based on the gauss's law;

$$\nabla.D = \delta_v, D = \epsilon E \tag{6.4}$$

Where, D is the electrical flux density in C/m^2, E is the electrical field intensity in V/m, ϵ is the permittivity in F/m and δ_v is the volume space charge in C/m^3, if present. In the absence of space charge the Poisson's equation $\nabla^2 V = -\delta/\epsilon$ is reduced to zero based on the relation of electric field derived from the gradient of voltage, $E = -\nabla V$. Therefore, the pre-requisites for the prediction of electric field strengths over a given geometry under AC voltage is the permittivity of the dielectric ($\epsilon_r; \epsilon = \epsilon_o.\epsilon_r$) and the values of electrical potential (V).

In case of DC, the electrical currents physics interface solves for the equation of current continuity derived from the Ampere-Maxwell's law;

$$J = \sigma E + \frac{\partial D}{\partial t} \tag{6.5}$$

$$\nabla.J = Q_v \tag{6.6}$$

Where, J is the current density in A/m^2, σ is the electrical conductivity in S/m and Q_v the resultant volume charge density in C/m^3. The first term to the right in Eq. 6.5

depicts the conductive current, while the second term represents the displacement current as a result of the rate of change of the electrical flux density. The prerequisites for the implementation of a time-domain study for DC field estimation are the values of electrical conductivity (σ) and the electric potential (V). The electrical conductivity for the dielectric medium is implemented based on Eq. 6.7, in order to incorporate its dependency on temperature and electric field stress [6].

$$\sigma(T,E) = A.exp(\frac{-0.98q}{K_B T})\frac{sinh(2.7755 \times 10^{-7} \times |E|)}{|E|} \tag{6.7}$$

Where, A is a dimensionless variable value in the range of 3.2781×10^{11} that can be tuned to obtain the desired range of conductivity, T is the temperature in K, q is the value of elementary charge equal to 1.6×10^{-19} C and K_B is the Boltzmann constant equal to $1.38 \times 10^{-23}\ m^2 kg s^{-2} K^{-1}$.

6.3.2. Results and Observations

The resultant values of tangential electrical field stress along the air-dielectric interface is shown in Figure 6.3. Figure 6.3a gives the AC field distribution. It can be observed that the electrical field reaches a maximum value close to the triple-point (electrode-air-dielectric) which causes the local breakdown of the dielectric interface, producing surface PD.

The same arrangement is simulated for the DC case with the electrical conductivity of the dielectric (sample) implemented based on Eq.6.7. The sample's dielectric conductivity is chosen based on the maximum and minimum measured values presented in section 6.2 and based on these 4 different combinations/ cases are simulated as listed on Table 6.3. For case I, II and III the sample's electrical conductivity (volumetric) is chosen to be in the range of 5×10^{-15} S/m and the electrical conductivity of the surrounding air medium is changed using the parameter sweep feature in COMSOL. The conductivity of air varies over a wide range between 10^{-13} to 10^{-9} S/m based on the location, humidity, composition and several other variables [7]. The DC field in Figure 6.3b is simulated for three cases of $\sigma_{air} = [10^{-13}, 10^{-12}, 10^{-11}]$ S/m. The results presented are all at steady state when the electrical field reaches the stable DC field distribution. And the DC field distribution can be determined by plotting the field transition over time. Figure 6.4 demonstrates this process by plotting the transition of the electrical field from capacitive to resistive field for case II. Alternatively, it is also possible to plot the maximum of the tangential field component over the dielectric interface as a function of time to observe the change. This is shown in Figure 6.5 where the field value reaches steady state around 1000 s.

A stark contrast is observed in the electrical field distribution over the dielectric surface in the AC and DC cases. For the given simulated configuration, the DC field distribution shows a much softer peak around the triple-point and a much elevated field stress close to the ground electrode with respect to the AC case. Additionally, along with the results of the surface charge distribution for the respective cases (I, II and III) presented in Figure 6.6, the following observations can be made:

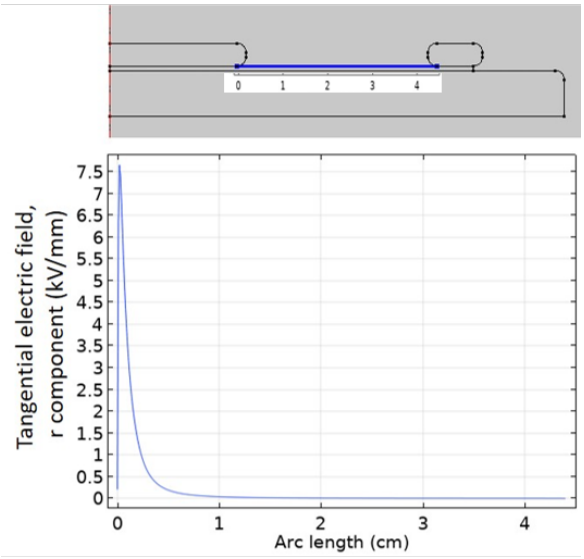

(a)

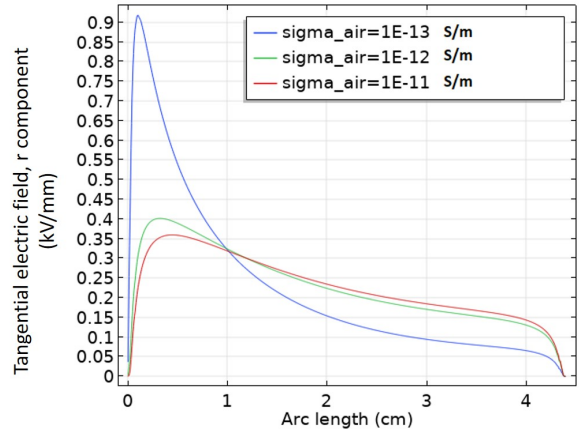

(b)

Figure 6.3: Plot of tangential electrical field along the dielectric interface (highlighted in the image above) under (a) AC and (b) steady state DC voltage stress conditions for sample conductivity, $\sigma_d = 5 \times 10^{-15}$ S/m and air conductivity as indicated on figure label [1].

- The lower the disparity in the resistivities of the two media (air and solid), the lower is the surface charge accumulation.
- The electrical field along the interface increases with increasing the resistivity of the surrounding air media (reducing the disparity between the resistivities

Table 6.3: Simulation results of the surface discharge model under DC field conditions.

Electrical conductivity of Air (σ_{air}) in S/m	Electrical conductivity of dielectric sample (σ_d) in S/m	Max. tangential electrical field stress E_{tan} in kV/mm	Max. surface charge density at 10 mm (arc length) in nC/cm^2	Approximate time to steady state
Increasing the resistivity of surrounding air medium with high resistive sample:				
Case I: 1×10^{-11}	5×10^{-15}	0.36	14	~ 4 s
Case II: 1×10^{-12}	5×10^{-15}	0.40	13.3	~ 16 min
Case III: 1×10^{-13}	5×10^{-15}	0.92	9	~ 1 h 40 min
Low resistivity of surrounding air with low resistive sample:				
Case IV: 1×10^{-11}	5×10^{-12}	3.6	2.1	~ 15 s

of the two media).

In other words, the extreme differences in resistivities of the interfacial media lead to charge retention on the dielectric surface which in turn opposes the applied electrical field and lowers the tangential electrical field stress which is the cause of the surface PD. An additional inference could be made regarding the time taken to reach steady state/ DC field distribution. High surface resistivities lead to large RC constants and hence longer time to DC resistive fields. This parameter gives very useful information regarding the waiting time (also known as charging time).

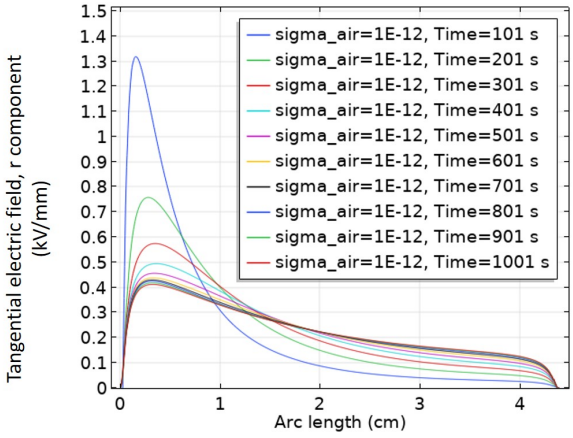

Figure 6.4: Tangential electrical field distribution plotted along the dielectric interface with sample conductivity, $\sigma_d = 5 \times 10^{-15}$ S/m and air conductivity $\sigma_{air} = 1 \times 10^{-12}$ S/m under DC stress at specified time instances [1].

Case IV involves the simulation of a dielectric with higher electrical conductivity ($\sigma_d = 5 \times 10^{-12}$ S/m and $\sigma_{air} = 10^{-11}$ S/m) to demonstrate the lowered waiting times. The resultant electrical field stress and the surface charge density are presented in Figure 6.7 and Figure 6.8 respectively. It can be observed that the tangential electrical field over the air-dielectric interface has predominantly increased (x4) and the distribution now resembles closely the AC field distribution though the intensity is still half that of the AC case. Nevertheless, unlike Case III, the time to

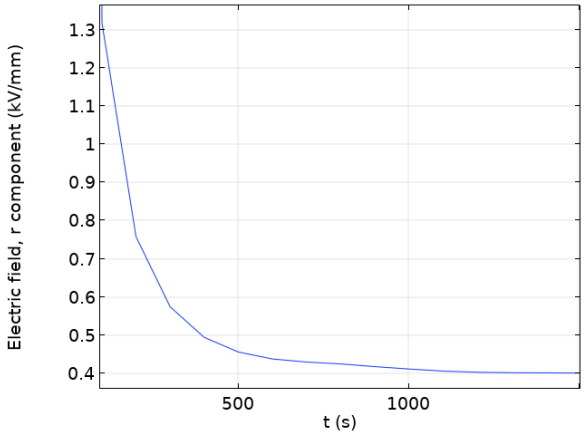

Figure 6.5: The maximum value of tangential electrical field component over the dielectric interface with sample conductivity, $\sigma_d = 5 \times 10^{-15}$ S/m and air conductivity $\sigma_{air} = 5 \times 10^{-12}$ plotted as a function of time [1].

DC steady state is now lowered as expected due to the smaller RC time constant.

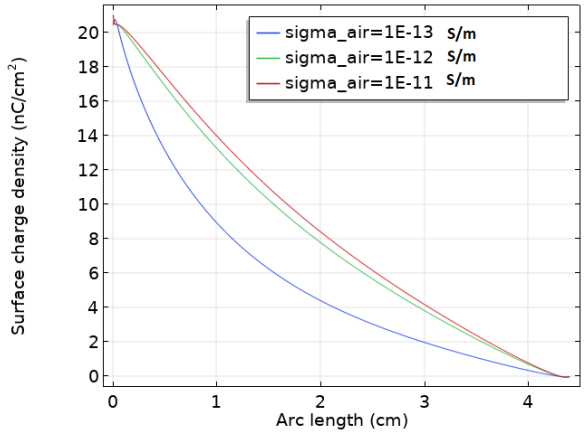

Figure 6.6: Plot of surface charge density on the air-dielectric interface under DC stress conditions for sample resistivity, $\sigma_d = 5 \times 10^{-15}$ S/m [1].

6.4. Partial discharge testing of surface defect model

The surface discharge tests are carried out under both AC and DC (positive and negative polarity) voltage stress. The defect arrangement used for both cases re-

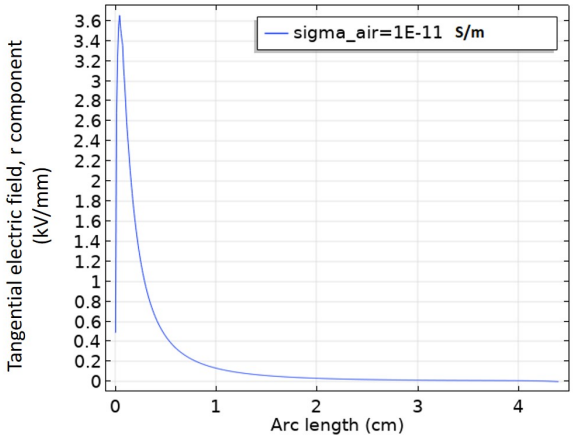

Figure 6.7: Plot of tangential electrical field along the air-dielectric interface under DC voltage stress conditions for low resistive sample [1].

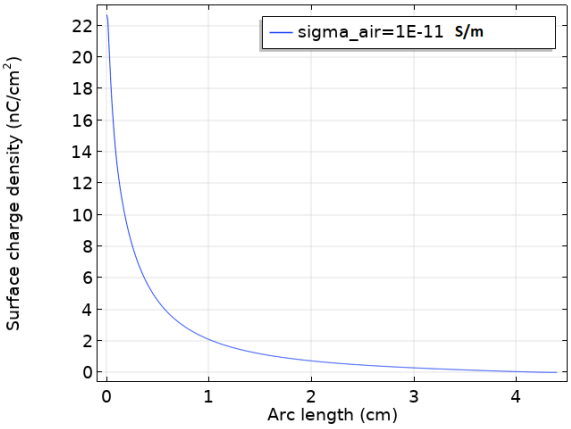

Figure 6.8: Plot of surface charge density over the air-dielectric interface under DC stress conditions for low resistive sample [1].

mains the same while the measuring circuit is modified as described in Chapter 3. The following subsections describe the results and observations of the tests.

6.4.1. AC test

The AC-PD tests are carried out prior to the DC tests to confirm the presence and behavior of the PD defect based on the well-known PRPD patterns. In this specific case, since goal of the research is to study DC partial discharge process using pulse sequences, the AC discharge raw data is also sampled in a similar manner. This is done so as to be able to generate the same set of plots that are used in the study

of DC discharges.

Based on the recursive testing of several dielectric samples, it could be concluded that with increasing test voltage, all dielectric samples begin to exhibit surface discharge (when the localized tangential electrical field exceeds the breakdown field strength). The PD inception voltage and the discharge magnitude differ with different samples. However, the PRPD pattern remains similar. The PRPD pattern of surface discharge tests on the resin impregnated transformer pressboard (Sample D) is shown in Figure 6.9. The PRPD plots have been displayed in a unipolar format to demonstrate the symmetrical discharge peaks on both voltage half-cycles. The discharge progression for the respective case, along with the plot of charge vs. voltage is shown in Figure 6.10. Figure 6.10a plots the variation of discharge magnitude corresponding to the test voltage as a function of time. The values of discharge magnitude are presented in a special format that is specific to AC PD and prescribed by the IEC 60270 [8] known as Q_{iec}. It is the peak value of discharge (Q_{pk}) recorded at the time instance as a function of a defined pulse train response. The plots in Figure 6.10 present both values, Q_{iec} and Q_{pk}. The discharge magnitude in the particular test case quickly increases to very high nC levels and hence the voltage steps are limited.

The PD raw data is sampled through the externally connected oscilloscope and the pulse sequence analysis (PSA) plots are developed for the case. The resultant PSA plots are shown in Figure 6.11 along with a sample of the pulse stream of the discharge process. Multiple clusters are seen over the PSA plot of Δt_i vs. ΔQ_i and Δt_{i+1} vs. Δt_i. These arise due to the 20 ms voltage cycle. The absence/reduced number of pulses on the declining/falling edge of the voltage cycle creates this clustering. The PSA plots involving discharge magnitude have been developed by taking into consideration the polarity of the discharge pulse. A detailed commentary on the plots in relation to the respective DC plots is given in section 6.4.2.

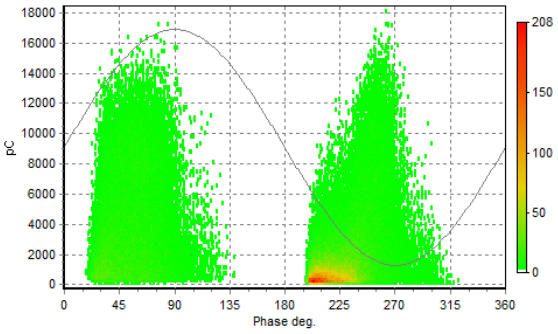

Figure 6.9: The PRPD pattern of the surface discharge defect of the resin impregnated pressboard- sample D [1].

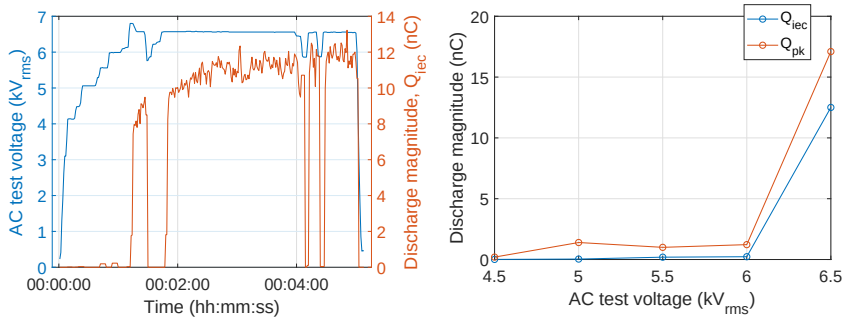

(a) (b)

Figure 6.10: (a) The discharge (PD) progression of a surface defect (sample D) and (b) the plot of charge vs. applied voltage in the respective case under AC stress [1].

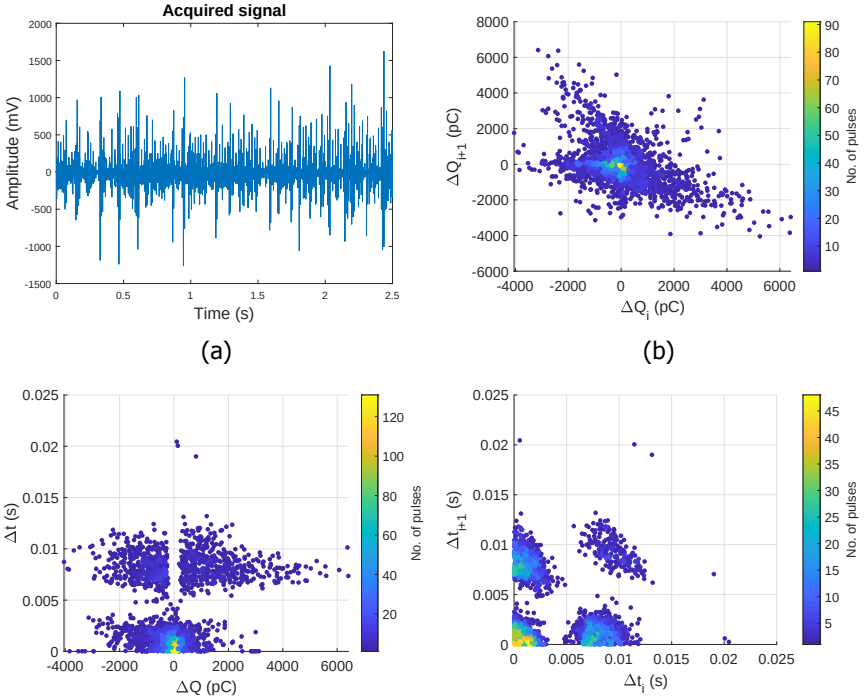

(a) (b)

(c) (d)

Figure 6.11: The results of surface discharge measurement under AC voltage for sample D (a) pulse stream, plot of (b) ΔQ_{i+1} vs. ΔQ_i, (c) Δt_i vs. ΔQ_i and (d) Δt_{i+1} vs. Δt_i [1].

6.4.2. DC tests

The DC-PD tests were performed on the different dielectric samples listed in Table.1. Not all samples exhibited surface discharge activity under DC stress. Based on the tests performed, samples A and C showed no discharge activity over the DC steady state (discharge pulses occur only during voltage ramps). Sample B shows declining PD activity, indicating a polarization current. This was also confirmed through the measurements made in section 6.2 , in which a slow polarization current is seen over a 30 min period. Hence, this cannot be considered as a stable and repetitive stage of discharge since the discharges fade out after the polarization phase is complete. Sample D which has the lowest electrical resistivity of them all exhibits the highest and most stable PD activity. Thus, this sample is chosen to study and understand the surface discharge process under DC with comparison to AC since it exhibits repetitive discharges with low waiting time (time lag). This section limits itself to the results of the DC-PD measurement on the resin impregnated pressboard sample (Sample D).

Negative DC test

The dielectric sample is stressed with negative DC voltage and the resultant pulse stream is recorded using the externally connected oscilloscope. A sample pulse stream is displayed in Figure 6.12a. The discharge pulses are all unipolar with a positive polarity. The discharge data is post-processed to derive the resultant pulse sequence plots as shown in Figure 6.12. While investigating for visible patterns, a unique distribution is seen on the PSA plot of time between discharges, Δt_{i+1} vs. Δt_i which distinctly resembles a fish. This plot on Figure 6.12d has been displayed on a logarithmic scale in order to visualize the distribution sufficiently.

Further, the defect progression in the respective case has been presented in Figure 6.13 along with the plot of charge vs. voltage. From Figure 6.13b, a near linear (increasing) trend in charge magnitude with increasing voltage can be observed. This is similar to the AC discharge trend, where the discharge magnitude increases with each increasing voltage step.

Positive DC test

The DC-PD tests are repeated on sample D under positive DC voltage. An identical procedure as described in section 6.4.2 is followed. The results of the tests are presented in Figure 6.14. The discharge pulses are all negative in polarity and the form of the PSA plots presented in Figure 6.14 is similar to the ones obtained in the negative DC case. However, from Figure 6.15b which presents the plot of charge vs. voltage it can be observed that though the discharge magnitude follows an increasing trend with increasing voltage, the rate of increase is very small. The discharge magnitude is less than 30 pC up to 25 kV_{dc}. The form of the PSA plot of time between discharges presented in Figure 6.14d though slightly different from the negative DC case still looks uniquely distinguishable.

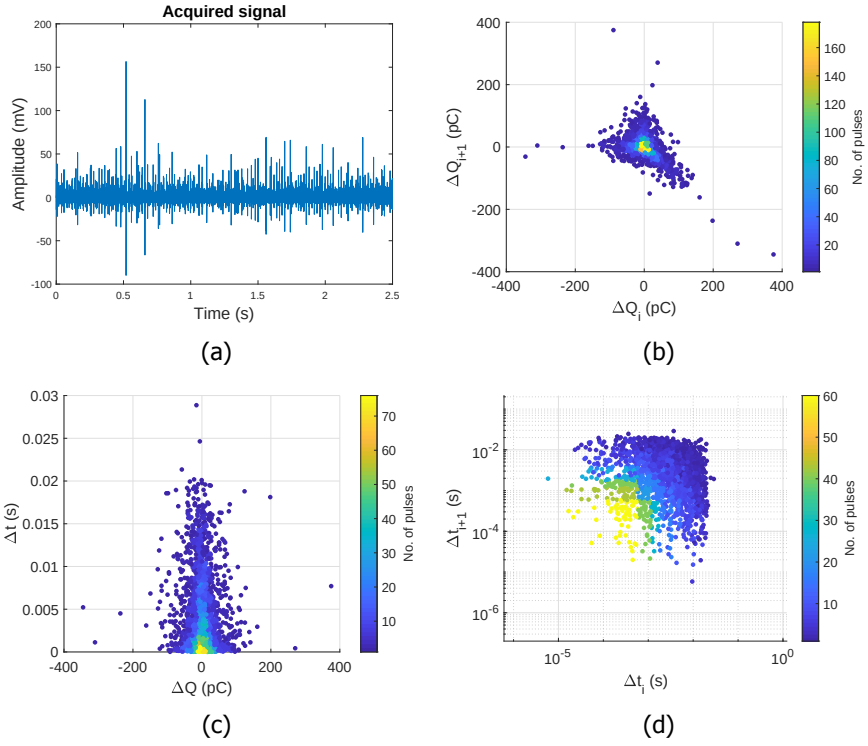

Figure 6.12: The results of surface discharge measurement under negative DC voltage for sample D (a) pulse stream, plot of (b) ΔQ_{i+1} vs. ΔQ_i, (c) Δt_i vs. ΔQ_i and (d) Δt_{i+1} vs. Δt_i [1].

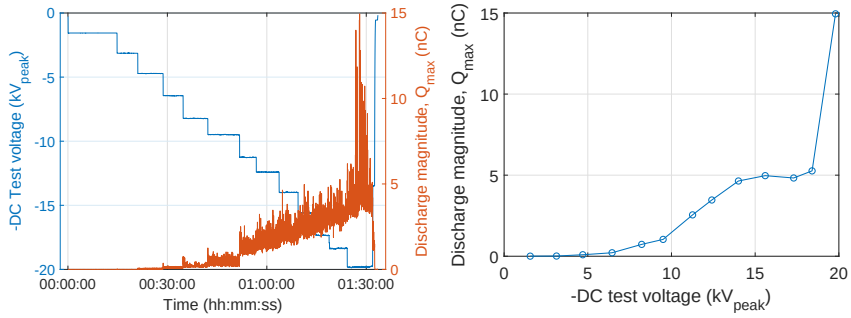

Figure 6.13: (a) The discharge (PD) progression of a surface defect (sample D) and (b) the plot of charge vs. applied voltage in the respective case under negative DC stress [1].

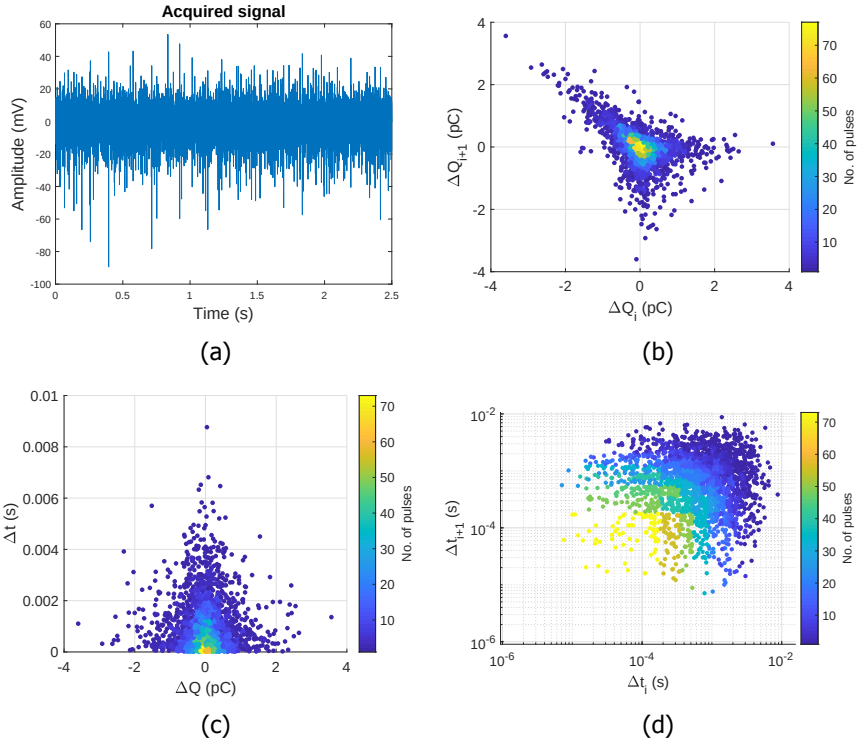

Figure 6.14: The results of surface discharge measurement under positive DC voltage for sample D (a) pulse stream, plot of (b) ΔQ_{i+1} vs. ΔQ_i, (c) Δt_i vs. ΔQ_i and (d) Δt_{i+1} vs. Δt_i [1].

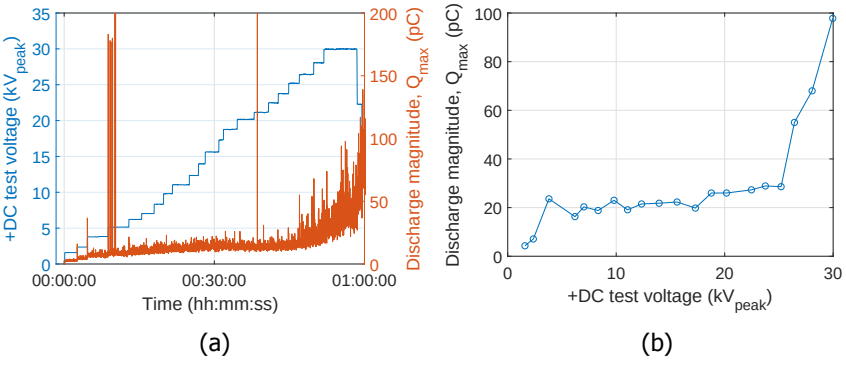

Figure 6.15: (a) The discharge (PD) progression of a surface defect (sample D) and (b) the plot of charge vs. applied voltage in the respective case under positive DC stress [1].

Observations on DC Surface discharge

Based on the results of the DC-PD tests the following observations can be made:

(i) There is a disparity in the discharge magnitude under +DC and -DC i.e. the discharge magnitude under -DC is higher than +DC. This phenomenon can be based on the theories of dielectric barrier discharge (DBD or surface discharge) found in literature. In [9], studying the mechanism of a single dielectric barrier plasma actuator, C.L. Enloe et al. describe the surface discharge process as quoted below;

"The DBD can maintain such a discharge because the configuration is self-limiting... To maintain a DBD discharge, an ac applied voltage is required. Figure 6a illustrates the half-cycle of the discharge for which the exposed electrode is more negative than the surface of the dielectric and the insulated electrode, thus taking the role of the cathode in the discharge. In this case, assuming the potential difference is high enough the exposed electrode can emit electrons. Because the discharge terminates on a dielectric surface, however (hence the term "dielectric barrier"), the build-up of surface charge opposes the applied voltage, and the discharge shuts itself off unless the magnitude of the applied voltage is continually increased. The behaviour of the discharge is similar on the opposite half-cycle: a positive slope in the applied voltage is necessary to maintain the discharge. In this half-cycle, the charge available to the discharge is limited to that deposited during the previous half-cycle on the dielectric surface (which now plays the role of the cathode) …"

Similarly, [10] defines the term 'back discharges' describing that the negative charges generated by the original surface discharge that propagate backwards to the electrode when the potential of the electrode drops.

Therefore, based on [9][10], the actual surface discharge current is actually the electron current flowing during the negative half of the AC wave. The discharge pulses seen on the positive half is the return current arising from the electrons deposited on the surface in the previous negative half-wave. Which would explain the increased discharge magnitude in the case of -DC stress and very low discharge magnitude under +DC. The pulse recorded under +DC could even be classified as the result of impact ionization at the positive electrode instead of the surface current. Figure 6.16 shows the stark difference in the charge distribution over the two voltage polarities of DC. While the same sample when tested under AC stress shows an almost similar charge distribution under both positive and negative half-cycles of the AC sine wave, as can be seen in Figure 6.16. As C.L. Enloe et al. mentions, surface discharges are self-limiting and therefore need an AC voltage to sustain. Which implies that repetitive DC discharge is only possible when the dielectric surface/interface has a higher conductivity which inhibits surface charge accumulation.

(ii) Not all dielectric samples exhibit surface discharge under DC stress as they hold large surface charge which reduces the tangential component of the electrical field.

The argument made in (i) based on the self-limiting nature of the discharge is an explanation to the absence of surface PD activity in several other dielectric samples which have higher resistivities. As these samples exhibit high surface

charge accumulation it limits the surface discharge activity as it opposes the applied electric field stress.

(iii) The unique 'fish' shaped pattern in the PSA plot of time between discharges (Δt_{i+1} vs. Δt_i).

The DC surface discharge tests on the dielectric samples have revealed a distinct pattern in the plot of Δt_{i+1} vs. Δt_i which resembles closely a fish like pattern as shown in Figure 6.17. Although this is a valuable visual tool in defect identification, the properties of the distribution can be explained using the WePSA (Weighted PSA) plots that were introduced in [11]. The shape of the distribution in Figure 6.17 is reflected in the WePSA plot of W vs. ΔQ where the angle intercepts between the lower (x-axis) and upper tangents gives the dispersion in the value of Δt. While the slope of the lower and upper tangent gives the value of smallest and largest values of Δt. In the case of the surface defect, the value of Δt goes from a very small value (the lower tangent almost incident with the x-axis) to a certain value of $\Delta t = x$. This randomized distribution of the pulses over time is what creates the fish like pattern when translated to the PSA plot of Δt_{i+1} vs. Δt_i. The WePSA plots are introduced and described in detail in the next chapter.

6.5. Surface defect: Similarities between AC and DC patterns

Based on the observations presented in section 6.4.2, the surface discharge process in principle is the movement of the negative charge/electrons during the negative half-cycle in case of AC or negative polarity in case of DC. The discharge mechanism by itself is not exclusive to AC or DC. It relies on the excess tangential electrical field that causes a partial breakdown over the dielectric interface. This implies that the pulse sequence plots for the two cases should be similar if not identical since the underlying physics remains the same. Therefore, this section investigates the possibility of unifying the patterns under both cases to verify the claim. The two major inconsistencies between the AC and DC discharge stream is the clustering of the pulses over the rising edge of the voltage sine wave and its bipolar nature. To unify the two cases, the AC surface discharge raw data/pulse stream is modified to represent a DC pulse stream. As the graphical depiction in Figure 6.19 shows, the original pulse stream has discharge pulses distributed predominantly over the rising edges of the voltage wave. Firstly, the time between these two clusters on successive half-cycles is removed in step 1 through an algorithm that recognizes the last negative pulse on the positive half-wave and the first positive pulse on the negative half-wave. In step 2, all the pulses are made unipolar (with a positive polarity in this case).

The PSA plots are developed based on the modified PD data, Figure 6.20 shows the resultant plots. It can be observed that the distribution becomes very similar to the DC PSA plots presented in Figure 6.12. This verifies the claim made in the

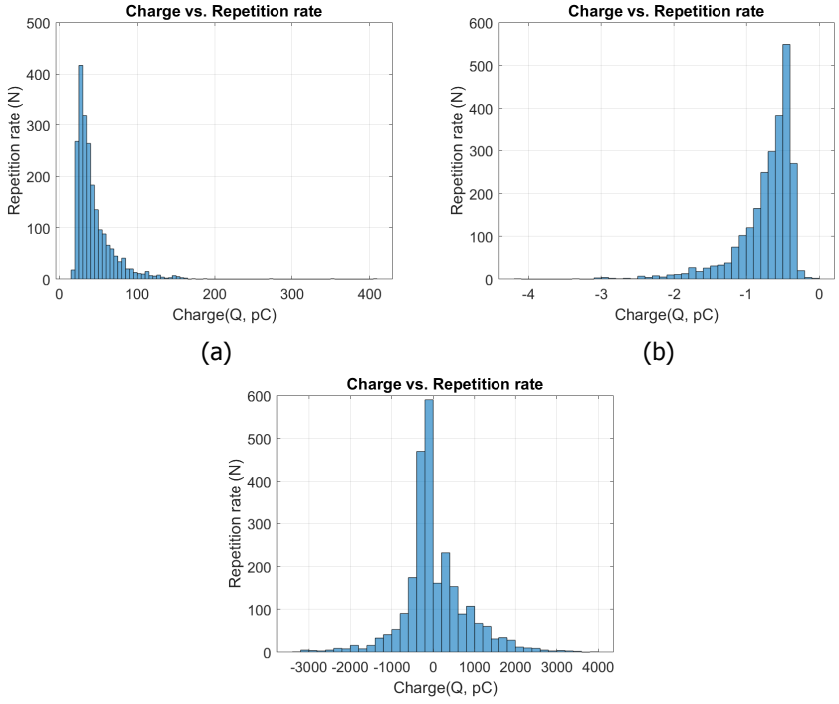

Figure 6.16: Histogram of repetition rate (*N*) of charge (*Q*) for the surface discharge tests under (a) -4.7 kV_{dc} (b) +3.8 kV_{dc} and (c) 6.5 $kV_{ac,RMS}$ [1].

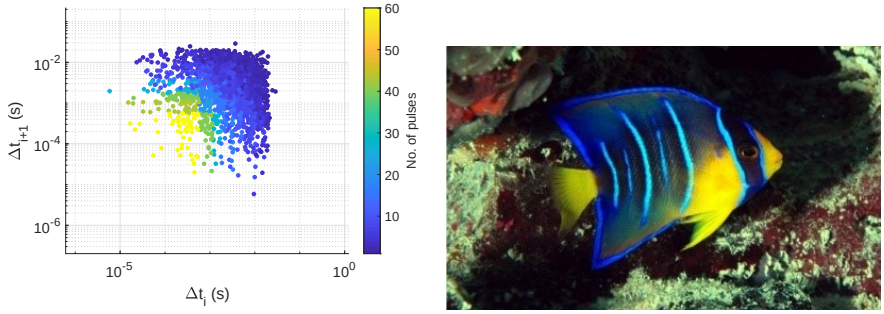

Figure 6.17: The PSA plot of surface PD under -DC stress and its resemblance to an Angel fish [12], [1]

beginning of the section that the surface discharge phenomenon in the AC and DC case are not exclusive but share the same underlying discharge process and hence

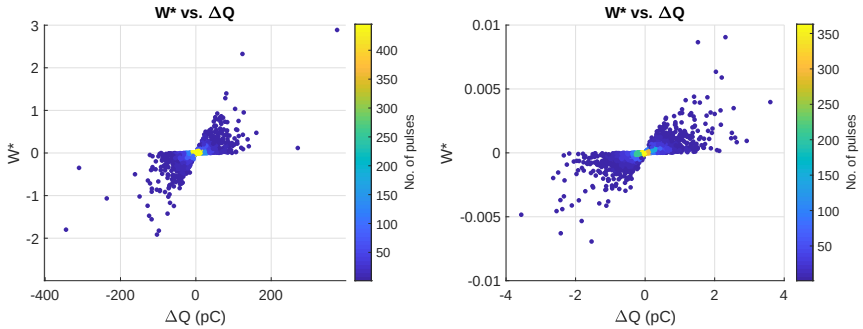

Figure 6.18: The WePSA plots for surface discharge, W vs. ΔQ under (a) -DC and (b) +DC [1].

still remain comparable.

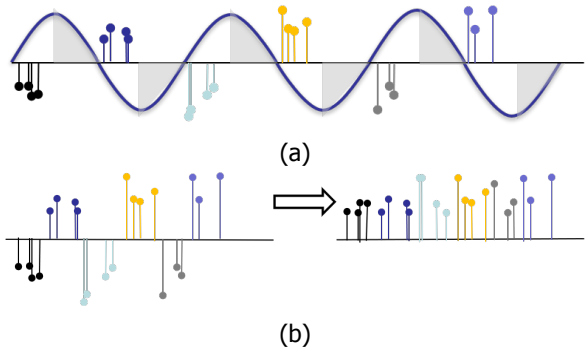

Figure 6.19: (a) A depiction of the partial discharge pulse stream over the AC voltage cycle, (b)(left) the modified pulse stream by removing/ignoring the time between the voltage half-cycle with no discharge pulses and (b)(right) the further modified pulse stream with unipolar pulses obtained by ignoring the pulse polarity [1].

6.6. Conclusion

This investigation on the surface discharge phenomenon under DC stress is conducted with the final goal of providing tools for defect identification under HVDC. The research approaches the problem by studying the DC defect in order to identify dominant features that are representative of the underlying discharge mechanism rather than investigating deeply on the final patterns alone. The systematic approach to study the electrical properties of the dielectric samples under test and

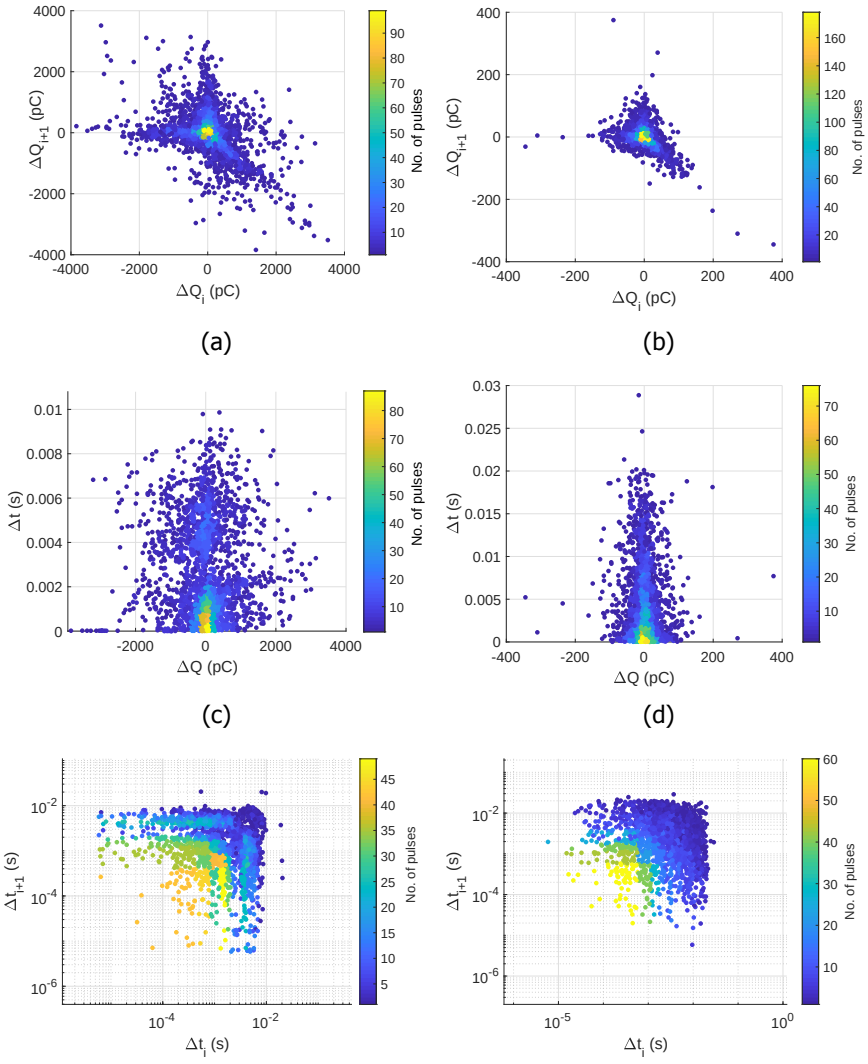

Figure 6.20: The results of surface discharge measurement on sample D under AC voltage after modification (left:(a), (c) and (e)) of the pulse stream compared to the results of the surface discharge measurement under Negative DC voltage (a) and (b) ΔQ_{i+1} vs. ΔQ_i, (c) and (d) Δt_i vs. ΔQ_i, (e) and (f) Δt_{i+1} vs. Δt_i [1].

to later simulate the field conditions and time to DC steady state for generic cases provide valuable explanation to the observed discharge phenomenon during the PD testing phase.

The research also studies the AC surface discharge patterns not just based on its correlation/variation with the AC sine wave (PRPD patterns) but based on the pulse sequence within each half-cycle of the voltage wave. For the DC defects with stable and repetitive discharges, the striking similarities between the AC and DC PSA patterns reveal that the surface discharge mechanism under DC stress is not exclusive but rather similar to the AC discharge process. However, additional parameters that need further investigation are the surface charge density/holding capacity and time to steady state that heavily influence the repeatability/rate of DC-PD. Nevertheless, this research demonstrates that in case of a measurable and repetitive surface discharge source as in the case of the resin impregnated pressboard, the DC pulse patterns resemble a unique 'fish' like pattern over the PSA plot for time between discharges (Δt_{i+1} vs. Δt_i).

During the course of the investigation, a great deal of variation with respect to the DC-PD activity was observed with various dielectric samples under study. One interesting feature that may serve as a future point of investigation is the selectivity of the dielectric sample to exhibit DC-PD activity that follows the DC ripple of the applied voltage.

references

[1] **S. Abdul Madhar**, A. Rodrigo Mor, P. Mraz, and R. Ross. "Study of DC partial discharge on dielectric surfaces: mechanism, patterns and similarities to AC". In: *International Journal of Electrical Power and Energy Systems* 126 (Mar. 2021), p. 106600. issn: 0142-0615. doi: 10.1016/j.ijepes.2020.106600.

[2] S. Boggs, D. H. Damon, J. Hjerrild, J. T. Holboll, and M. Henriksen. "Effect of insulation properties on the field grading of solid dielectric DC cable". In: *IEEE Transactions on Power Delivery* 16.4 (2001), pp. 456–461. issn: 08858977. doi: 10.1109/61.956720.

[3] T. Christen. "Characterization and robustness of HVDC insulation". In: *Proceedings of IEEE International Conference on Solid Dielectrics, ICSD*. 2013, pp. 238–241. isbn: 9781479908073. doi: 10.1109/ICSD.2013.6619804.

[4] Standard IEC 62631-3-1:2016. *Dielectric and resistive properties of solid insulating materials- Part 3-1: Determination of resistive properties (DC methods)- Volume resistance and volume resistivity- General method*. International Electrotechnical Commission (IEC), 2016.

[5] Standard IEC 62631-3-2:2015. *Dielectric and resistive properties of solid insulating materials- Part 3-2: Determination of resistive properties (DC methods)- Surface resistance and surface resistivity*. International Electrotechnical Commission (IEC), 2015.

[6] **S. Abdul Madhar**, M. Brunner, A. Rodrigo Mor, and P. Mraz. "Measurement of key dielectric properties for surface PD model under HVDC". In: *Proceedings of International conference on Dielectrics, ICD*. Valencia: IEEE, 2020.

[7] E. Seran, M. Godefroy, E. Pili, N. Michielsen, and S. Bondiguel. "What we can learn from measurements of air electric conductivity in222Rn-rich atmosphere". In: *Earth and Space Science* 4.2 (2017), pp. 91–106. issn: 23335084. doi: 10.1002/2016EA000241.

[8] Standard IEC 60270. *High-voltage test techniques–Partial discharge measurements*. International Electrotechnical Commission (IEC), 2000.

[9] C. L. Enloe, T. E. McLaughlin, R. D. VanDyken, K. D. Kachner, E. J. Jumper, T. C. Corke, M. Post, and O. Haddad. "Mechanisms and Responses of a Single Dielectric Barrier Plasma Actuator: Geometric Effects". In: *AIAA Journal* 42.3 (2004), pp. 595–604. issn: 00011452. doi: 10.2514/1.3884.

[10] A. Kumada, M. Chiba, and K. Hidaka. "Potential distribution measurement of surface discharge by Pockels sensing technique". In: *Journal of Applied Physics* 84.6 (1998), pp. 3059–3065. doi: 10.1063/1.368460.

[11] **S. Abdul Madhar**, P. Mraz, A. Rodrigo Mor, and R. Ross. "Empirical analysis of partial discharge data and innovative visualization tools for defect identification under DC stress". In: *International Journal of Electrical Power & Energy Systems* 123 (Dec. 2020), p. 106270. issn: 01420615. doi: 10.1016/j.ijepes.2020.106270.

[12] Keywestaquarium.com. *Most Common Fish in the Florida Keys*. 2020. url: https://www.keywestaquarium.com/common-fish-florida-keys.

7

Defect Identification under DC: Corona, Floating and Surface defect

This chapter presents several approaches to the analysis of partial discharge (PD) data. In the previous chapters, three common defects namely corona, floating electrode and surface discharge were studied in depth. Based on the findings of these chapters combined with modern, existing data processing tools, the available information is analysed with the final goal of defect identification under DC stress conditions. One of the major concerns when it comes to DC-PD testing, is its non-repetitive/erratic pulse pattern. This chapter, however, only deals with the analysis of repetitive stages of discharge that will allow the study of their resultant patterns and trends. The chapter first introduces the analysis through visual tools such as the well-known PSA patterns. It also describes in which way a three-pulse PSA diagram cannot serve as a stand-alone figure and hence requires a change in perspective by either adding or reducing a dimension. In order to improve the visual recognition possibility of such a plot, a weighted scale is proposed, introducing the innovative Weighted PSA or the WePSA diagrams which are more intuitive and provide a clear distinction between various defects. The chapter also investigates a defect identification scheme based on statistical classification of discharge parameters. Several unique features such as the formative trend in the probability plot of time between discharges for the three common defect types show promise in the quest for defect identification under DC. The discharge trend with voltage also referred to as the Q(V) plot or Q-V plot are also presented for all three defects. The last part of the chapter presents a test methodology to identify the discharge source based on the acquired

Parts of this chapter have been published in Elsevier's International Journal of Electrical Power and Energy Systems, **123**, (2020), 106270, ISSN 0142-0615, https://doi.org/10.1016/j.ijepes.2020.106270 [1]

knowledge on various discharge features.

7.1. Introduction

Partial discharge (PD) testing has become an indispensable tool in type testing and quality certification for AC applications in the past decades. It has come to be a part of several international standards such as the IEC, IEEE and other European standards. With the global boom of HVDC transmission, a similar application of PD under DC stress is a popular prospect. Though the relationship between PD levels under DC and ageing or quality is not very well-known yet, the ability to verify a system's fitness or quality through PD testing is treated with great anticipation. It is a known fact that the discharge activity under DC is more complex than AC. The charge transport mechanism under DC is influenced by several properties of the surrounding material media. Some influencing factors are conductivity, temperature, humidity, material bonding/structure, surface roughness, electron-traps and its associated energy. For the design of DC high voltage (HV) components, material properties, their DC response and a complete knowledge of the transition stages (during turn-on, turn-off and polarity reversal) are a pre-requisite [2]. Some stray discharge pulses may perhaps occur on DC-PD tests that are not concerned with PD activity associated with any defect but only from space-charge or other external factors. Hence these are often ignored. The standard IEC 65700-19-03:2014 for DC bushings only sets a limit on the number of pulses in the last 30 min of the 2-hour test [3]. The interim Cigre report of WG D1.63 explicitly states that the state-of-the-art, up to now can detect and barely differentiate between stray pulses and real PD but cannot yet perform defect identification or risk assessment through partial discharge tests under DC [4].

So far, the most popular means of studying and characterizing insulation defects under DC has been through Pulse Sequence Analysis (PSA) of the partial discharge pulses. It was first introduced by Hoof and Patsch in 1995 to study PD induced ageing under DC [5]. In later years, some other statistical parameters were studied with the object of creating unique defect fingerprints under DC [6][7]. Nevertheless, the fingerprints presented have failed to match the effectiveness of the Phase Resolved PD (PRPD) plots which revolutionized the AC asset diagnostic and maintenance business [8]. Research on DC partial discharges has either focused on the study and understanding of the discharge mechanism or purely on its statistical classification alone. They both lead to interesting results but do not provide a direct solution to defect identification. Therefore, this chapter presents different approaches to partial discharge defect identification under DC stress conditions through various empirical analysis of the discharge data. The in-depth study of the individual defects presented here were conducted prior to the analysis in order to determine which discharge stage strongly represents the defect nature/character [9][10]. Characteristic features of every defect type were identified and are further used in this research to generate visual patterns for defect recognition. The PD raw data (pulse stream) has been established to have contained discharge pulses only from a single defect with the help of additional optical measurements as were described in [10]. The goal of the contribution is to suggest means of DC defect identification that are both perceptive and practical. Table 7.1 lists the various different defects that were included in the analysis and details about the sampled

Table 7.1: Details of the stream length and no. of pulses for each defect type.

Defect type	Test voltage (kV_{dc})	Recording time (s)	No. of pulses
Pos. corona	6.5	2.5	1239
Neg. corona	8.7	0.23	30000
Surface	+6.8	120	1023
(sample A)	-6.5	120	908
Surface	+3.8	2.5	2484
(sample B)	-4.7	10	2175
Floating electrode	+29.5	2.5	532
	-29.5	5	10253

data such as time of recording and the number of pulses within the recorded data stream. The surface discharge measured with two different samples, A and B is relevant to section 7.3. Sample A is a polyethylene based material and sample B is resin impregnated pressboard. In all other sections, the results presented for surface discharge defect pertain to sample B alone.

7.2. Analysis based on visual patterns

Visual patterns are the most powerful since they directly interact with the human eye which is trained for pattern recognition and easily open to interpretation. However, the shape, contrast and the contours or shape of the visual patterns play an important role in their recognition. Visual images with same contours and different scaling and contrast for example may be indistinguishable in comparison to a visual pattern with the same scaling and contrast but different contours. Therefore, this section explores the various possible visual patterns that can be used for PD defect identification under DC stress. It weighs in the factor for easy user comprehension based on the simplicity and unambiguity of the plot.

7.2.1. PSA patterns

The plots of ΔQ_{i+1} vs. ΔQ_i and Δt_{i+1} vs. Δt_i (3-pulse PSA) commonly referred to as PSA plots often appear to have the same outlines/shapes for several defect types. For instance, the PSA plot for negative corona and surface discharge on positive DC shown in Figure 7.1 appear nearly identical. However, both the discharge scenarios are dissimilar from each other and follow a unique discharge process. The advantages and possible alternative solutions to this are evaluated in this section.

The PSA plot of ΔQ_{i+1} vs. ΔQ_i, plots the variation in discharge magnitude with no information about the pulse rate or time between the respective pulses. Similarly, the PSA plot of Δt_{i+1} vs. Δt_i plots the variation in time between discharges but with no information on the discharge magnitude of these respective pulses. On the contrary, a 2-pulse PSA, plot of Δt vs. ΔQ, includes both the quantities of change

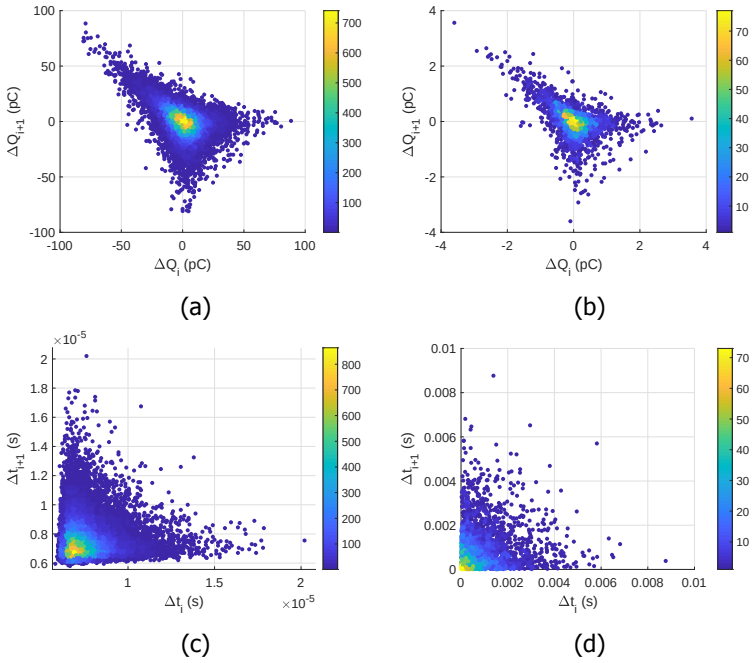

Figure 7.1: The PSA plots of ΔQ_{i+1} vs. ΔQ_i for (a) negative corona and (b) positive surface discharge and Δt_{i+1} vs. Δt_i for (c) negative corona and (d) positive surface defect. These heatmap show the density of pulses [1].

in discharge magnitude and pulse rate. However, is limited to the pulse sequence information of just two successive pulses. Therefore, if the goal is to represent the pulse sequence information of three successive pulses, the PSA plots of change in discharge magnitude and time need to be considered together to create a complete three dimensional (3-D) image as illustrated in Figure 7.2. This would show each of the plots with a unique distribution without omitting the information of either quantities. For instance, the plots of negative corona (Configuration IV has been used for the following illustration) and positive surface discharge shown in Figure 7.1 are combined to form the three-dimensional PSA in Figure 7.3

It can be seen that the pulse distributions in 3-D are distinct from one and other. In order to highlight the difference, the curve-fitting tool in MATLAB is used to plot a plane for the given pulse distribution using a second order polynomial equation. The plane is not used to fit the data accurately but to demonstrate the differences in the density of the data on the two plots. The coefficients of the polynomial used in this process are presented in Table 7.2.

The phenomenon of partial discharge like any other in nature exhibits regularities in its characteristics but not absolute congruence. The goal of its analysis should be to highlight or magnify the underlying regular pattern while minimizing the effect of outliers. However, the 3-pulse PSA tries to look into great detail towards the

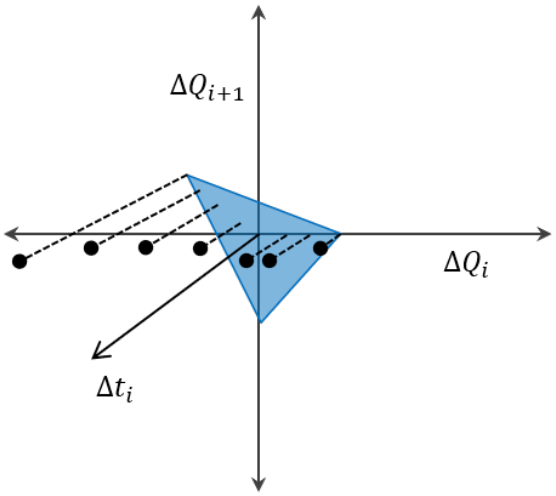

Figure 7.2: Illustration of the three-dimensional PSA [1].

sequence in which the amplitudes of the pulses have emerged or the manner of evolution of pulse rate. This magnifies the differences in the pulse stream creating a chaotic pattern in many cases. For instance, the corona discharge is the most stable in terms of magnitude of charge and repetition rate. Instead of seeing a narrow scatter over a mean value, the 3-pulse PSAs in Figure 7.1 displays an elaborate distribution. Seeming to reveal that the difference in pulse magnitudes change over a range of 0 to $\pm$100 pC (taken from the vertex of Figure 7.1a). The magnitude variation of 100 pC might have taken place in a small percentage of the total pulses while the majority of the pulses were close to each other in magnitude. This needs careful examination by looking at the heat map of the plot and interpreting the density of pulses in each range. The three-dimensional PSA on the one hand is complete and distinctive for various PD defects while on the other hand is complex to interpret and lacks intuitiveness. The 3-D plot suffers an added disadvantage as the three-dimensional plot also requires higher graphical processing power for its rendering and display. Therefore, due to the high level of complexity an alternative plot with weighted charge/time variables on the plot axis is proposed in the next section. The goal is to reach a level of effectiveness and simplicity comparable with the PRPD diagrams in AC where the outline/shape of the pattern is sufficient to distinguish various dielectric defects. Instead of requiring expert examination of multiple aspects prior to identification of defect type.

7.2.2. Weighted PSA or WePSA patterns

As described in section 7.2.1, the 3-pulse PSA plots cannot be used as stand-alone plots since they either lack information on time or magnitude of charge. In order to have information on both change in time and change in charge magnitude on the

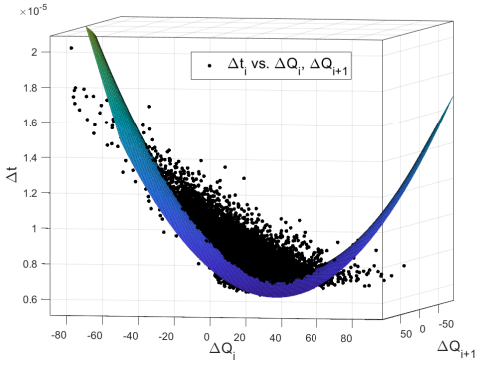

(a)

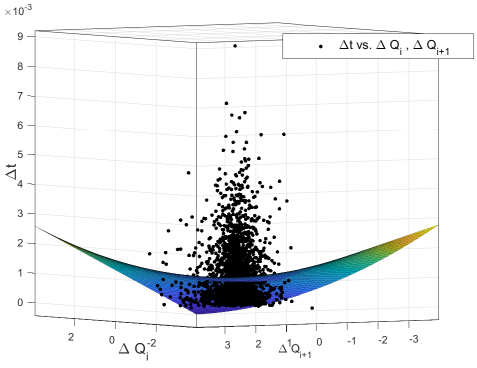

(b)

Figure 7.3: The three-dimensional PSA plots of (a) negative corona and (b) positive surface defect [1].

same plot one of the plot axis is used to represent a weighted quantity (represented by the variable *W*). The plot also helps minimize the effect minor differences in the magnitude of discharge and discharge rate, and two plots are created, weighted with respect to time between discharges (W vs. Δt) and weighted with respect to change in discharge magnitude (W vs. ΔQ). The weighted quantity W is the product of the two quantities (ΔQ and Δt). It is derived as shown in Eq. 7.1.

$$W_{i=1\ to\ N} = \Delta Q_i \times \Delta t_i \tag{7.1}$$

Where N is the number of discharge pulses in the given recorded stream. As the weighted quantity is a product of two other pulse parameters, the plot helps minimize the effect minor differences in the magnitude and rate of the discharge. Only the extreme/large differences in magnitude and rate outline the pattern. The following sections describe the features of the plots in more detail.

Table 7.2: The coefficients of the polynomial used for the curve fitting in example Figure 7.3

f(x,y)=p00+p10.x+p01.y+p21.x^2+p11.xy	
Negative corona	p00=7.314e-06 p10=-4.59e-08 p01=2.43e-08 p20=1.16e-09 p11=-5.91e-10
Positive surface	p00=8.19e-04 p10=-3.92e-05 p01=2.11e-05 p20=4.18e-05 p11=7.79e-05

Plot of W vs. ΔQ

To illustrate the meaningfulness of the plot a sample weighted PSA plot of W vs. ΔQ is shown in Figure 7.4 The slope and dispersion over the red lines shown on the figure can be derived as follows.

$$slope = tan\,\theta = \frac{\Delta W}{\Delta(\Delta Q)} = \frac{W_i - 0}{\Delta Q_i - 0} = \frac{\Delta Q_i.\Delta t_i}{\Delta Q_i} = \Delta t_i \tag{7.2}$$

$$dispersion = slope_1 - slope_2 = \Delta t_1 - \Delta t_2 = \Delta(\Delta t) \tag{7.3}$$

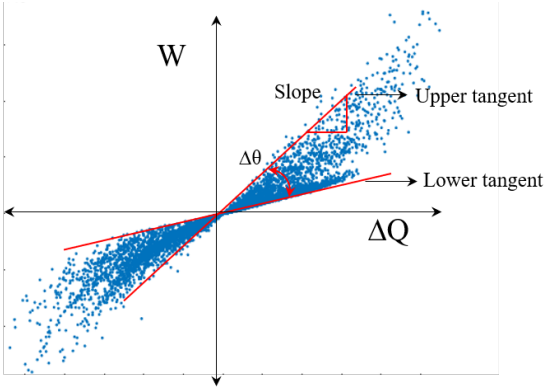

Figure 7.4: An example to illustrate the features of a weighted PSA plot of weighted quantity W vs. change in discharge magnitude (ΔQ) [1].

The plot for negative corona shown in Figure 7.5a shows a very narrow scatter in the values of Δt which is representative of the corona Trichel pulse cluster that have

almost a constant rate. On the contrary, the surface discharge pattern in Figure 7.7a and 7.7c exhibit a full range variation from zero upwards to a maximum value which is depictive of the randomness in the surface discharge process. A unique form of asymmetry is seen in the pattern of floating discharge shown in Figure 7.6a and 7.6c. This arises from the nature of the discharge which switches between breakdown of the gap and corona over the floating electrode (in the repetitive stage). The floating electrode defect exhibits a peculiar characteristic wherein a large breakdown pulse is followed by a series of small corona pulses and this pattern repeats itself. This imbalance in density of large vs. small pulses leads to an asymmetry in its discharge pattern. The similarity in the pattern of positive corona and surface discharge is dealt with at the end of the chapter.

In conclusion, the following set of inferences can be drawn from the weighted PSA plots of W vs. ΔQ:

(i) The dispersion in the scatter plot of W vs. ΔQ is the dispersion in the value of Δt.

(ii) The slope of the external tangent enclosing the distribution gives the smallest and largest values of Δt.

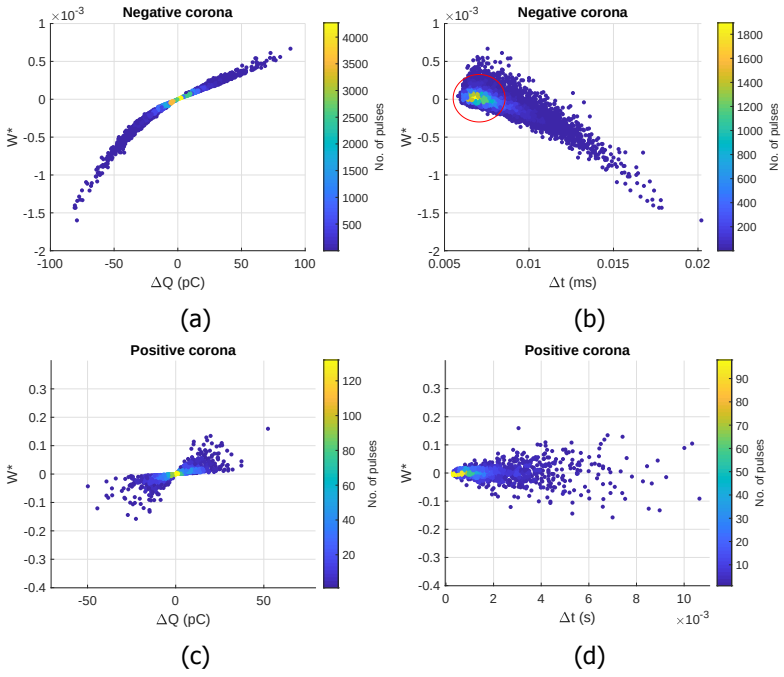

Figure 7.5: The weighted pulse sequence plots (left column) W vs. ΔQ and (right column) W vs. Δt for (a) & (b) Corona on -DC and (c) & (d) Corona PD on +DC [1].

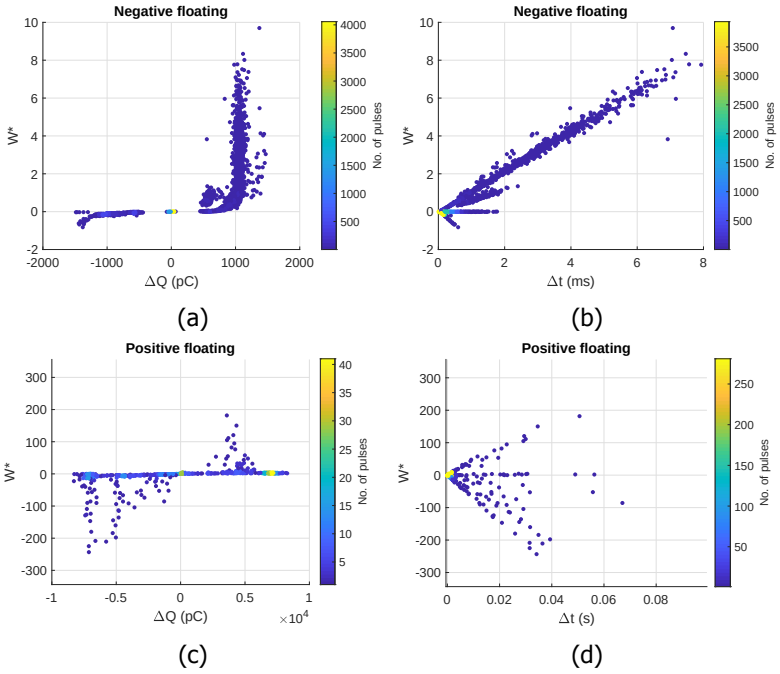

Figure 7.6: The weighted pulse sequence plots (left column) W vs. ΔQ and (right column) W vs. Δt for (a) & (b) Floating PD on -DC and (c) & (d) Floating PD on +DC [1].

7

(iii) The symmetry in the diagram depicts that the variation in Δt is regular and does not follow a specific scheme. While on the contrary, an asymmetry such as in Figure 7.6a and 7.6c shows multiple discharge process occurring systematically causing the data to group in a unique fashion.

Plot of W vs. Δt

The weighted PSA plot of W vs. Δt is shown in Figure 7.8, the slope and dispersion over the red lines shown in the figure can be derived as follows.

$$slope = tan\,\theta = \frac{\Delta W}{\Delta(\Delta t)} = \frac{W_i - 0}{\Delta t_i - 0} = \frac{\Delta Q_i . \Delta t_i}{\Delta t_i} = \Delta Q_i \tag{7.4}$$

$$dispersion = slope_1 - slope_2 = \Delta Q_1 - \Delta Q_2 = \Delta(\Delta Q) \tag{7.5}$$

That is the dispersion in the plot of W vs. Δt depicts the scatter in the values of ΔQ. In this case, the nature of the defect can be inferred from the axis of distribution. In case of corona there is a point distribution (shown in red in Figure 7.5b) over W equal to zero, which would mean the quantity ΔQ varies about zero and Δt varies over a mean value, reflecting the stable repetitive discharges under negative

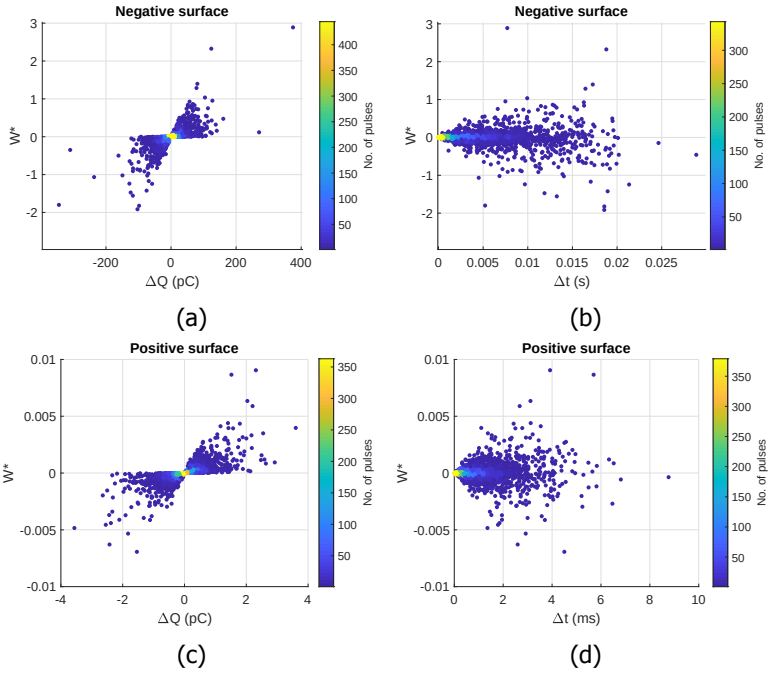

Figure 7.7: The weighted pulse sequence plots (left column) W vs. ΔQ and (right column) W vs. Δt for (a) & (b) Surface PD on -DC (Sample B) and (c) & (d) Surface PD on +DC (Sample B) [1].

DC voltage (configuration I). Similarly, for surface PD (shown Figure 7.7b and 7.7d) it is distributed symmetrically over the horizontal axis with a dispersion, $\Delta\theta$. Which indicates that the change in discharge magnitude in case of surface discharge is randomly distributed between zero and a maximum value defined based on the slope of the external tangent enclosing the distribution. The plots for floating discharge display an asymmetrical distribution due the systematic switching between the gap breakdown and corona over floating body.

In conclusion, the following set of inferences can be drawn from the weighted PSA plots of W vs. Δt:

(i) The dispersion in the scatter of W vs. Δt gives the dispersion in the values of ΔQ.

(ii) The slope of the external tangent enclosing the distribution gives the largest values of ΔQ (positive/increasing trend or negative/decreasing trend).

(iii) Based on the axis of symmetry of the distribution, the nature of the discharge is determined (point symmetry, horizontal line symmetry, asymmetry with multiple clusters).

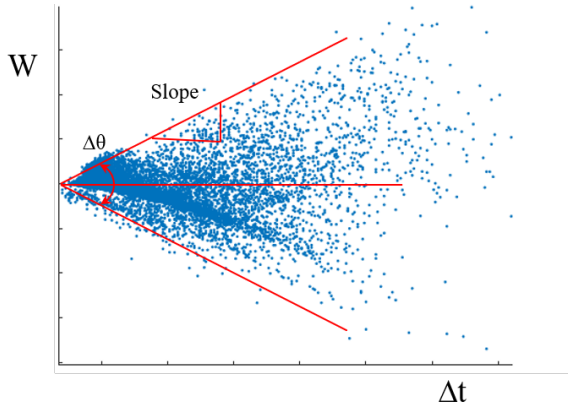

Figure 7.8: An example to illustrate the features of a weighted PSA plot of weighted quantity *W* vs. time between discharges (Δt) [1].

The weighted PSA plots for positive corona and surface discharge shown in Figure 7.5 and 7.7 appear to be similar. The repetitive stage of positive corona (self-sustaining discharge state [10]) which is unlike Trichel seems to have similarities with the process of surface PD. However, the plot of repetition rate of the charge (*N* vs. *Q*) for the two defect sources are dissimilar. In case of positive corona, the range of discharge magnitude varies over a median value as shown in Figure 7.9a. However, in the case of surface defect the magnitude of discharges varies from the smallest value possible to be measured (the charge threshold, Q_{th} set by the measuring system) to a maximum value.

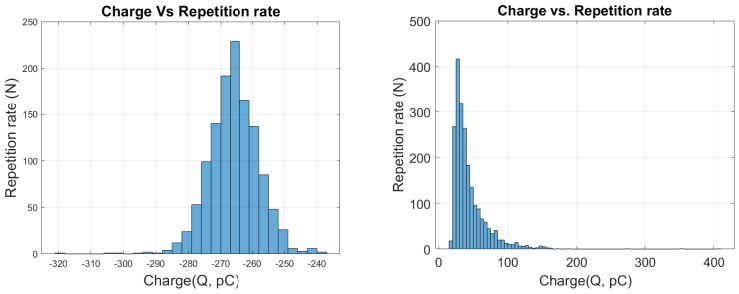

(a) (b)

Figure 7.9: Plot of charge (*Q*) vs. repetition rate (*N*) for (a) Corona on +DC and (b) Surface PD on -DC [1].

In the first assessment of sorts, the weighted PSA plots appear to reveal more information than the, 2-pulse PSA, 3-pulse PSA, 3-D PSA and are more perceptive and stable. They possess visible differences and exhibit unique patterns for various

defect types and hence may be a suitable alternative to the latter.

7.2.3. Other derived patterns

In the case of certain defect types such as corona that was studied in Chapter 4, specific derived patterns such as the plot of charge (Q_{i+1}) and time to discharge (Δt_{i+1}) have proven to be more reliable and useful in the defect identification process. These discharge patterns help differentiate the configuration of corona depending on the presence and absence of a relationship between the two quantities of charge and time to discharge. The linear rising relationship with the value of charge and time to discharge (Q_{i+1} vs. Δt_{i+1}) is shown in Figure 7.10a and 7.10b for configuration I and IV of the corona arrangement when the needle is placed at HV with -DC applied and when the needle is placed at ground with +DC applied respectively. Similarly, Figure 7.10c demonstrates the absence of such a relationship for configuration II of the corona arrangement with the needle placed at ground and -DC applied.

However, this plot has shown benefit only in the identification of corona. No single, stand-alone plot has so far benefited in the identification of all PD defect types.

7.3. Analysis based on statistical classification of discharge parameters

The probability distribution of the discharge quantities is studied in this section. Two quantities namely, difference in magnitude of successive charge (ΔQ) and time between successive charge (Δt) are considered. Both are normalized from 0 to 1 using the expression given in Eq. 7.6.

$$x' = \frac{x - min(x)}{max(x) - min(x)} \tag{7.6}$$

Where x' is the normalized value and x is the actual value. An exponential distribution is used to construct the probability plots shown in Figure 7.11 and 7.12.

7.3.1. Classification of time between discharge occurrence

Figure 7.11 shows the probability distribution of the normalized time between discharges (Δt) for various PD defect types. Three distinctive distributions can be seen on this figure. First, the cumulative probability distribution of floating electrode defect that follows a log-normal distribution. The defect under -DC discharges at a steady rate and the distribution of Δt values well represent/fit the lognormal curve. The floating defect under +DC on the other hand has a slow repetition rate and only up to 80 % of the points fit the lognormal distribution while the tail on the upper end poorly fits the curve. Secondly, can be observed the exponential distribution of the surface discharge quantity of Δt. The surface defect tested for both samples A

and B under both positive and negative DC showcases a similar distribution. The Δt distribution for positive corona also appears to follow an exponential distribution. Negative corona, however, follows a unique Weibull distribution. All the curves (lognormal, exponential and Weibull) are fitted for the showcased data series. Despite the poor fit of positive floating defect to the lognormal distribution and the likelihood of positive corona towards the exponential distribution rather than the Weibull distribution that negative corona follows, this analysis shows potential in aiding in the defect identification process.

7.3.2. Classification of difference in discharge magnitude

The other discharge quantity that is available from a DC-PD measurement is the quantity of charge. A similar analysis is made on the ΔQ distributions of various

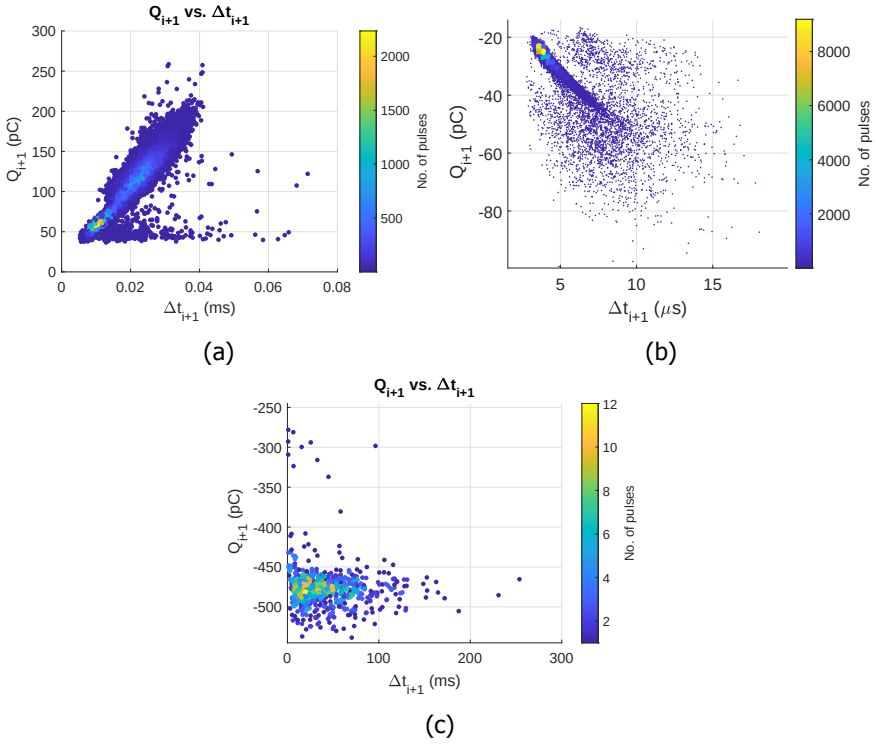

Figure 7.10: Discharge pattern of Charge (Q_{i+1}) vs Time to discharge (Δt_{i+1}) (a) when the needle is placed at negative DC voltage (Configuration I), (b) when needle is placed on ground with positive DC voltage (Configuration IV), note that the x-axis is presented in μs in this case and (c) when needle is placed on ground with negative DC voltage (Configuration II).

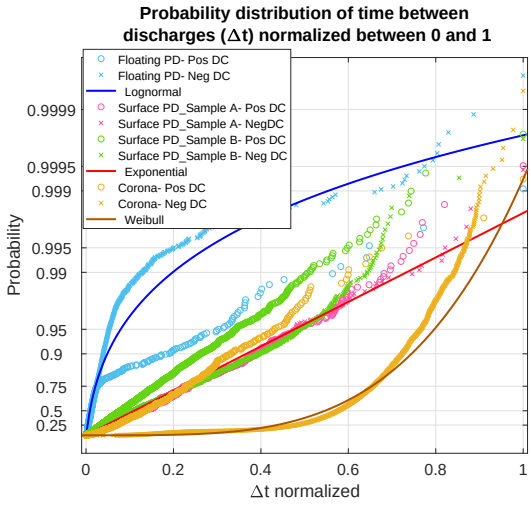

Figure 7.11: Cumulative Probability distribution of time between discharges (Δt) for various defects normalized between 0 and 1 [1].

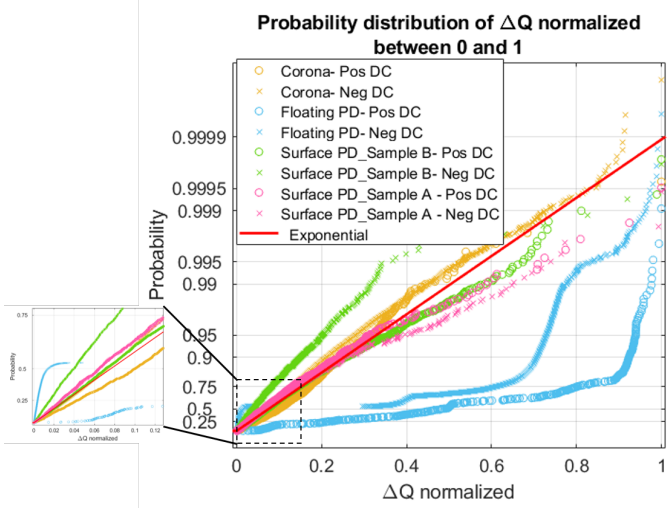

Figure 7.12: Cumulative Probability distribution of change in discharge magnitude (ΔQ) for various defects normalized between 0 and 1 (insert with zoom) [1].

defect sources with the same available data. The probability distribution of the normalized values of difference in magnitude of successive charge (ΔQ) are presented in Figure 7.12

Only two distinctive groups are seen on this plot. An exponential distribution of

the normalized ΔQ values for corona and surface discharge, and a discontinuous distribution of the values of floating discharge. From [9] it can be noted that the floating PD under DC alternates between breakdown of the gap and corona over the floating body (in the repetitive discharge stage). And there is a disparity in discharge magnitudes of these two phenomena. This disparity reflects as the discontinuity in values of ΔQ. The initial part of the distribution follows a lognormal distribution (can be seen from the insert on Figure 7.12) while the latter part follows a Weibull or double exponential curve.

7.4. Discharge trends with respect to voltage

In case of AC PD analysis, one of the most commonly used supplementary figures alongside the Phase resolved PD (PRPD) plots is the *Q(V)* plot, also known as the Q vs. V plot. It provides useful information on the trend in discharge magnitude with respect to increasing and decreasing voltage. It is particularly useful in the discrimination of internal defects from surface discharge defects, since the PRPD plots of a surface defect and internal defect can sometimes look similar. However, the difference in inception and extinction voltage of an internal defect, generating a hysteresis-like curve helps differentiate the two defect types under AC. Though this research has not studied the DC discharge from an internal defect, it still explores the benefit of the Q(V) plots under DC for the three different defects studied in this research. Figures 7.13, 7.14 and 7.15 show the Q(V) plots of the respective defects namely corona, floating electrode and surface discharge under AC, -DC and +DC test voltages. And this section evaluates their effectiveness in the defect identification process.

Consider the discharge trends for corona given in Figure 7.13a for the AC test case. The discharge process is a combination of the Trichel/negative corona and the streamer discharges/ positive corona. The corona defect under AC incepts with the trichel pulses of relatively small magnitude ($\sim$ 200 pC in this case) and at higher voltages translates to the streamer discharges also known as positive corona that has a relatively high magnitude (a few nC in this case). A similar overall trend can be noted while considering Figures 7.13b and 7.13c together for corona under -DC and +DC voltages. By putting together the information on the two plots one would conclude that it belongs to the corona defect. In addition, given the many nuances in the discharge process of corona that are described in chapter 4, such as pulse-free zone and self-sustaining corona, the Q(V) plots for the particular defect look unique in their own way.

The floating electrode defect follows a similar trend with its AC discharge process in comparison to its -DC and +DC discharge processes put together. The sustainable pulse stage on -DC voltage has a discharge magnitude comparable to the floating discharge under AC with a magnitude of $\sim$2 nC. However, the inception voltage under -DC is slightly higher than under AC voltage. This is because the singular discharge pulses preceding the sustainable pulse stage charge the floating electrode lowering the electrical field across the floating gap (explained in section 5.3). Similarly, the discharge magnitude under +DC is of a similar magnitude com-

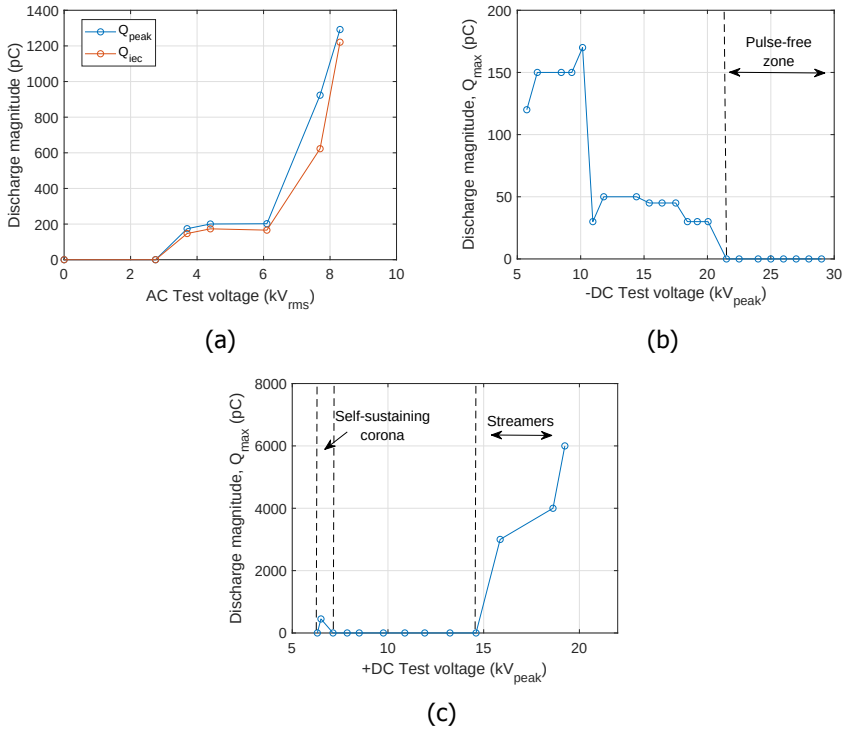

Figure 7.13: The plot of discharge magnitude with respect to voltage (Q vs. V) for the corona defect tested under (a) AC (b) -DC (configuration I) and (c) +DC (configuration II) voltage.

pared to the corona over floating body observed under AC voltage. However, the Q(V) plot by itself does not provide any information on the non-repetitive or repetitive stage of the discharge. Neither does it reflect the information on the PSA plot of time between discharges presented in Figure 5.9c. The Q(V) plot for the floating electrode defect could easily be taken as the discharge progression of corona or surface discharge presented in Figures 7.13 and 7.15.

The Q(V) plots of the surface discharge defect do not exhibit such a coherence in terms of inception value of voltage or charge magnitude. The Q(V) plots for the -DC tests solely seems to follow the AC discharge trend. The +DC plot does not seem to correspond in terms of discharge magnitude or inception voltage to the AC process. The reason for which has been described in detail in section 6.4.2. The Q(V) plots for the surface discharge defect do not provide any significant benefit to the defect identification process due to the absence of any manifest features in the discharge process.

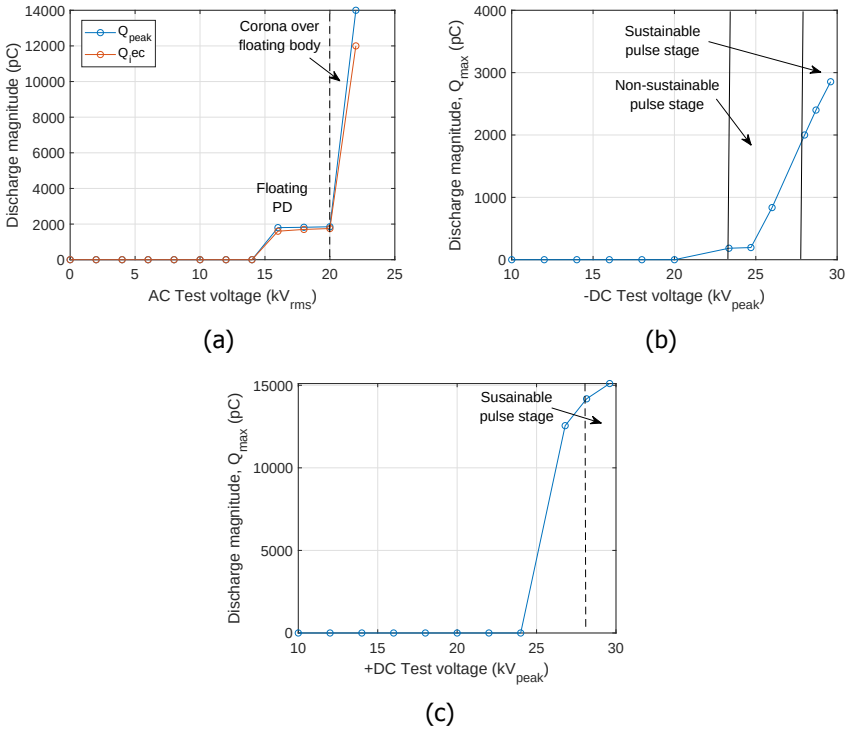

Figure 7.14: The plot of discharge magnitude with respect to voltage (Q vs. V) for a floating electrode defect tested under (a) AC (b) -DC and (c) +DC voltage.

7.5. Discriminatory process

Defect identification under DC stress has gained tremendous traction in the recent years due to a wide spectrum of new DC applications. The ability to qualify the insulation quality and fitness of DC systems is the goal of partial discharge testing. So far partial discharges under DC have been treated as insufficient to produce a repeatable and well-shaped pattern due to their low pulse rates and erratic nature. However, several defect cases, such as the ones discussed in this chapter, discharge at a stable rate (comparable to AC). This raises the significance of defect identification under DC with the aid of visual tools. Defect identification not just provides insight into the type of insulation system defect but also broadens the fundamental understanding on the insulation's DC behaviour. This chapter investigates several ways of analysing discharge data under DC, exploring the possibilities of the most promising visual tool that is closest to the AC-PRPD diagrams. Based on the presented visual tools a decision tree is devised to distinguish between the different defect types. The flow chart shown in Figure 7.16 categorizes the repetitive PD pulses using the weighted PSA plots (WePSA). The key towards visual pattern iden-

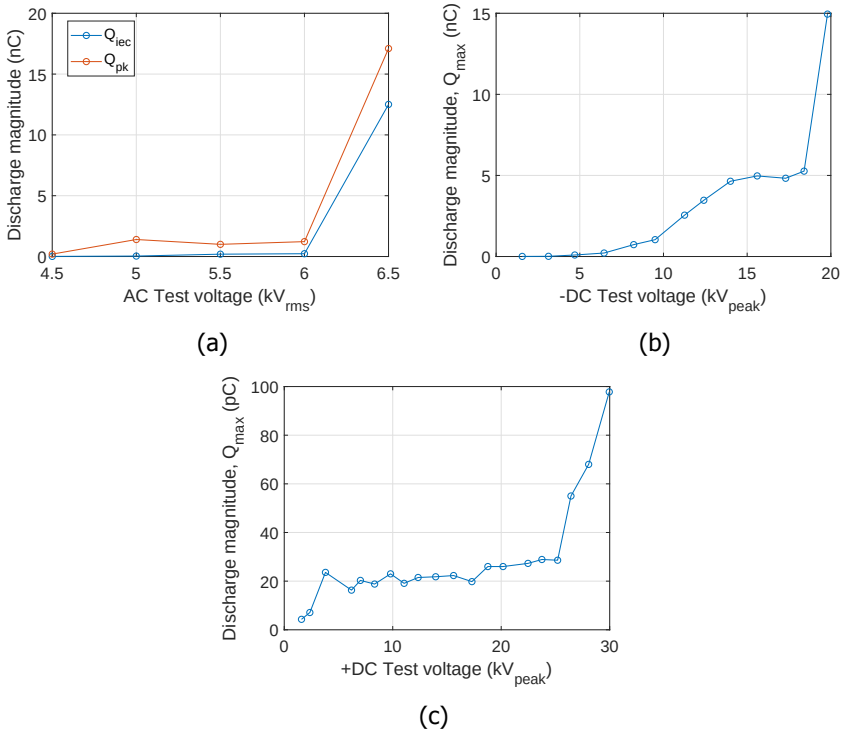

Figure 7.15: The plot of discharge magnitude with respect to voltage (Q vs. V) for a surface discharge defect tested under (a) AC (b) -DC and (c) +DC voltage.

tification, is the possibility of recording sufficient number of pulses that will produce a pattern with adequate contrast. Therefore, the first decision block on the flow chart looks for selection of 'measurable and repetitive PD pulses'. In some cases, the PD pulses may be smaller in amplitude so that they are below the noise threshold of the acquisition system. In these cases, it will not be probable to build visual patterns with such an acquisition stream. In other cases, the PD pulse stream is non-recurrent, i.e. such as the singular pulses in a floating electrode defect or the pulse-free zone of corona. In these cases, the non-repetitive nature of the pulses, renders the acquisition ineffective due to lack of sufficient pulses. For the defect conditions that can be suitably measured and are repetitive in nature, WePSA plots are used in their classification. A narrow scatter range of Δt in the plot of W vs. ΔQ along with a point distribution around W=0 in the plot of W vs. Δt is indicative of negative corona. A double check can be made by verifying the probability distribution of Δt and the unique trend in the correlation between $Q_{i+1}$and Δt_{i+1} [10]. The random/wide Δt scatter in the plot of W vs. ΔQ and a line distribution about the W=0 intercept in the plot of W vs. Δt is indicative of a surface defect

or positive corona. One or the other can be confirmed based on the distribution of Q (plot of N vs. Q). Floating discharge under DC has several unique features [9]. This procedure has been formulated for the identification of singular defect sources under DC. The scenario with several defect sources interacting with each other has not been tackled. This may be recommended as a step for future research in the field, where de-clustering techniques for PD source separation under DC voltage can be investigated.

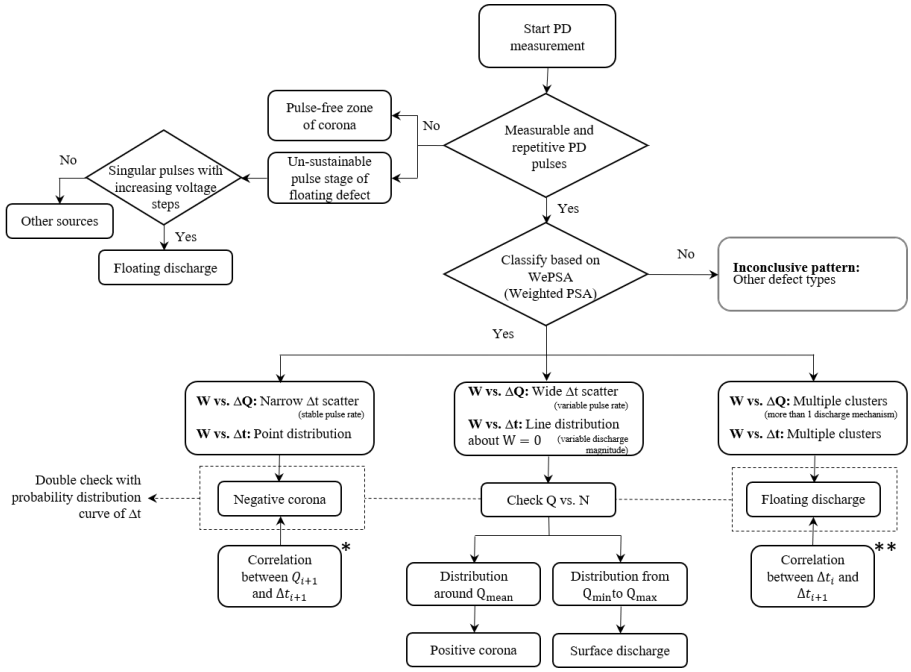

Figure 7.16: Flow chart identifying the defect sources based on the weighted PSA plots [1]. *The unique relationship between the quantities of charge(Q_{i+1}) and time between discharge (Δt_{i+1})[10] **The unique discharge patterns of Δt_i vs. Δt_{i+1} for floating electrode defect are presented in [9]

7.6. Conclusion

The chapter summarizes the PD patterns obtained from three different partial discharge defects. It selects the data for processing based on previous studies [9][10] that designate a specific discharge characteristic to the particular defect configuration. For instance, the repetitive stage of floating electrode and the self-sustaining positive corona that are unique features based on which the defect could be identified are utilized in this research. The following points recapitulate the various sections of the chapter.

- It presents the unique probability distribution of the quantity 'Δt' for three different defects, except positive corona that closely resembles the surface discharge defect. This could serve as a diagnostic tool in PD defect identification.
- The new perspective to PSA, demonstrating the possibility of a three dimensional or 3D-PSA plot by combing two plots has been proposed.
- The novel weighted PSA (WePSA) plots proposed in the chapter are not only visibly distinctive but also perceptive and simple to interpret to a great extent.
- The plots of discharge trend with respect to voltage, Q(V), provide an overall understanding the discharge process of the defect with the possibility of comparing it with the already well known AC defect behaviour.
- The decision chart presented in the last section of the chapter devises a diagnostic procedure by means of which one can investigate the nature of discharge under DC stress conditions.

It is understood that PD under DC does not manifest itself as clearly and systematically as under AC (repetitive with each voltage cycle). And even in conditions in which it does, a single figure/pattern may not be entirely sufficient to determine the source. Therefore, the multiple patterns and methods of analysis presented in this chapter are proposed with the final goal of implementation in the PD diagnostic phase aiding in the identification of the PD defect type. The results presented show great promise, especially with the novel 'Weighted PSA' plots or WePSA patterns that come a step closer to the DC version of PRPD.

references

[1] **S. Abdul Madhar**, P. Mraz, A. Rodrigo Mor, and R. Ross. "Empirical analysis of partial discharge data and innovative visualization tools for defect identification under DC stress". In: *International Journal of Electrical Power & Energy Systems* 123 (Dec. 2020), p. 106270. issn: 01420615. doi: 10.1016/j.ijepes.2020.106270.

[2] T. Christen. "Characterization and robustness of HVDC insulation". In: *Proceedings of IEEE International Conference on Solid Dielectrics, ICSD*. 2013, pp. 238–241. isbn: 9781479908073. doi: 10.1109/ICSD.2013.6619804.

[3] Standard IEC 65700-19-03:2014. *Bushings for DC application*. International Electrotechnical Commission (IEC), 2014.

[4] A. Abbasi, J. Castellon, A. Cavallini, F. Esterl, T. Gotz, M. Kharezy, S. Markalous, S. Neuhold, R. Pietsch, A. Pirker, R. Plath, U. Richert, M. Rossner, and M. Seltzer-grant. "Progress on Partial Discharge Detection under DC Voltage Stress". In: (2019).

[5] M. Hoof and R. Patsch. "Pulse-sequence analysis: a new method for investigating the physics of PD-induced ageing". In: *IEE Proceedings-Science, Measurement and Technology* 142.1 (1995), pp. 95–101.

[6] P. Morshuis and G. Hoogenraad. "Partial discharge diagnostics for DC equipment". In: 1 (1996), pp. 407–410.

[7] P. H. Morshuis and J. J. Smit. "Partial discharges at dc voltage: Their mechanism, detection and analysis". In: *IEEE Transactions on Dielectrics and Electrical Insulation* 12.2 (2005), pp. 328–340. issn: 10709878. doi: 10.1109/TDEI.2005.1430401.

[8] B. Fruth and L. Niemeyer. "The importance of statistical characteristics of partial discharge data". In: *IEEE Transactions on Electrical Insulation* 27.1 (1992), pp. 60–69.

[9] **S. Abdul Madhar**, P. Mraz, A. Rodrigo Mor, and R. Ross. "Physical interpretation of the floating electrode defect patterns under AC and DC stress conditions". In: *International Journal of Electrical Power and Energy Systems* 118 (June 2020), p. 105733. issn: 01420615. doi: 10.1016/j.ijepes.2019.105733.

[10] **S. Abdul Madhar**, P. Mraz, A. Rodrigo Mor, and R. Ross. "Study of Corona Configurations under DC Conditions and Recommendations for an Identification Test Plan". In: *International Journal of Electrical Power and Energy Systems* 118 (June 2020), p. 105820. issn: 01420615. doi: 10.1016/j.ijepes.2020.105820.

8

Conclusions and Recommendations

8.1. Conclusions

The research studied the partial discharge behaviour of three of the most common defect types under DC namely corona, surface and floating electrode. The PD defect sources were studied in-depth and analysed extensively to recognize differences in their behavior and discharge patterns. As stated in chapter 1, the goal of this research was to develop a methodology for the classification/identification of various common insulation defects through electrical partial discharge measurement under DC voltage stress. The sub-objectives defined in section 1.4 are recapitulated in this chapter and the results related to each sub-objective have been summarized.

In-depth study of PD characteristics of various defect sources

(i) Three common defect types namely, corona, floating electrode and surface discharge were studied in this thesis. The defects were studied both under AC and DC voltage stress.

(ii) This thesis demonstrates that the decision to focus on individual defects and their in-depth behaviour has yielded through its study, characteristic defect fingerprints.

(iii) In case of the study of corona under DC, the self-sustaining pulse stream of configuration II (section 4.2.2) and the intermittent corona of configurations II and III (section 4.2.3) were found through detailed observation and analysis of the discharge phenomenon.

(iv) The research on floating discharge defect has elucidated the discharge physics under AC. This was accomplished through the interpretation of the PRPD (Phase resolved PD) pattern and the phenomenon of moving/sliding pulses in the active discharge diagram. The PD behavior under AC has been explained through an analytical model implemented in MATLAB as described in section 5.2.

(v) Through the careful study of the floating electrode defect under DC, a criterion for its repetitive discharge state has been defined in section 5.3.

(vi) The study of surface discharge defect revealed differences in the behavior of dielectric samples towards positive and negative DC test voltages. The reasons for this differences have been adequately studied and analysed. The research has also demonstrated an increased similarity between the DC and AC discharge processes in certain test cases.

(vii) Based on the study of dielectric properties of the materials involved in the DC surface discharge tests, it was concluded that with a lower disparity in the conductivity of the two involved media (in this case, air and surface PD sample), lower will be the surface charge accumulation. And this lowered surface charge accumulation led to the increase in the tangential electrical field component along the interface that in turn led to the inception of surface discharge during the steady-state DC.

Development of an optimal post-processing strategy for the analysis of the acquired PD data

(i) This work demonstrates that for conventional electrical PD measurements, with PD data recorded through continuous streaming at a rate of 10-20 MS/s, it is possible to obtain meaningful patterns through special analysis.

(ii) As a part of this research, a special set of algorithms was developed to recognize individual pulses from the data stream, for post-processing and analysis of the PD raw data as described in section 3.5.1.

(iii) It has been shown that three basic parameters namely, discharge magnitude, time of discharge occurrence and polarity are sufficient to analyse the PD discharge stream sufficiently.

(iv) In certain cases, such as in the study of surface discharge defect, software simulations using COMSOL have given more insight to the effects of dielectric parameters of the surface PD sample under study.

Evaluation of the PD defect characteristics to find a defect identification methodology

(i) The final goal of the research was to discover characteristic differences in the PD behaviour of the different defects in order to develop a defect identification strategy. This has been made possible by the detailed study of individual defect sources and a careful study of the discharge and material physics as mentioned previously.

(ii) The analysis of the discharge parameter Δt for the three defects has revealed that each of the defect sources has a unique probability distribution of Δt as presented in section 7.3.1.

(iii) The research has highlighted the lack of intuitiveness and the trouble in interpreting PSA (pulse sequence analysis) plots. The PSA plots have also shown to magnify the differences in discharge magnitudes and time between discharges as demonstrated in section 7.2.1.

(iv) A new perspective to the PSA plots, by combining two plots to form a 3-D PSA plot has been proposed.

(v) The novel "WePSA" or Weighted PSA patterns have been developed based on the analysis of the discharge parameters of the repetitive stage of the three defect types under study. The WePSA plots as presented in section 7.2.2 have demonstrated to be visibly distinctive and easy to interpret for each of the individual defects.

(vi) The causality in the relationship between the quantities of discharge magnitude Q_{i+1} and time to discharge Δt_{i+1} has shown to exhibit a unique trend in the plot of Q_{i+1} vs. Δt_{i+1} in the case of corona configurations I and IV as presented in section 7.2.3.

(vii) The repetitive stage of floating discharge defect under negative DC voltage manifests itself through a unique pattern on the PSA plot of time between successive discharges in a 3-pulse sequence (Δt_{i+1} vs. Δt_i) as seen in Figure 5.9d.

(viii) The PSA plot for time between discharges (Δt_{i+1} vs. Δt_i) for the surface discharge defects has revealed a unique 'fish' shaped pattern. This is shown in Figure 6.17.

(ix) Based on the overall analysis, this research has devised and proposed a comprehensive diagnostic procedure in section 7.5 through the formulation of a flowchart for PD defect identification under DC voltage. The procedure developed so far is limited to the identification of the three singular defects studied in this research.

8.2. Recommendations for future work

This research has been able to focus on the study of three common PD defect types under air as dielectric. There is certainly the scope for the research to be extended to the study of defects under other dielectric media such as liquid (mineral and synthetic oils as in transformers), solids (epoxy resin as in GIS spacers or XLPE as in cables) and other gaseous dielectric (SF_6 as in GIS), as well as the study of internal defects such as voids and intrusions. The discriminatory procedure proposed in Figure 7.16 is based on the findings of this research. It is recommended that this procedure be extended to include multiple other defect scenarios in the future to create one comprehensive defect identification procedure. There is also a need to develop clustering strategies for partial discharges under DC in order to identify multiple defects that discharge simultaneously.

There is also a need to test the proposed methodologies for defect identification on real industrial defects. With this it will become possible to build more experience and gain feedback on the performance of the strategy. In the real world scenarios it is also most probable for test objects to have more than one defect. This will have to be tackled independently by the development of clustering techniques for DC-PD before the application of the knowledge on defect identification. Lastly, based on the study of DC-PD, certain suitable recommendations could be made to the international standardization committees that formulate the testing criteria. However, to do this, one needs to further the research in the direction of influence of DC-PD on the ageing of the dielectric or the level of risk based on the defect behavior. In conclusion, this research is a start that will serve as a base for future research in this field.

Conceptual WePSA plots for various defect types

Negative corona

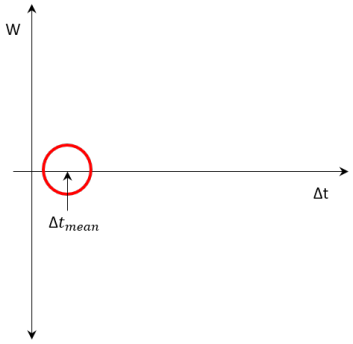

(a) Point distribution over Δt_{mean}

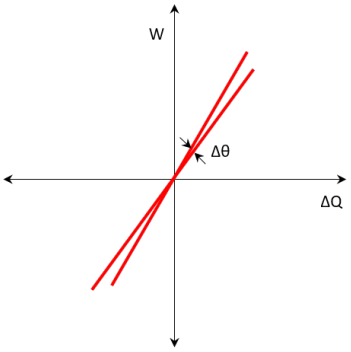

(b) Narrow dispersion of $\Delta\theta$

Positive corona or Surface discharge

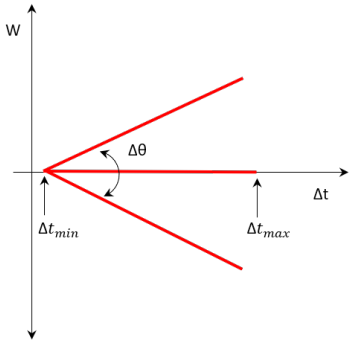

(c) Line symmetry over Δt

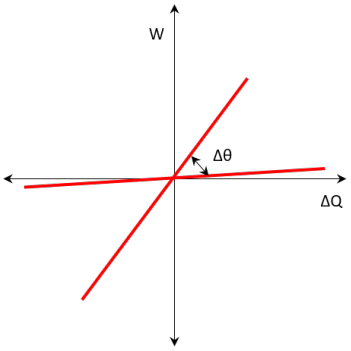

(d) Wide dispersion of $\Delta\theta$ full range variation from zero upwards to a maximum value

Negative or Positive Floating discharge

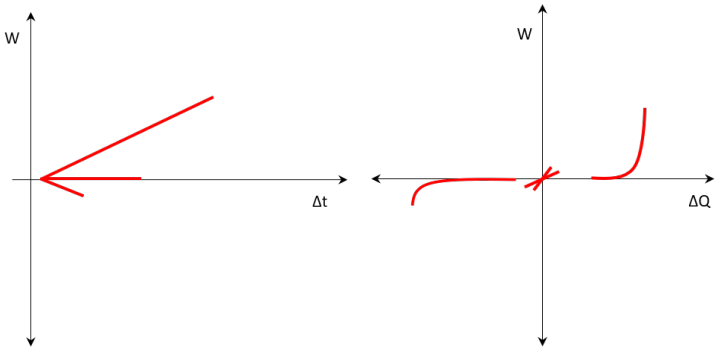

(a) Multiple clusters and asymmetrical

(b) Multiple clusters and asymmetrical

List of Abbreviations

AC	Alternating current
BW	Bandwidth
DC	Direct current
DUT	Device under test
EHV	Extra high voltage
EM	Electromagnetic
EV	Electric vehicle
FAT	Factory acceptance test
FEM	Finite element method
GIL	Gas insulated line
GIS	Gas insulated switchgear
GND	Ground
GS	Giga samples
HF	High frequency
HFCT	High frequency current transformer
HP	High pass
HV	High voltage
HVAC	High voltage alternate current
HVDC	High voltage direct current
IEC	International Electrotechnical Commission
IEEE	Institute of Electrical and Electronics Engineers
LP	Low pass
MS	Mega samples
PD	Partial discharge
PDE	Partial differential equation
PDIV	Partial discharge inception voltage
PRPD	Phase resolved partial discharge
PSA	Pulse sequence analysis
PV	Photovoltaic
RH	Relative humidity
SAT	Site acceptance test
TDR	Time domain reflectometry
UHV	Ultra high voltage
USD	US Dollar
UV	Ultra violet
VNA	Vector network analyser
WePSA	Weighted pulse sequence analysis
WG	Working group

Acknowledgements

Firstly, I acknowledge that nothing is possible without the willingness of the Almighty. All praise be to Allah who gave me the strength to understand, learn and perform in my duties. His mercies upon me have no bound. *Alhamdulillah*.

This PhD journey has been a special one and will remain close to my heart. Apart from having been given the chance to work in beautiful Switzerland, I have also had the pleasure of working with HAEFELY AG, a name that is synonymous with High Voltage and considered a legend by most of us who belong to this field. And not to forget the cherry on the cake, I got to do this PhD together with the Delft University of Technology, which I very much call my own.

I would like to start by thanking my co-promoter and daily supervisor at TU Delft, Dr. Armando Rodrigo Mor for his constant support, his gentle motivation and timely advice. He has helped me push my capabilities through the review and criticism of my work. Next I would like to thank Dr. Petr Mráz, my mentor and supervisor at Haefely. I would like to thank him for the countless discussions which have moulded this research to what it is today. Petr has been the kind of mentor who provides his back for the mentee to climb higher. His guidance has come a long way. Apart from being my supervisor, he has also been a good friend and a well-wisher. I am immensely grateful to him for his continued support.

I would like to extend my gratitude to my Promoter Prof. dr. Robert Ross for his valuable time and wise advice. In this short time, I am glad to have learnt from his profound experience and his vast knowledge. I would also like to thank my Manager, Santiago Gonzalez for giving me the time and flexibility to complete my thesis and being a part of several useful brainstorming sessions. I am also grateful to the European Horizon 2020 research initiative, the MEAN4SG consortium for this amazing opportunity. I would like to thank all my colleagues at Haefely who have worked with me directly or indirectly. Special thanks to the 2 pm coffee group for the deep discussions over coffee. A special mention to Marc Brunner for helping me with the material testing by sharing his in-depth knowledge on the instruments. There are countless more people who have helped me during this journey, with a kind word, a genuine prayer or a helping hand, a heart-felt thanks to all of them.

Certainly, over the top of all my countless blessings is my family. They are my source of happiness and comfort. How does one thank a devoted father who has given his entire life to give me the wings to fly and a selfless mother who has been the wind beneath those wings. No amount of thanks can do that. Not to forget my younger sister, who earnestly ignores me and later secretly emulates me. I genuinely believe that it is their prayers that has got me so far. The prayers of my nana, amma (grandparents), aunts, uncles and all my cousins included.

When the whole world was dealing with the new pandemic a new chapter of my

life began. Therefore, thanks is also due to my parents-in-law for now I belong in their prayers too. And of course, God bless my kind husband, who believes I can do anything. Life would be incomplete without him.

Saliha Abdul Madhar
4th March, 2021, Basel

Curriculum Vitæ

Saliha ABDUL MADHAR

23-04-1994 Born in Chennai, India.

Education

2015–2017 M.Sc in Electrical Sustainable Energy at Delft University of Technology

Master thesis at the Delft University of Technology and the Asset Management department of DNV GL Energy, The Netherlands.

Thesis: Feasibility study of sensitive partial discharge measurements on long cable systems.
Committee: Prof.ir. P. Vaessen, Prof.dr.ir. E.F. Steennis, Dr. A. Rodrigo Mor, Ir. B.C. van Maanen.

2018–2020 PhD Researcher

(Jan 2018–Dec 2019) Marie Skłodowska Curie Research Fellow under the Mean4sg project group, employed with HAEFELY AG, Switzerland.
(Jan 2020–Dec 2020) PhD Researcher and Product Engineer with the Product Management department of HAEFELY AG, Switzerland.

Promoter: Prof.dr. R. Ross.
Co-promoter: Dr. A. Rodrigo Mor.
Supervisor: Ing. P. Mráz, Ph.D.

Work experience

2020–Present Product Engineer at HAEFELY AG, Switzerland

List of Publications

Journals

S. Abdul Madhar, P. Mraz, A. Rodrigo Mor, and R. Ross. "Study of Corona Configurations under DC Conditions and Recommendations for an Identification Test Plan". In: *International Journal of Electrical Power and Energy Systems* 118 (June 2020), p. 105820. issn: 01420615. doi: 10.1016/j.ijepes.2020.105820

S. Abdul Madhar, P. Mraz, A. Rodrigo Mor, and R. Ross. "Physical interpretation of the floating electrode defect patterns under AC and DC stress conditions". In: *International Journal of Electrical Power and Energy Systems* 118 (June 2020), p. 105733. issn: 01420615. doi: 10.1016/j.ijepes.2019.105733

S. Abdul Madhar, P. Mraz, A. Rodrigo Mor, and R. Ross. "Empirical analysis of partial discharge data and innovative visualization tools for defect identification under DC stress". In: *International Journal of Electrical Power & Energy Systems* 123 (Dec. 2020), p. 106270. issn: 01420615. doi: 10.1016/j.ijepes.2020.106270

S. Abdul Madhar, A. Rodrigo Mor, P. Mraz, and R. Ross. "Study of DC partial discharge on dielectric surfaces: mechanism, patterns and similarities to AC". in: *International Journal of Electrical Power and Energy Systems* 126 (Mar. 2021), p. 106600. issn: 0142-0615. doi: 10.1016/j.ijepes.2020.106600

Conferences

S. Abdul Madhar, P. Mraz, S. Barrios Pereira, and N. Akroud. "Frequency response of a real cable network and its impact on field PD measurements". In: *2019 International Conference on Electricity Distribution (CIRED)*. 1492. 2019, pp. 1–5

S. Abdul Madhar and P. Wenger. "Simultaneous Electrical and UHF Measurement of DC-PD from Point-Plane Defect". In: *The International Symposium on High Voltage Engineering*. Springer, 2019, pp. 991–1003

P. Mraz, **S. Abdul Madhar**, P. Treyer, and U. Hammer. "Guidelines for PD measurement according to IEC 60270". In: *The International Symposium on High Voltage Engineering, Hungary*. 2019

P. Wenger, **S. Abdul Madhar**, and M. Beltle. "Simultaneous Electrical, UHF, Current and Optical PD Measurements on Floating Potential under DC Stress". In: *2019 IEEE Conference on Electrical Insulation and Dielectric Phenomena (CEIDP)*. 2019, pp. 287–290

S. Abdul Madhar, M. Brunner, A. Rodrigo Mor, and P. Mraz. "Measurement of key dielectric properties for surface PD model under HVDC". in: *Proceedings of International conference on Dielectrics, ICD*. Valencia: IEEE, 2020